ISTANBUL TECHNICAL UNIVERSITY ★ INSTITUTE OF SCIENCE AND TECHNOLOGY

MICROSTRUCTURAL AND THERMAL CHARACTERIZATION STUDIES OF NON-DOPED AND ERBIUM DOPED BINARY GeO_2 – PbF_2 GLASSES

M.Sc. Thesis by
Mithat Cem ELBİZİM

Department : Advanced Technologies

Programme : Materials Science and Engineering

JANUARY 2010

ISTANBUL TECHNICAL UNIVERSITY ★ INSTITUTE OF SCIENCE AND TECHNOLOGY

MICROSTRUCTURAL AND THERMAL CHARACTERIZATION STUDIES OF NON-DOPED AND ERBIUM DOPED BINARY GeO_2 – PbF_2 GLASSES

M.Sc. Thesis by
Mithat Cem ELBİZİM
(521071021)

Date of submission : 25.12.2009
Date of defence examination: 27.01.2010

Supervisor (Chairman) : Prof. Dr. M. Lütfi ÖVEÇOĞLU (ITU)
Members of the Examining Committee : Asst. Prof. Dr. Burak ÖZKAL (ITU)
Prof. Dr. Fatma TEPEHAN (ITU)

JANUARY 2010

İSTANBUL TEKNİK ÜNİVERSİTESİ ★ FEN BİLİMLERİ ENSTİTÜSÜ

KATKISIZ VE ERBİYUM KATKILI İKİLİ GeO_2 – PbF_2 CAMLARININ MİKROYAPISAL VE TERMAL KARAKTERİZASYON ÇALIŞMALARI

YÜKSEK LİSANS TEZİ
Mithat Cem ELBİZİM
(521071021)

Tezin Enstitüye Verildiği Tarih : 25.12.2009
Tezin Savunulduğu Tarih : 27.01.2010

Tez Danışmanı : Prof. Dr. M. Lütfi ÖVEÇOĞLU (İTÜ)
Diğer Jüri Üyeleri : Y. Doç. Dr. Burak ÖZKAL (İTÜ)
Prof. Dr. Fatma TEPEHAN (İTÜ)

OCAK 2010

FOREWORD

Firstly, I would like to express my greatest gratitude and thanks to my supervisor Prof. Dr. M. Lütfi ÖVEÇOĞLU for his guidance and help during both my graduate studies and my dissertation work. I would like to thank Prof. Dr. Gönül ÖZEN for her support and advices for my thesis studies. I would also like to thank Assist. Prof. Dr. Burak ÖZKAL for providing convenient investigation enviroment conditions in the Particulate Materials laboratories.

I am very grateful to Res. Assist. Demet TATAR for her everlasting support and guidence throughout my thesis studies. I am also grateful to Res. Assist. Hasan GÖKÇE and Res. Assist. Ahmet Umut SÖYLER for their great help in my experimental work.

I am thankful to the members of the Particulate Materials laboratories, Res. Assist. Selim COŞKUN, Şeyma DUMAN, Aziz GENÇ, Nida YILDIZ USLU, Sezen Seda YAKAR, Deniz YILMAZ and Hatice Kübra YUMAKGİL for their support and contribution to my studies. I am also thankful to Çiğdem ÇAKIR KONAK for her patience and help during my electron microscopy investigations.

I am deeply grateful to my parents Yasemin ELBİZİM and Şevket Ersin ELBİZİM and my brother Faruk Can ELBİZİM for their understanding, companionship, support and advices, this study wouldn't exist without them.

December 2009 Mithat Cem Elbizim

Physics Engineer

TABLE OF CONTENTS

Page

ABBREVIATIONS

GeO_2	**:** Germanium dioxide
PbO	**:** Lead oxide
PbF_2	**:** Lead difluoride
Er_2O_3	**:** Dierbium trioxide
DTA	**:** Differential Thermal Analysis
XRD	**:** X-Ray Diffraction
SEM	**:** Scanning Electron Microscope
EDS	**:** Energy Dispersive Spectrometry
°C	**:** Celsius
% wt	**:** Weight Percentage

LIST OF TABLES

Page

LIST OF FIGURES

Page

MICROSTRUCTURAL AND THERMAL CHARACTERIZATION STUDIES OF NON-DOPED AND ERBIUM DOPED BINARY GeO_2 – PbF_2 GLASSES

SUMMARY

Germanium oxide glasses are not widely investigated as silicate, borate and phosphate glass. In recent years, germanium oxide based glasses become an important glass-former among other glasses formers, due to their applicability to optical materials like visible, infrared and upconversion lasers, linear and non-linear optical lasers.

When germanium oxide combined with heavy metal oxides and fluorides, they gain interesting properties. They have smaller phonon energies and higher refractive indices than silicate and borate glass which makes it an excellent source for photonic, optoelectronic, passive and active optical fibers and non-linear optical devices. In addition to that, heavy metal oyfluoride glasses become the most promising materials due to their efficient optical, enhanced mechanical and thermo-stable properties. Fluoride ions in the glass matrix can help the removal of OH^- groups in the glass host and they reduce multiphonon decay between excited states of rare-earth ions.

Among the heavy metal glasses, lead germanate glasses have low non-radiative transitions and phonon energy, they can be applied as host materials to non-linear optic and upconversion lasers while their crystallite phases can be applied in fields of pyroelectric, ferroelectric and electrooptic. Moreover, lead germanate glass systems gain interesting physical and chemical properties when they are doped with rare-earth elements like erbium, thulium and europium.

In this study, germanium-rich binary GeO_2 – PbF_2 glasses are aimed to investigate for their thermal properties and identification of their crystalline phases with differential thermal analyzer (DTA), X-ray diffractometer (XRD) and scanning electron microscope (SEM) techniques.

Non-doped and doped GeO_2 – PbF_2 binary glasses are investigated with varying PbF_2 and Er_2O_3 contents for their thermal behavior and characterization temperatures which are the glass transition temperature, crystallization peak temperatures and melting temperatures and effects of varying compositions on characterization temperatures is reported. Thermal effects for different heating rates are also reported for non-doped binary GeO_2 – PbF_2 glass system. Crystal phases on the heat-treated glass-ceramic samples are identified and effects of PbF_2 and Er_2O_3 to crystalline phases are reported with X-ray diffraction scans and scanning electron microscope micrographs.

KATKISIZ VE ERBİYUM KATKILI İKİLİ GeO_2 – PbF_2 CAMLARININ MİKROYAPISAL VE TERMAL KARAKTERİZASYON ÇALIŞMALARI

ÖZET

Germanyum oksit camları, silikat, borat ve fosfat camları kadar detaylı çalışılmamışlardı. Son yıllarda, germanyum oksit esaslı camlar, görünür, kızılötesi ve yükseltme lazerlerinde, lineer ve lineer olmayan optik lazerleri gibi optik malzemelerde kullanılabilir olmalarından dolayı diğer cam yapıcılara arasında bir öneme sahip olmuştur.

Germanyum oksit ağır metal oksit ve fluorürlerle birlikte kullanıldığında çok ilgi çekici özelliklere sahip olmaktadırlar. Silikat ve borat camlarından düşük fonon enerjilere ve yüksek kırılma indisine sahip olmalarından dolayı fotonik, optoelektronik, pasif ve aktif optik fiberler ve lineer olmayan optik cihazlar için mükemmel bir kaynak olmaktadır. Buna ek olarak ağır metal oksit camları, etkili optik, gelişmiş mekanik ve ısıl kararlı özelliklerinden dolayı en çok gelecek vaat eden malzemeler olmaktadırlar. Ayrıca cam matris içindeki flüorür iyonları, OH-gruplarının uzaklaştırımasına ve nadir toprak iyonlarının çoklu fonon bozunmalarının azaltılmasına yardımcı olur.

Ağır metal camları arasında, kurşun germanate camları düşük ışımasız geçişlere ve fonon enerjilerine sahip olmalarından dolayı lineer olmayan optik ve yükseltme lazerlerinde kullanılırken kristal fazları ise piroelektrik, ferroelektrik ve elektrooptik alanlarında kullanılmaktadır. Ayrıca kurşun germanate cam sistemleri, erbiyum, tulyum ve evropyum gibi nadir toprak elementleri ile katkılandırıldıklarında çok ilginç fiziksel ve kimyasal özelliklere sahip olmaktadırlar.

Bu çalışmada germanyumca zengin GeO_2 – PbF_2 camları, termal özeliklerinin ve oluşan kristal fazların diferansiyel termal analiz (DTA), X-ışınları kırınımı (XRD) ve taramalı elektron mikroskopu (SEM) yöntemleri kullanılarak araştırılması amaçlanmıştır.

Katkılı ve katkısız ikili GeO_2 – PbF_2 camları, değişen PbF_2 and Er_2O_3 miktarı ile termal davranışının ve cam geçiş sıcaklığı, kristalizasyon tepe sıcaklığı ve erime sıcaklıkları gibi karakterizasyon sıcaklarının değişimi incelenmiştir. İkili GeO_2 – PbF_2 camlarında, farklı ısıtma hızlarının etkisi ayrıca incelenmiştir. X-ışınları kırınımı ve taramalı elektron mikroskopu yöntemleri kullanılarak ısıl işlem görmüş cam-seramiklerde görülen fazlar tanımlanmış ve PbF_2 and E_2O_3 katkısının bu kristal fazlara olan etkisi incelenmiştir.

1. INTRODUCTION

Non-crystalline lead germanate materials doped with rare-earth ions have potential applications due to their physical and chemical properties which allow to fabricate optical fibers, laser hosts and optoelectronic materials (Scavini et al., 2001; Zhereb et al., 2008; Conçalves et al., 2002). In addition, different compositions of crystalline phases of lead germanate materials provide promising ferroelectric, pyroelectric, electrooptic and photorefractive properties (Scavini et al., 2001; Tomasi et al., 2002; Ghigna et al., 2002).

There are some recent studies carried out on glass systems which accommodate lead germanates with fluoride network (Tambelli et al., 2004; Dominiak-Dzik et al., 2008; Bueno et al. 2008; Klimesz et al., 2008). Fluoride ions aid the removal of OH residual groups and decrease melting temperature, as well they diminish the connectivity in the network thus they are accepted fluoride ions as non-bridging atoms in mixed oxyfluoride glass compositions (Tambelli et al., 2004). Especially, fluoride systems have more potential in luminescence applications than oxide systems due to their relatively lower phonon energies which allow them to have non-radiation transitions (Mortier and Patriarche, 2000; Bueno et al., 2008; Lucas et al., 2001; Adam, 2001). However, in oxyfluoride glass network, the real fluoride concentration is lower than theoretical values for samples which are heated at relatively higher temperatures. In these systems, Ge^{+} ions usually tend to react with fluorine ions and combine compounds of elusive germanium fluorides (GeF, GeF_2, GeF_4) which usually evaporate from the melted samples (Bueno et al., 2005; Klimesz et al., 2008), yet fluoride ions are sensitive to oxygen atoms and traces of water (Mortier and Patriarche, 2000; Ghigna et al., 2002).

Thermal stability in glass networks is critical to be studied for the non-crystalline and crystalline phases which is required to affirm the technological advantages (Scavini et al., 2001; Nie et al., 2007). In this study, GeO_2 – PbF_2 – Er_2O_3 system is investigated for its thermal stability and microstructure. Er^{+} ion was selected in this study because it is one of the most efficient rare-earth ion for accomplishing infrared

and visible upconversion lasers, thus it has been widely studied (Gouveia-Neto et al, 2004a). In literature, several authors (Speranskaya, 1959; Phillips and Scroger, 1965; Gouju et al., 1968; Bush and Venevtsev, 1981; Scavini et al., 2001) studied the GeO_2 – PbO phase diagram. However, these studies contradict each other and authors identified different crystal phases at the same compositional range. Moreover, nucleation of PbF_2 in GeO_2 – PbO – PbF_2 environments which are generally doped with rare earth elements (Gouveia-Neto et al, 2004a; Dominiak-Dzik et al., 2008; Mortier et al., 2006). Nevertheless, this study intensifies on thermal study and microstructure of GeO_2 – PbF_2 where PbO agent was excluded. Glass compositions were selected as $(1 - x)\ GeO_2 - x\ PbF_2$ and $(1 - x - y)\ GeO_2 - x\ PbF_2 - y\ Er_2O_3$ where x = 0.1, 0.2 and 0.3 and y = 0.005 and 0.02 mol%. Thus, effect of substitution of PbO with PbF_2 on GeO_2 – PbO phase relation and intervention of Er_2O_3 were investigated.

2. GERMANIUM OXIDE BASED GLASSES

2.1 Germanium Oxide

Indirect gap elemental semiconductors like Si and Ge attract many interests because of their ability to luminescence in visible region (Amato et al., 1997; Setlur et al., 2006). Their structural, optical and electronic properties have been studied widely in the last decades. Germanium dioxide (GeO_2) is one of the most attractive materials among dielectric oxides in fields of optical applications. In addition to that, germanium oxide based glasses are more refractive then commercial SiO_2 based glasses and also nanocrystalline GeO_2 can be used in the applications of nano-fiber communications (Viswanathamurthi et al., 2004).

GeO_2 has two distinct crystalline phases which are rutile and quartz like structures which are shown in Figure 2.1 (Margaryan and Piliavin, 1993; Ghingna et al., 2002; Anan'ev et al., 2008). When GeO_2 is heated to temperature above 1049 °C, germanium dioxide transforms into hexagonal (β-quartz) phase from tetragonal (rutile structure). Following cooling to 1000 °C causes the transformation of unstable β-quartz into stable α-quartz, thus stable α-quartz can be obtained at room temperatures. Rutile-like structure is in the form of tetragonal structure with a germanium atom and 6 oxygen atoms, while quartz-like structure has hexagonal form (Margaryan and Piliavin, 1993; Viswanathamurthi et al., 2004; Anan'ev et al., 2008). Moreover, the piezoelectric properties of α-quartz GeO_2 couldn't be investigated due to absence in nature and growth difficulties before discovering transformation of rutile GeO_2 to α-quartz GeO_2 phase (Balitsky et al., 1997).

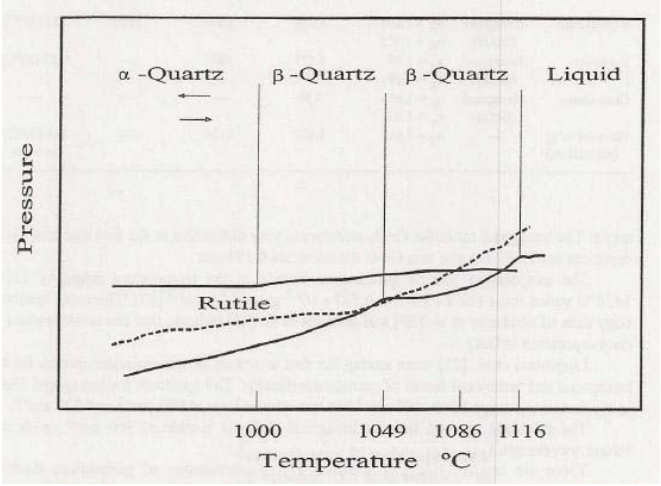

Figure 2.1 : Polymorphic Transition of GeO_2 with pressure and temperature (Margaryan and Piliavin, 1993).

Balitsky et al., (1997) succeeded on crystal growth of prismatic α-GeO_2 crystals and many of them reside at solution-wall boundary. They also accomplished on nucleating thin dendrite crystals of α-GeO_2 on the surface of the solution (Balitsky et al., 1997).

2.2 Germanium Oxide Glasses

SiO_2, B_2O_3, GeO_2 and P_2O_5 are called as main glass formers (Doremus, 1994). Compared to SiO_2 and B_2O_3, GeO_2 has not been investigated widely as a glass-former oxide. Because of aspiration to materials which have less absorption losses in the middle IR range, germanium oxide glasses have become more essential glass-formers as silicate based glasses (Anan'ev et al., 2008). Germanate glasses and their crystals which are demonstrated in Figure 2.2 are usually utilized at high pressures in place of silicates, due to their structural similarities with silicates. For instance, rutile-like GeO_2 is isostructural with the polymorph of silicate at high pressure (Peng and Stebbins, 2007). Scavini et al. (2001) devitrified pure GeO_2 glass in order to investigate its crystal structure and X-ray diffraction results showed only α-GeO_2. Although α-GeO_2 is stable above 1050 ºC, crystallization of tetragonal β-GeO2 could not be accomplished even after a long heat treatment process which was 660 ºC at 360 h (Scavini et al., 2001).

Combination of silicates, germanates and borates with alkali oxides are primary oxide glasses and their characteristic properties are usually affected by alkali ions with low oxygen coordination. Besides, alkali ions can influence each glass network

modifier individually (Peng and Stebbins, 2007). Among the GeO_2 based glasses, alkaline metal oxides enclose one of the most detailed studies while their preparation procedures are easier than other GeO_2 based glasses (Ghinga et al., 2002). Some of these properties like density and glass transition temperature can change slightly in silicate glasses, but they show maximum and minimum values in germanate and borate glasses with change of alkali amount in the network (Peng and Stebbins, 2007).

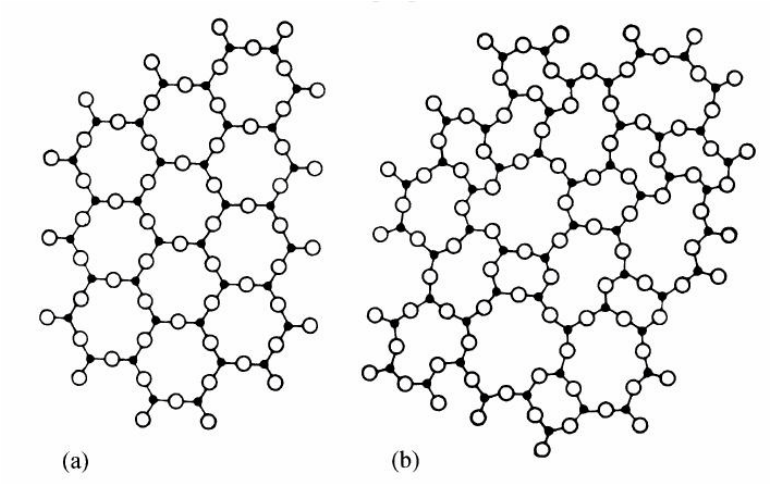

Figure 2.2 : Two dimensional illustration of crystal (a) and glass (b) arrangement (Yamane and Asahara, 2000).

In these glasses, this change can be basically associated with transition of trigonal B^{3+} and tetrahedral Ge^{4+} to highly coordinated structures which contain more oxygen ions and these oxygen atoms bridge and connect two differently coordinated cations (Du et al., 2007).

Pure glassy GeO_2 are formed with GeO_4 tetrahedra units and they have non-oriented network arrangement (Micolaut et al., 2006). Formation GeO_4 occurs with bridging of oxygen atoms and germanium atoms have four-coordinated structure. When additional compounds (M_aO_b) are introduced to pure GeO_2 glass, amount of modifier oxide can affect thermophysical properties like characteristic temperatures and glass density and these properties can have their maximum or minimum values at specific composition range (Du et al., 2007; Hannon et al., 2007). In alkali germanate glass systems, this behavior set in between 10 – 20 mol% A_2O content in the binary GeO_2 – A_2O glasses. This behavior is called as germanate or germanium anomaly (Henderson, 2007) and coordination change is illustrated in Figure 2.3. This anomaly basically depends on increment and reduction of GeO_6 octahedra number in the

network (Hannon et al., 2007; Anan'ev et al., 2008, Ghinga et al., 2002, Henderson et al., 2009). This anomaly is also a sign of eccentric polymorphism of pure GeO_2, where it can be existed in both rutile-like and quartz-like structure in room temperature (Ghinga et al., 2002).

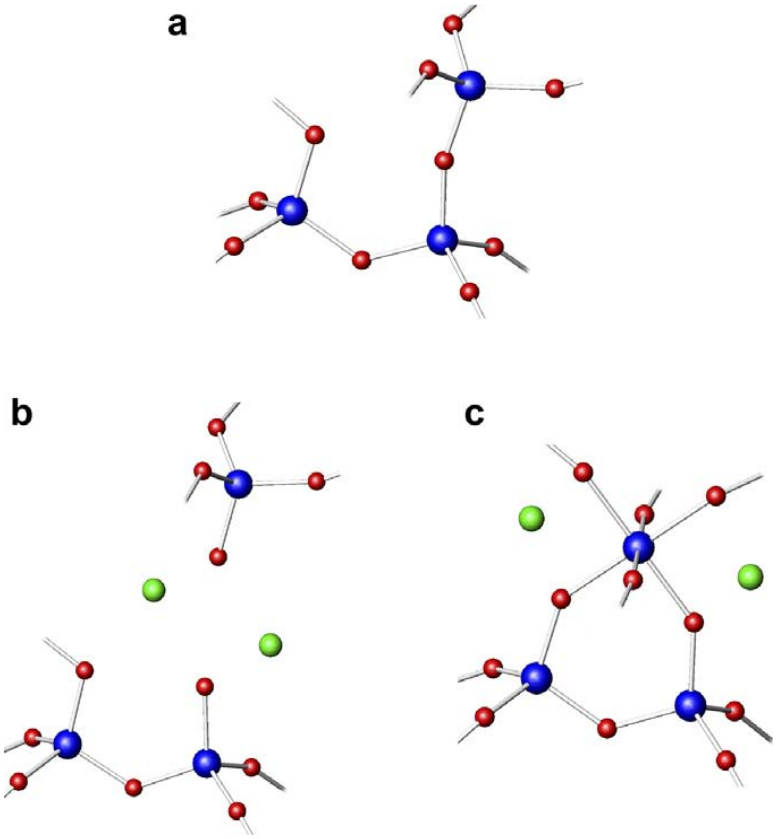

Figure 2.3 : Illustration of coordination change on alkali germanate glasses: (a) Pure GeO_2 glass which is formed by [GeO_4] tetrahedral, (b) alkali germanate glass which has two bridging and two non-bridging atoms per germanium atom, (c) alkali germanate glass which is formed by [GeO_4] tetrahedra and [GeO_6] octahedral (Hannon et al., 2007).

In oxide glass networks, ions are surrounded by oxygen atoms, which are non-bridging atoms or bridging atoms. Common belief is such that ionic motion is only possible between regular ionic sites and smaller ions cause mechanical stress in large sites while larger ions are dissolved in the surrounding matrix in the oxide glasses (Henderson, 2007; Belostotsky, 2007). Thus, motional ions which reach to extrinsic sites cannot affect the integrity of network (Belostotsky, 2007). When a modifier oxide is added to germanate glass network, it increases number of oxygens and force them to host more oxygen than they already have. Increase of oxygen in the germanium environment could result with two possible scenarios which are formation of non-bonding oxygens (NBOs) or lower coordinated germanium atoms

(GeO_4) can converse into highly coordinated germanium atoms (GeO_6) (Hannon et al., 2007).

Hannon et al. (2007) reported that two details on germanate anomaly in germanate glasses contradict each other. First of them is about the formation of highly coordinated which doesn't exist and doesn't affect the germanate anomaly. Second contradiction is about presence of highly coordinated germanium and even if they are found, they are only five or six coordinated germaniums in the network or it could be mixture of them. From this aspect, Hannon et al. (2007) suggested that combination of two GeO_4 tetrahedra can turn out five coordinated trigonal bipyramidal GeO_5 units with addition of modifier oxide. For instance at lower alkali oxide Na_2O, the transformation of GeO_4 units to GeO_5 units occurs and the average number of Ge – O coordination increases. On the other hand, for relatively higher Na_2O content formation of non-bridging oxygens (NBOs) is found and results in a decrease on the number of Ge – O coordination. But NBOs are usually observed at the higher Na_2O contents and if NBOs are not in the presence, oxygens atoms tend link two GeO_4 tetrahedra or GeO_4 tetrahedron and highly coordinated Ge unit. Because there are no oxygen atoms which are coordinated by three GeO_6 octahedra, sufficient formation of GeO_5 and GeO_6 units exist in the network (Hannon et al., 2007).

Bonding of oxygen atom in the network in germanium alkali oxide systems can be expressed by the equation (2.1) where oxide atoms bond with germanium tetrahera and formation of either GeO_6 or GeO_5 and no non-bridging oxygens occur (Du et al., 2007).

$$Na_2O + {}^{[4]}GeO_{4/2} = ({}^{[6]}GeO_{6/2})^{2-} + 2Na^{+} \quad \textbf{(2.1)}$$

Formation of non-bridging oxygen in the network in germanium alkali oxide systems can be expressed by the equation (2.2) where high amount of alkali content forces most or all of the GeO_6 or GeO_5 transform back to GeO_4 tetrahedra with non-bridging oxygen (Du et al., 2007).

$$Na_2O + {}^{[4]}GeO_{4/2} = {}^{[4]}GeO_{3/2}O^{-} + Na^{+} \quad \textbf{(2.2)}$$

Hoppe et al. (2000) stated that distinguishing of GeO_5 and GeO_6 units are not possible by using only diffraction studies, but they claimed that differentiation of formation of GeO_5 and GeO_6 units can be possible when change on the coordination number (n_{GeO}) is taken consideration with compositional change.

Hannon et al. (2007) provide a model where negatively charged GeO_n units cannot come closer than specific distance and their negatively charged center should be substantially away from other negatively charged centers. They claimed that their model was based on six different postulates for germanates glass. First of all, all germanium atoms in the matrix should be in four or n-coordinated where value of n is either 5 or 6. Secondly, there shouldn't be any evidence of three-coordinated oxygen atoms. Thirdly, number of GeO_n units in the matrix should have its maximum value while number of NBOs in the network should be minimal. They also claimed two GeO_n units cannot be connected and these units don't have any NBOs in their formation. Finally, they mentioned formation of GeO4 tetrahedra which has more than NBOs could be possible when highly coordinated GeO_n units are absent in the glass network.

Since GeO_2 is a well-known as glass-former chemical compound (Nie et al., 2007), thermal stability of the oxide systems can be increased with adding GeO_2 to the glass system and thus prevention of crystallization is achieved. However, Nie et al. (2007) found in their studies that GeO_2 acts completely different in bismuth-borate glasses and it decreases ΔT temperature difference in these glasses which shows that GeO_2 cannot prevent crystallization in these glass compositions.

2.3 Heavy Metal Glasses

Germanium, tellurium, gallium antinomy oxides are investigated as glass maker oxides and due to the combination with heavy metals, they are called as heavy metal oxide (HMO) glasses. These glasses are important because of their relatively small phonon energies and high refractive indices when compared to borate, silicate and phosphate glasses. Moreover, heavy metal oxide glasses are permeable for middle infrared lights, thus they are provide essential characteristics for applications in photonic, passive and active optical fibers and non-linear optical devices (Lezal et al., 2001). Especially, PbO based heavy metal oxide glasses have attractive physical properties like high density, high linear and non-linear refractive index which allow them to be used widely on optical and optoelectronic devices (Knoblochova et al., 2009).

Due to the possibility of development of passive, active and non-linear optical applications, studies on heavy metal oxide glass systems are focused. Since these

glasses are used in optical devices, it's necessary to improve the quality of glass with using high purity chemical compounds while this way helps to decrease impurities on the glass network and yield better luminescence results. Lezal et al. (2001) stated that their study showed:

1. The OH groups can be removed from the system efficiently where the OH concentration is below $3x10^{-3}$ mol%, if reactive atmosphere (like Chloride environment was used for development of Heavy Metal Oxide based glasses.

2. Heavy Metal Oxide glasses' physical properties like color of the glass and optical efficiency can be adjusted with fabrication conditions.

3. Heavy Metal Oxide glasses have better rare earth element solubility than tellurite glasses.

Knoblochova et al. (2009) studied that addition of GeO_2 and PbO instead of B_2O_3 leads increment on not only density but also molar volume. Moreover, it also decreases the glass transition temperature which could be as a result of increment of PbO in the glass network. Knoblochova et al. (2009) showed that addition of PbO and GeO_2 content increased the number of non-bridging oxygen atoms which leads to network disorder and it was concluded that decrease on glass transition values with addition of heavy metal oxide content is related with this network opening.

2.4 Fluoride Glasses

Fluoride ions in oxide based glasses cause changes on the physical properties of the glass systems. Fluoride ions in the glass environment tend to decrease refractive index and melting temperatures, help elimination of OH^- groups and provide ion conductivity. In oxyfluoride glass systems, fluoride anions act as nonbridging atoms and they decrease connectivity in the glass network. Moreover, small part of the fluoride anions bond to glass network weakly and act as charge carriers which improve conductivity and allow the development of electrochemical devices like halide sensors, solid-state batteries and glass purifiers (Tambelli et al., 2004). Like heavy metal oxide glasses, fluoride glasses can be applied to many photonic devices, however their chemical durability is not good as metal oxide glasses. When compared to each other, heavy metal oxide glasses have almost analogous properties like glass transition temperature, refractive index and phonon energies, but they cut-

off at different short and long wavelengths (Lezal et al., 2001). Zhang et al. (2008) proved that increasing the number of the fluoride anions in the system can result as decrease on refractive index and phonon energy which leads efficient upconversion process. Besides, oxyfluoride glass systems can accommodate unique crystalline phases (Dantelle et al., 2006; Dominiak-Dzik et al., 2008). Especially, nucleation metal fluoride nanocrystals on the glass host with controlled crystallization is one of the interesting study on the ultra-transparent glass ceramics (Tambelli et al, 2004).

Heavy metal oyfluoride glass is now one of the attractive materials due to their efficient optical, enhanced mechanical and thermo-stable properties (Gouveia-Neto et al, 2004b; Bueno et al, 2008). In these glasses, despite presence of oxygen atoms in network, fluoride ions reduce phonon energy and contribute removal of OH^- groups in the glass host where reduction of multiphonon decay between excited states of rare-earth ions is accomplished and the quantum efficiency of the glass network can be improved (Zhang et al., 2008).

2.5 Rare earth elements and effects on the glasses

Rare-earth doped materials are mainly preferred for designing photonic devices and they are investigated extensively. In many of rare-earth elements systems, erbium doped glass systems and their applications prevail because of their luminescence lifetime, emission bandwidth and upconversion efficiency and allow them to be studied widely (Mortier et al., 2001; Gouveia-Neto et al., 2008). However, in rare-earth doped systems non-radiative losses or cut-off optical phonon energies should be kept minimal in order to improve intensity of the radiative luminescence. Since, fluoride based glasses have low cut-off optical phonon energy while showing bad chemical durability and oxide systems have high cut-off optical phonon energy but good mechanical and chemical durability, oxyfluoride systems can be investigated for both physical properties (Kassab et al, 2007).

But it is necessary to investigate stability of un-doped glass in order to prepare same glasses with rare-earth elements like Er^{3+}, Tm^{3+}, Eu^{3+} (Lezal et al., 2001). Although Er^{3+} doped tellurite glasses display one of the best stimulated emission properties within the various glass hosts, when compared with the rest of the glass formers they have low thermal stability and their ambiguity on upconverison luminescence, thus it prevents them to be applied in industrial designs (Nie et al., 2007).

Among these laser and luminescence applications, upconversion lasers diode has been investigated widely because of promising designs like optical data storage, under-water optical fibers, biomedical devices, sensors and infrared excited visible lasers where rare-earth ions excited (Figure 2.4) in the transparent hosts with infrared laser (Joubert, 1999). Er^{3+} ions are one of most preferred rare-earth ion which is used as an activator in upconversion process. Although, the rare-earth element takes a significant role in upconversion lasers, the host choice is also important because glass host dominates most of the spectroscopic properties (Zhang et al., 2008).

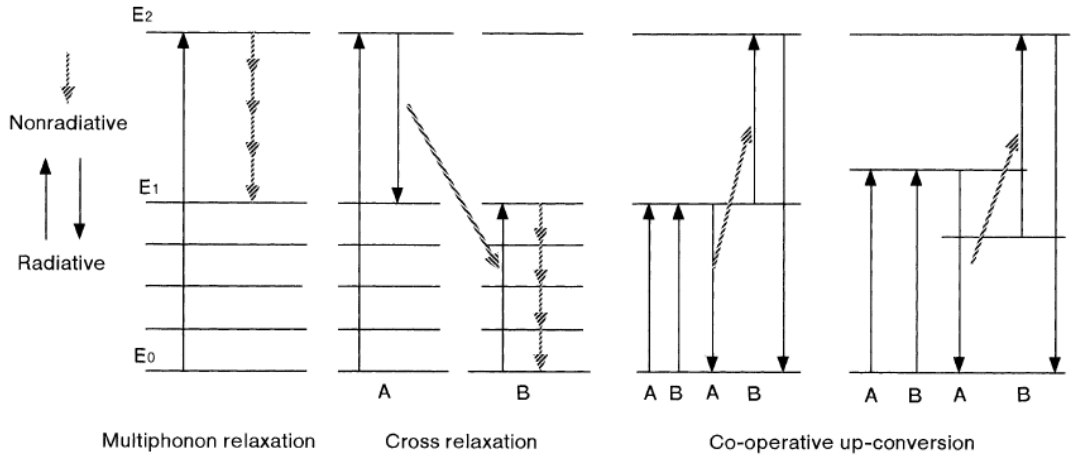

Figure 2.4 : Illustration of relaxation phenomenon of rare-earth elements (Yamane and Asahara, 2000).

When GeO_2-based glasses are doped with rare earth elements which have low phonon energy, they gain numerous optical spectroscopic properties (Mortier, 2003, Gouveia-Neto et al., 2008). Due to their lower phonon energy, they show high quantum efficiency of luminescence and they are attractive as laser and luminescent applications (Klimesz et al., 2008).

2.6 Lead Germanate Glasses

In most of the glass compositions, lead germanate of the binary system PbO-GeO_2 glasses become one of the brightest materials as laser applications (Ghingna et al., 2002; Kassab et al, 2007). Among the other oxide systems, they have low cut-off optical phonon energy and low non-radiative transitions, thus these properties makes them good candidates for upconversion lasers. Moreover, they can be used in waveguide non-linear optics due to their high linear and non-linear refractive indexes (Kassab et al, 2007). These glass systems and their crystalline compounds are

favorable in technological applications like fiber optics in optoelectronics and in the fields of pyroelectric, ferroelectric and electrooptic when compared to other germanate glass systems due to their interesting physical and chemical properties especially when they are doped with rare earth ions (Tomasi et al., 2002; Ghinga et al., 2002; Tomasi et al., 2005; Zhereb et al., 2008). On the other hand, these glasses are not studied as widely as alkali germanate glasses and several studies (Speranskaya, 1959; Phillips and Scroger, 1965; Gouju et al.,1968 ; Bush and Venevtsev, 1981; Scavini et al., 2001) on binary GeO_2 – PbO system contradict each other and stable crystalline phases are not determined completely.

2.6.1 Binary GeO_2 – PbO glasses

Binary GeO_2 – PbO glasses can transmit the light up to 4.5 μm in the infrared region (Lezal et al., 2001). It is possible to improve glass stability to crystallization with addition other several of glass modifiers. Homogenous glasses can be produced with 50 mol% PbO content in binary GeO_2 – PbO glass system. Basic OH vibration in the glass network causes an extrinsic absorption band which is usually detected at the value of 2.93 μm (Lezal et al., 2001). In germanate glasses, lead oxide content occupy as a network modifier. Even a small percent of PbO addition into germanate glass causes formation of non-bridging oxygens in the network and formation of non-bridging oxygens results with decrease of the glass transition temperature (Ghinga et al, 2002).

In GeO_2 – PbO glass systems (Scavini et al., 2001; Ghinga et al. 2002; Zhereb et al., 2008), glass transition temperature (T_g) changes between 472 and 442 °C which is shown in Figure 2.5 while onset crystallization temperature is between 610 and 670 °C for $0.30 \leq x \leq 0.50$ PbO content (Lezal et al., 2001). While Ghinga et al. (2002) reported that their pure GeO_2 glassy sample showed a glass transition temperature around 525 °C. When they added PbO to the system, glass transition temperature tended to make a rapid decrease until PbO content reached 10 mol%. With more addition of PbO, glass transition temperature value did not change. When PbO content became more that 25 mol%, glass transition temperature values showed continuous decrease with PbO content. Ghinga et al. (2002) obtained 0.75 GeO_2 – 0.25 PbO glass which has a glass-transition temperature at 460 °C and an on-set crystallization at 560 °C while they reported that similar behavior was also observed

for different compositions. Furthermore, their XANES and EXAFS studies evidenced that Ge coordination is mainly in tetrahedral coordination for all of the glassy samples which they studied and glassy GeO_2 is almost similar with hexagonal GeO_2 crystals. On the other hand, they reported that number of octahedral GeO_6 units increased briskly with addition of PbO, but number of octahedral GeO_6 units were almost constant at more than 10 mol% PbO content. However, Ghinga et al. (2002) reported that results of several authors contradict with each other about the existence of six-fold [GeO_6] units in the lead germanate glasses.

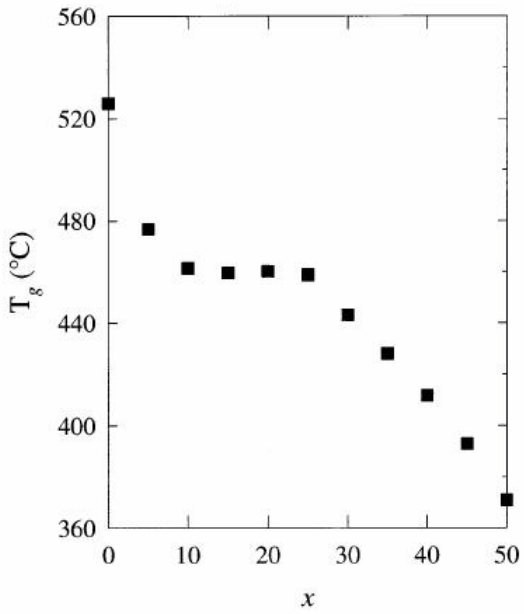

Figure 2.5 : Change of glass-transition with x mol% PbO content (Ghingna et al., 2002).

Speranskaya (1959) was the first who studiedand exhibited the PbO-GeO_2 binary phase diagram (Figure A.1) by using differential thermal analysis and X-ray powder diffraction techniques where samples were annealed at high temperature for long times. He identified five lead germanate crystalline phases which are Pb_6GeO_8, Pb_3GeO_5, $Pb_5Ge_3O_{11}$, $PbGeO_3$, and $PbGe_3O_7$ as stable crystallines in the binary PbO-GeO_2 system. Phillips and Scroger (1965) asserted the constitution of a much different binary GeO_2-PbO phase diagram (Figure A.2) where they reported four stable lead germanate crystal phases which are Pb_4GeO_6, $Pb_3Ge_2O_7$, $PbGeO_3$, and $PbGe_4O_9$ crystalline phases at room temperature and $PbGe_2O_5$ phase is the one at temperature in the range between 700–740 ºC. On the other hand, Gouju et al. (1968) suggested that lead germanate binary phase system accommodates (Figure 2.6) four different stable crystalline phases which are Pb_3GeO_5, $Pb_3Ge_2O_7$, $PbGeO_3$, and

$PbGe_4O_9$. Bush and Venevtsev (1981) proposed three phase diagrams for the GeO_2-rich end of the GeO_2 – PbO binary system. In their stable phase diagram (Figure A.3), they obtained both α-$PbGeO_3$ and rutile-like GeO_2 phase after a prolonged high-temperature annealing. There is an eutectic point at 760 °C for 60 mol% GeO_2 in their phase diagram. On the other hand, Scavini et al. (2001) was suggested a metastable phase diagram for the GeO_2-rich end of the GeO_2 – PbO binary system. They conducted their study using X-ray and neutron diffraction technique. In their phase diagram, they obtained $PbGe_4O_9$ phase in the metastable condition. On the other hand, after prolong heat treatment (360 h), they observed that $PbGe_4O_9$ phase transform to $PbGe_3O_7$ phase and they claimed that this phase is thermodynamically stable. In addition to that, they reported the presence of polymorphs of $PbGe_4O_9$ phases in their study.

Study of Scavini et al., (2001) demonstrated that intensity of peaks of hexagonal GeO_2 decrease with increasing PbO content up to 20 mol% PbO in binary GeO_2 – PbO glass. In addition to that, increasing PbO content up to 20 mol% instigates the formation of both monoclinic and hexagonal $PbGe_4O_9$ phases and $PbGe_3O_7$ phase. Ratio of the $PbGe_4O_9$ / $PbGe_3O_7$ peak intensity decreases with PbO content while $PbGe_3O_7$ phase becomes major phase in glass-ceramic for 20 mol% PbO. Thus, both $PbGe_4O_9$ and $PbGe_3O_7$ phases co-exist in this composition range. On the other hand, their thermal study indicated that $PbGe_4O_9$ phase becomes metastable for 25 – 50 mol% PbO content and these crystalline phases are observed because of their tendency to crystallize. Unlike low PbO glass compositions (up to 20 mol%), long heat treatments effect phase composition significantly and transformation of $PbGe_4O_9$ phase into $PbGe_3O_7$ was observed. Formation of monoclinic $PbGeO_3$ (2θ = 30.5 and 33.1º) phase is observed besides these phases. Intensity peaks of $PbGeO_3$ increase with PbO content while intensity peaks of polymorphs of $PbGe_4O_9$ phase disappears (Scavini et al., 2001).

Bush and Stefanovish (2002) stated that lead tetragermanate ($PbGe_4O_9$) crystals can take an important place in development of pyroelectric applications. $PbGe_4O_9$ crystals can be found in four different morphologies which are α, β_1, β_2 and γ. Although γ-$PbGe_4O_9$ doesn't transform into other polymorphs of its kind in range of 20 – 800 °C, α, β_1 and β_2 phases can undergo reversible phase transformations

around 250 – 260 °C with sufficiently high activation energies (Bush and Stefanovich, 2002).

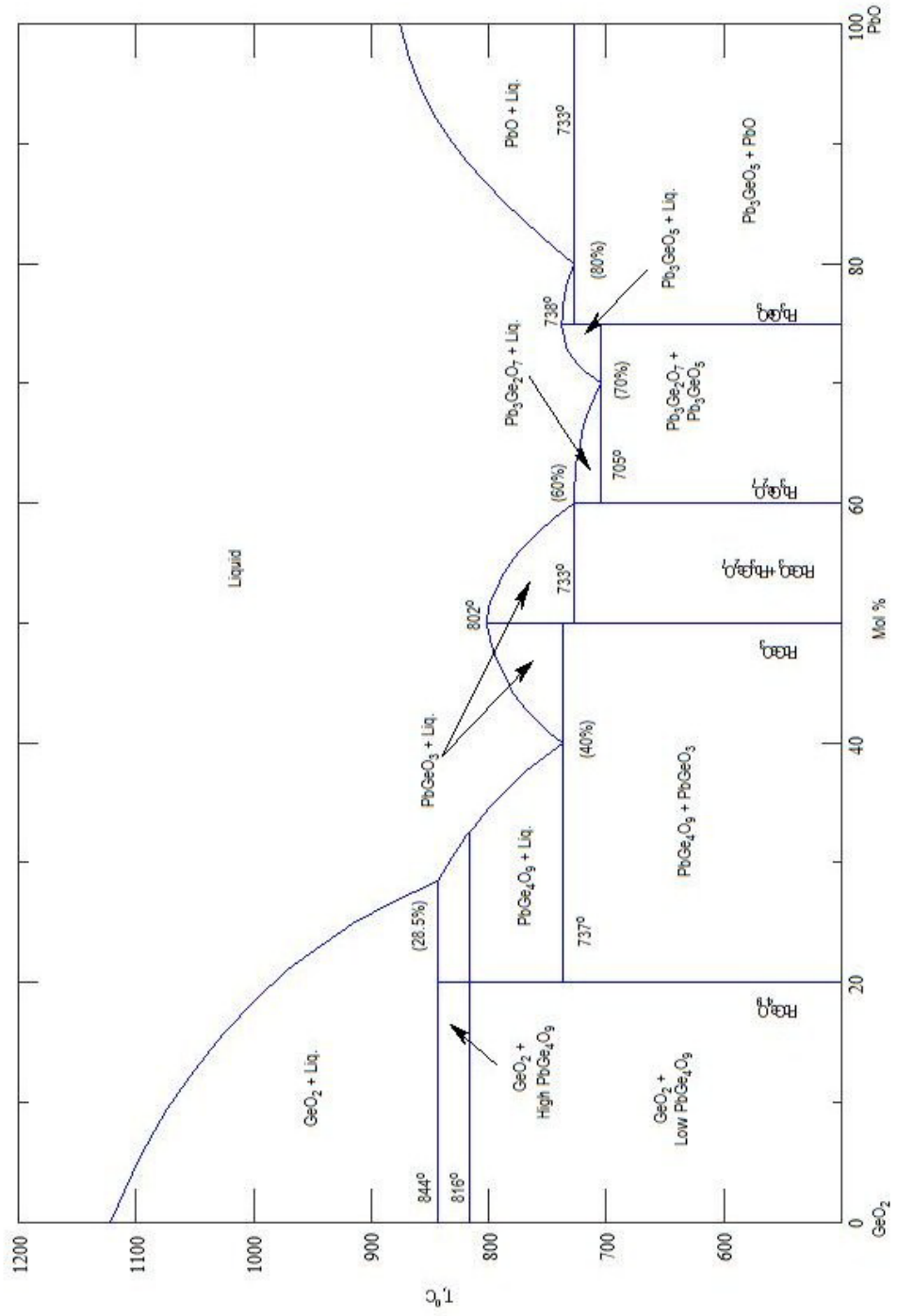

Figure 2.6 : System GeO_2-PbO (Gouju et al., 1968).

In normal conditions, α-$PbGe_4O_9$ crystals have trigonal structure with a space group of P321 and its lattice parameters in hexagonal setting are a = 11.420(2) A° and c =

4.753(1) A°. γ-$PbGe_4O_9$ crystals are formed in monoclinic system with a space group of C121 and its lattice parameters are a_m = 7.328(6) A°, b_m = 11.477(5) A°, c_m = 6.822(5) A° and β_m = 141.98(6)° (Bush and Stefanovich, 2002).

Structure of α-$PbGe_4O_9$ crystals are defined as coalition of tetrahedral and octahedral formation of germanium – oxygen. GeO_4 tetrahedra link at the corners and they form three-member rings of Ge_3O_9 perpendicular to c axis while GeO_6 octahedra bind these rings. Pb atoms accommodate in form of layers and they lay on broad conduits which spread along c axis. On the other hand, structure of γ-$PbGe_4O_9$ crystals are formed with only GeO_4 tetrahedra which coalesce as infinite $(Ge_3O_9)_\infty$ spirals and climb through c axis. α-$PbGe_4O_9$ and β_1-$PbGe_4O_9$ trigonal cell and β_2-$PbGe_4O_9$ pseudotrigonal structure distinct from each other with small atomic dislocations and assemblage on c axis (Bush and Stefanovich, 2002).

While α and γ-$PbGe_4O_9$ crystals are colorless and transparent, γ-$PbGe_4O_9$ crystals occur polysynthetic twins which allows them to distinguish from α-$PbGe_4O_9$. Thickness of these needle-like γ-$PbGe_4O_9$ crystallites can increase up to 100 μm (Bush and Stefanovich, 2002).

Gingha et al. (2002) reported that $PbGeO_3$ crystals which has monoclinic structure and isomorphous to $PbSiO_3$ alamosite structure (Tambelli et al., 2002) have three nonequivalent tetrahedral Ge units with twelve Ge-O bonds whose length change within range of 1.68 Å and 1.78 Å. The structure of crystalline also accommodates three nonequivalent Pb atoms and one of them resides at the top of a tetragonal (PbO_4) pyramid while other two locate at the top of a trigonal (PbO_3) pyramid. In addition to that, with heat treatments Raman studies (Tambelli et al., 2004) showed that the structure of $PbGeO_3$ is formed with twelve tetrahedral [GeO_4] units which is demonstrated as $(GeO_3)_n$ chains while each tetrahedral [GeO_4] unit has two bridging and non-bridging oxygen atoms.

2.6.2 Binary GeO_2 – PbF_2 glasses

GeO_2 – PbF_2 glasses have low melting temperatures and F^-/O^-_2 relation and Pb^{2+} amount affect their properties significantly. They are ideal for purpose of optical and laser glass designs (Ivanova, 1991). Recent years, rare earth doped oxyfluoride lead germanate glasses draw attention because of controlled crystallization of PbF_2 nanocrystalline phases (Klimesz et al., 2008).

3. EXPERIMENTAL PROCEDURE

In this study, the GeO_2 – PbF_2 and the GeO_2 – PbF_2 – Er_2O_3 binary glass systems were investigated because of limited investigations on the thermal and microstructural properties and compared with GeO_2 – PbO binary system and GeO_2 – PbF_2 – PbO glass systems.

3.1 Glass Synthesis

Nine different glass compositions (in moles) which are 0.9 GeO_2 – 0.1 PbF_2 , 0.8 GeO_2 – 0.2 PbF_2 , 0.7 GeO_2 – 0.3 PbF_2 , 0.895 GeO_2 – 0.1 PbF_2 – 0.005 Er_2O_3 , 0.795 GeO_2 – 0.2 PbF_2 – 0.005 Er_2O_3 , 0.695 GeO_2 – 0.3 PbF_2 – 0.005 Er_2O_3 , 0.88 GeO_2 – 0.1 PbF_2 – 0.02 Er_2O_3 , 0.78 GeO_2 – 0.1 PbF_2 – 0.02 Er_2O_3 , 0.68 GeO_2 – 0.1 PbF_2 – 0.02 Er_2O_3 were obtained by using high purity GeO_2 (99,99% purity, Aldrich), PbF_2 (99,5% purity, Aldrich) and Er_2O_3 (99,99% purity, Aldrich) powders. Mixtures are prepared by compensating molar weights of GeO_2 (104,609 gram/mole), PbF_2 (245,197 gram/mole) and Er_2O_3 (382,518 gram/mole). Powder batches of glass compositions which are given in Table 3.1 were weighted 4 grams using a Precisa^{TM} XB220A sensitive balance and grounded in an agate mortar for 5 minutes to have homogenous powders.

Table 3.1 : Weight amounts of the powders in this investigation

Compositions (mol)	GeO_2 (grams)	PbF_2 (grams)	Er_2O_3 (grams)
0.9 GeO_2 – 0.1 PbF_2	31.735	0.8264	0
0.8 GeO_2 – 0.2 PbF_2	25.220	14.779	0
0.7 GeO_2 – 0.3 PbF_2	19.954	20.045	0
0.895 GeO_2 – 0.1 PbF_2 – 0.005 Er_2O_3	31.193	0.8169	0.0637
0.795 GeO_2 – 0.2 PbF_2 – 0.005 Er_2O_3	24.804	14.626	0.0570
0.695 GeO_2 – 0.3 PbF_2 – 0.005 Er_2O_3	19.626	19.857	0.0516
0.88 GeO_2 – 0.1 PbF_2 – 0.02 Er_2O_3	29.641	0.7895	0.2463
0.78 GeO_2 – 0.2 PbF_2 – 0.02 Er_2O_3	23.602	14.185	0.2213
0.68 GeO_2 – 0.3 PbF_2 – 0.02 Er_2O_3	18.677	19.314	0.2009

Grounded powders were heated to 1100 °C with a heating rate of 10 °C/min in platinum crucible and kept for 20 minutes in an electrically heated furnace. Melted glassy samples in a platinum crucible were water-quenched immediately to prevent crystallization. Protherm™ furnace which was used for glass melting experiments and heat-treatment process is shown in Figure 3.1.

Figure 3.1 : Protherm™ furnace.

3.2 Thermal Characterizations

Non-isothermal differential thermal analysis (DTA) experiments were carried out for compositions of 10, 20, 30 mol% of PbF_2, 0.5 and 2 mol% of Er_2O_3 in a TA™ Q600 DTA/TGA/DSC which is shown in Figure 3.2. DTA scans were conducted by using 5-10 mg of as-cast samples with different heating rates of 5, 10, 15, 20 °C/min between 50 and 900 °C temperatures in a platinum crucible.

Figure 3.2 : TA™ Instruments Q600 DTA/TGA/DSC.

Glass transition temperatures (T_g), crystallization peak temperature (T_p) and melting temperatures (T_m) which are shown in Figure 3.3 were determined for different heating rates of 5, 10, 15 and 20 °C/min by using TA Instrument Universal Analysis Program™.

Changes on the exothermic and endothermic peaks were investigated through the thermal analysis results at different heating rates of 5, 10, 15 and 20 °C/min. As cast glass samples were heat-treated at above the crystallization peak temperatures which are measured from the DTA scans and quenched by dipping the platinum crucible in water immediately.

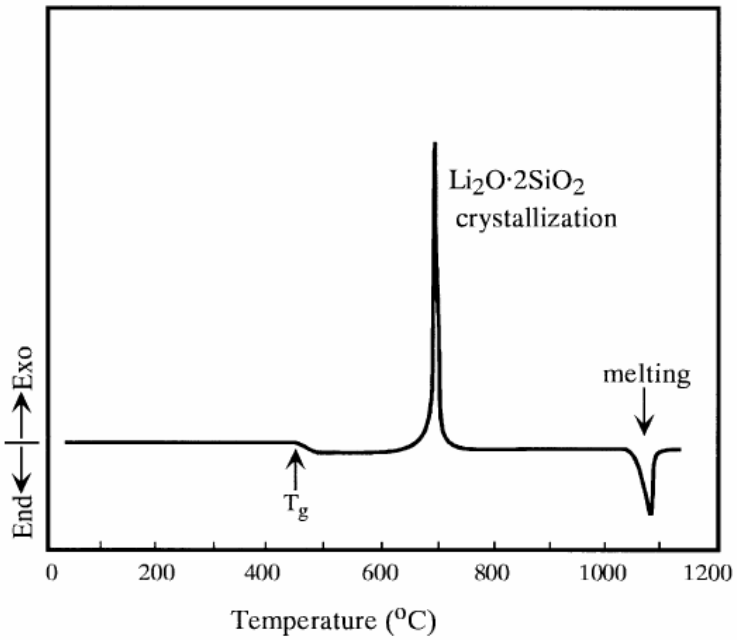

Figure 3.3 : DTA graph and characteristic temperatures of $Li_2O – SiO_2$ glass (Yamane and Asahara, 2000).

3.3 Microstructural Characterizations

3.3.1 X-ray diffraction (XRD) characterizations

In order to identify structural changes and phases in the microstructures of the annealed binary $GeO_2 – PbF_2$ glasses and $GeO_2 – PbF_2 – Er_2O_3$ glasses, X-ray diffraction (XRD) investigates were performed on the heat-treated glass samples. Glasses were annealed at certain temperatures obtained from DTA investigations followed by water quenching to freeze the structure at the heat-treated temperature.

This is followed by running XRD scans using a Bruker™ D8 Advanced Series powder diffractometer shown in Figure 3.4. All investigations were performed using Cu Kα radiation at 1.5406 Å wavelength and the diffractometer were set in the range of 2θ from 10° to 90° with a step size of 0.02.

Figure 3.4 : Bruker™ D8 Advanced Series powder diffractometer.

All samples were grounded to powder for XRD scans and Eva software® was selected for labeling intensity peaks and defining the crystalline phases which existed in the corresponding samples. The International Centre for Diffraction Data® (ICDD®) data files were used for identifying the crystalline phase of heat-treated glass samples by correlating the positions of the peaks and intensities.

3.3.1 Scanning electron microscope (SEM) characterizations

Scanning Electron Microscope (SEM) studies are performed on heat-treated samples in a JEOL™ JSM 5410 which is shown Figure 3.5 operated at 15kV and linked with Noran™ 2100 Freedom energy dispersive spectrometer (EDS) attachment. Samples were etched in %90 distilled water + %10 Hydrofluoric acid solution for 5 seconds and etched samples were coated with palladium-gold for the SEM and EDS operations.

Figure 3.5 : JEOL^{TM} JSM 5410 scanning electron microscope.

4. RESULTS AND DISCUSSION

4.1 0.90 GeO_2 – 0.10 PbF_2 Glass

As-cast 0.90 GeO_2 – 0.10 PbF_2 glass samples are shown in Figure 4.1. As seen in Figure 4.1, this glass shows transparency in visible light.

Figure 4.1 : As-cast 0.90 GeO_2 – 0.10 PbF_2 binary glass samples.

4.1.1 DTA investigations of the 0.90 GeO_2 – 0.10 PbF_2 glass

DTA curves for the as-cast 0.90 GeO_2 – 0.10 PbF_2 glass taken at different heating rates of 5, 10, 15, 20 °C/min are presented in Figure 4.2. DTA curves demonstrated that there are two exothermic peaks existed at each different heating rate and this might be a result of the formation of crystalline phases or transformation of phases. Subsequent to these two exothermic peaks, there are two endothermic peaks which correlate with melting temperatures of corresponding crystalline phases in the glass network. Characteristic temperatures and on-set crystallization temperatures (T_x) of the 0.90 GeO_2 – 0.10 PbF_2 glass are given in Table 4.1. Glass transition temperatures (T_g) for all different rates are almost constant at around 302±1 ºC while first and second crystallization peak temperatures (T_p) vary between 590±10 ºC and 640±10 ºC, respectively. Two melting temperatures (T_m) change within 831±1 ºC and 841±1 ºC, respectively.

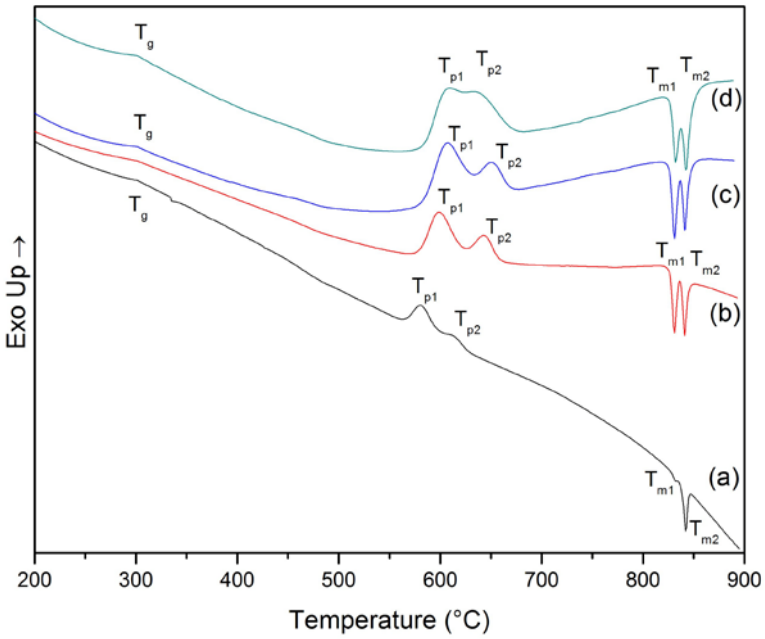

Figure 4.2 : DTA scans of the as-cast non-doped 0.90 GeO_2 – 0.10 PbF_2 glass with the heating rates of 5 (a),10 (b), 15 (c) and 20 (d) °C/min.

Although, glass transition temperatures were not affected by different heating rates, the crystallization peak temperatures were slightly shifted to the lower temperatures with decrement of the heating rates. Both exothermic and endothermic peaks decrease and second exothermic peaks start to deconvolute into two exothermic peaks when heating rates were decreased from 20 to 5 °C/min.

Table 4.1 : Characteristic temperatures of the 0.90 GeO_2 – 0.10 PbF_2 glass.

	0.90 GeO_2 – 0.10 PbF_2			
H.F.	5 °C/m	10 °C/m	15 °C/m	20 °C/m
T_g	301.89	302.17	301.82	302.29
T_x	279.31	296.66	305.61	307.29
T_{p1}	581.20	598.83	607.43	609.58
T_{p2}	614.15	642.60	650.58	633.29
T_{m1}	831.55	830.98	831.11	832.19
T_{m2}	842.34	841.23	841.42	842.52

Table 4.1 was used as reference for determining annealing temperatures of 0.90 GeO_2 – 0.10 PbF_2 glass sample for further investigations.

4.1.2 XRD analysis of the 0.90 GeO_2 – 0.10 PbF_2 glass

Figure 4.3 show XRD patterns of the 0.90 GeO_2 – 0.10 PbF_2 glass in the as-cast condition, and after annealing at 590 °C and 670 °C, respectively. In order to investigate crystalline phases of the 0.90 GeO_2 – 0.10 PbF_2 glass, specimens are

annealed at two different temperatures (590 °C and 670 °C) which are obtained from DTA results. When the glass is quenched right after the furnace annealed at 590 °C for 20 min with the heating rate of 10 °C/min, only the hexagonal α-GeO_2 crystalline phase exists in its microstructure.

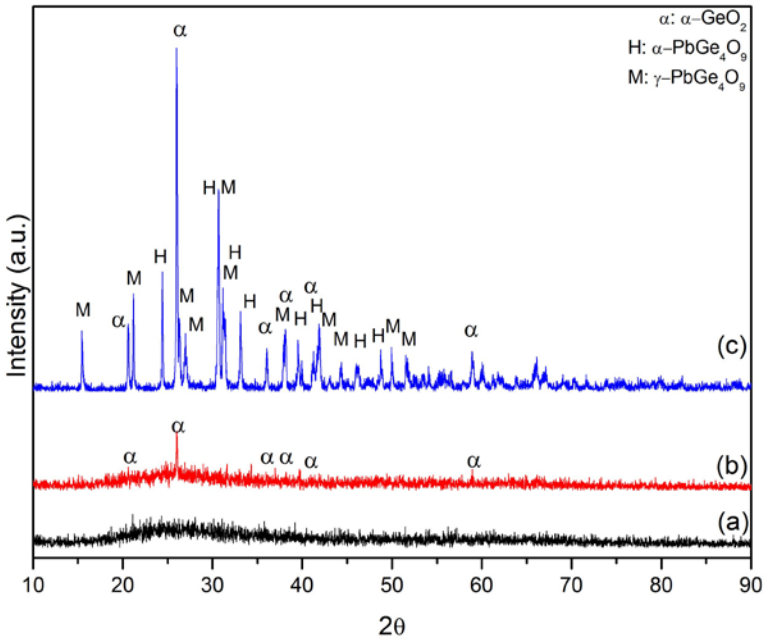

Figure 4.3 : XRD scans of the 0.90 GeO_2 – 0.10 PbF_2 non-doped glasses which are as-cast (a) and annealed at 590 °C (b) and 670 °C (c).

As seen in Figure 4.3, when the glass is annealed at 670 °C for 30 min with the heating rate of 10 °C/min, it has α-GeO_2 hexagonal α-$PbGe_4O_9$ and monoclinic γ-$PbGe_4O_9$ crystals in its structure. From these results, first exothermic peak in DTA results corresponds to the crystallization of the α-GeO_2, while second one is related with the formation of the $PbGe_4O_9$ polymorph. All of the crystals structures, lattice parameters, space groups and card numbers of the crystalline phases observed in the glasses are given in Table B.1.

4.1.3 SEM investigations of the 0.90 GeO_2 – 0.10 PbF_2 glass

In order to observe morphologically the crystalline phases which are identified in XRD investigations, SEM/SEI micrographs were taken from the surface of the non-doped 0.90 GeO_2 – 0.10 PbF_2 glass-ceramic samples which were annealed at 670 °C for 30 min with a heating rate of 10 °C/min and quenched in water afterwards. EDS measurements were taken from the crystalline regions.

Figures 4.4(a) – 4.4(d) are taken the SEM/SEI micrographs from the surface of the non-doped 0.90 GeO_2 – 0.10 PbF_2 glass-ceramic samples which were annealed at 670 °C for 30 min with a heating rate of 10 °C/min and quenched in water.

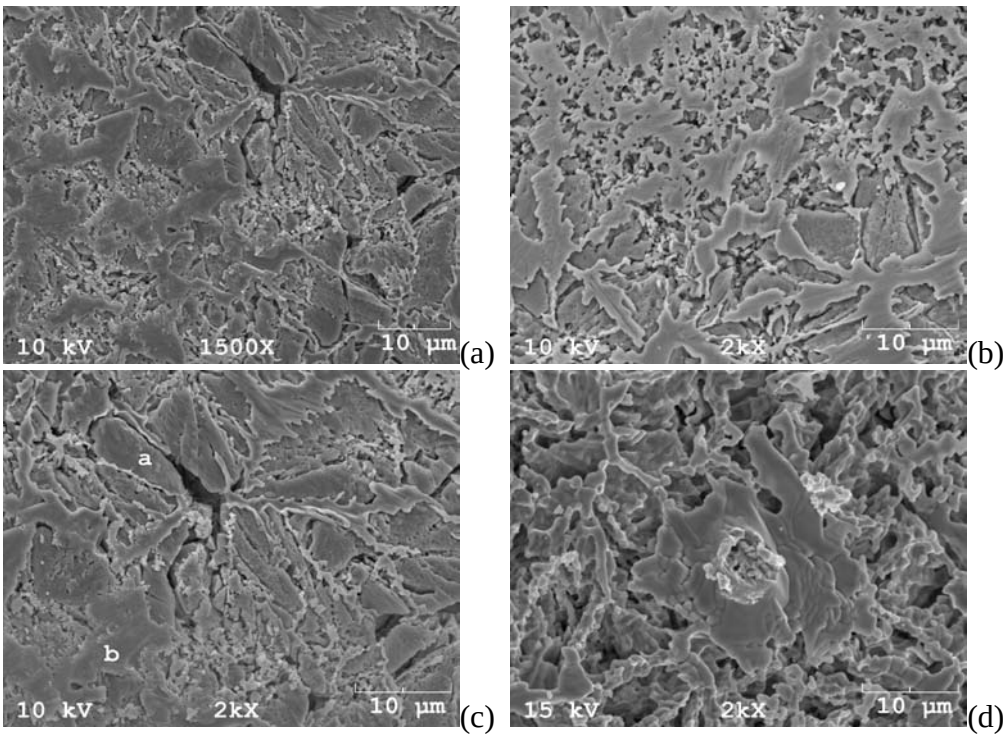

Figure 4.4 : SEM micrographs of the crystalline regions of the non-doped 0.90 GeO_2 –0.10 PbF_2 glass samples which was heat treated at 670 °C: (a) 1500x, (b) 2000x, (c) 2000x, (d) 2000x.

Formation of germanium rich crystals which cover the surface of the sample can be seen as dendrite-like structures on the surface in Figures 4.4(a) – 4.4(c). EDS were performed on the crystalline regions (a and b in Figure 4.4(c)) and revealed that (74.334 wt% Ge, 9.563 wt% Pb, 14.071 wt% O, 0.032 wt% F) the dendrite-like crystalline regions (labeled as a regions in Figure 4.4(c)) consist of α-GeO_2 crystals. The regions labeled as b in Figure 4.4(c) indicate glassy background (58.924 wt% Ge, 26.729 wt% Pb, 12.724 wt% O, 1.624 wt% F) of the glass-ceramic matrix. None of the polymorphs of $PbGe_4O_9$ crystals were observed in the SEM micrographs and their morphology could be covered by α-GeO_2 crystalline regions.

4.2 0.80 GeO_2 – 0.20 PbF_2 Glass

As-cast 0.80 GeO_2 – 0.20 PbF_2 glass samples are shown in Figure 4.5. As seen in Figure 4.5, this glass shows transparency in visible light.

Figure 4.5 : As-cast 0.80 GeO_2 – 0.20 PbF_2 binary glass samples.

4.2.1 DTA investigations of the 0.80 GeO_2 – 0.20 PbF_2 glass

DTA curves for the as cast 0.80 GeO_2 – 0.20 PbF_2 glass with different heating rates of 5, 10, 15, 20 °C/min are exhibited in Figure 4.6. As seen in Figure 4.6, glass transition temperature (T_g) remains constant when the heating rate is changed. Except for the heating rate of 5 °C/min, there exists one exothermic peak which shifts to higher temperatures with heating rates, as expected. A small second crystallization peak is observed before the main crystallization peak for the DTA curve at a scan rate of 5 °C/min. On the other hand, samples which are heated with 5, 10, 15 °C/min has only two endothermic peak while presence of another endothermic peak is observed for heating rate of 20 °C/min.

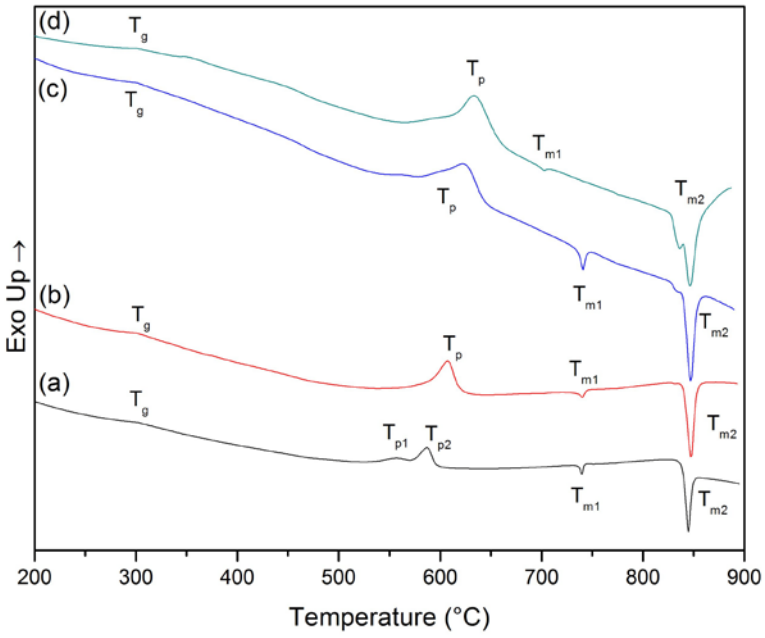

Figure 4.6 : DTA scans of the as-cast non-doped 0.80 GeO_2 – 0.20 PbF_2 glass with the heating rates of 5 (a),10 (b), 15 (c) and 20 (d) °C/min.

Characteristic temperatures and on-set crystallization temperatures (T_x) of the DTA curves of the 0.80 GeO_2 – 0.20 PbF_2 glass are given in Table 4.2. Glass transition

temperatures (T_g) lay at 302±1 ºC while first and second crystallization peak temperatures (T_p) exist at 556 ºC and 610±25 ºC, respectively. Two melting temperatures (T_m) change within 740±1 ºC and 846±1 ºC, respectively.

Table 4.2 : Characteristic temperatures of the 0.80 GeO_2 – 0.20 PbF_2 glass.

	0.80 GeO_2 – 0.20 PbF_2			
H.F.	5 °C/m	10 °C/m	15 °C/m	20 °C/m
T_g	301.75	302.10	301.68	301.63
T_x	254.6	305.27	320.33	331.65
T_{p1}	556.35	-	-	-
T_{p2}	586.12	607.37	622.01	633.28
T_{m1}	739.62	740.29	740.92	740.94
T_{m2}	844.89	847.42	847.09	846.45

Table 4.2 was used as reference for determining annealing temperatures of 0.80 GeO_2 – 0.20 PbF_2 glass sample for further investigations

4.2.2 XRD analysis of the 0.80 GeO_2 – 0.20 PbF_2 glass

Binary GeO_2 – PbF_2 glass containing 20 mol% PbF_2 demonstrates amorphous structure in the as-cast condition as seem in Figure 4.7(a).

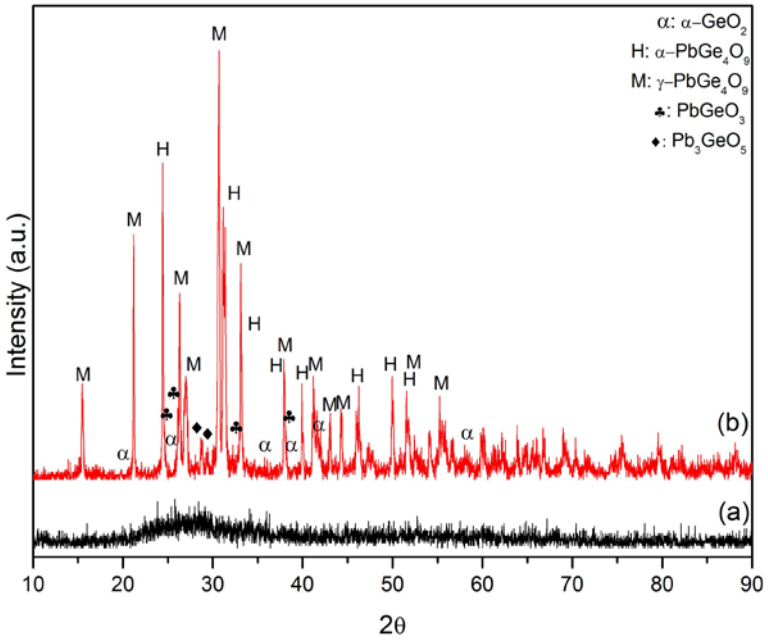

Figure 4.7 : XRD scans of the 0.80 GeO_2 – 0.20 PbF_2 non-doped glasses which are as-cast (a) and annealed at 630 °C (b).

In order to investigate crystalline phases of 0.80 GeO_2 – 0.20 PbF_2 glass, specimens are annealed at 630 °C which is beyond the peak crystallization temperatures of the DTA curves (Figure 4.6). The glass which was heat treated at 630 °C for 30 min with

the heating rate of 10 °C/min demonstrates both α-$PbGe_4O_9$ and γ-$PbGe_4O_9$ crystals with the addition of very small amount of α-GeO_2, monoclinic α-$PbGeO_3$ and Pb_3GeO_5 phases in its structure. The structures of the crystals, lattice parameters, space groups and card numbers of the crystalline phases observed in the glasses are given in Table B.1.

4.2.3 SEM investigations of the 0.80 GeO_2 – 0.20 PbF_2 glass

In order to examine the microstructural features of the crystalline phases observed in the XRD investigations, SEM/SEI were conducted. SEM/SEI micrographs were taken from the surface of the non-doped 0.80 GeO_2 – 0.20 PbF_2 glass-ceramic samples which were annealed at 630 °C for 30 min with a heating rate of 10 °C/min and quenched in water afterwards. EDS measurements were taken from the crystalline regions.

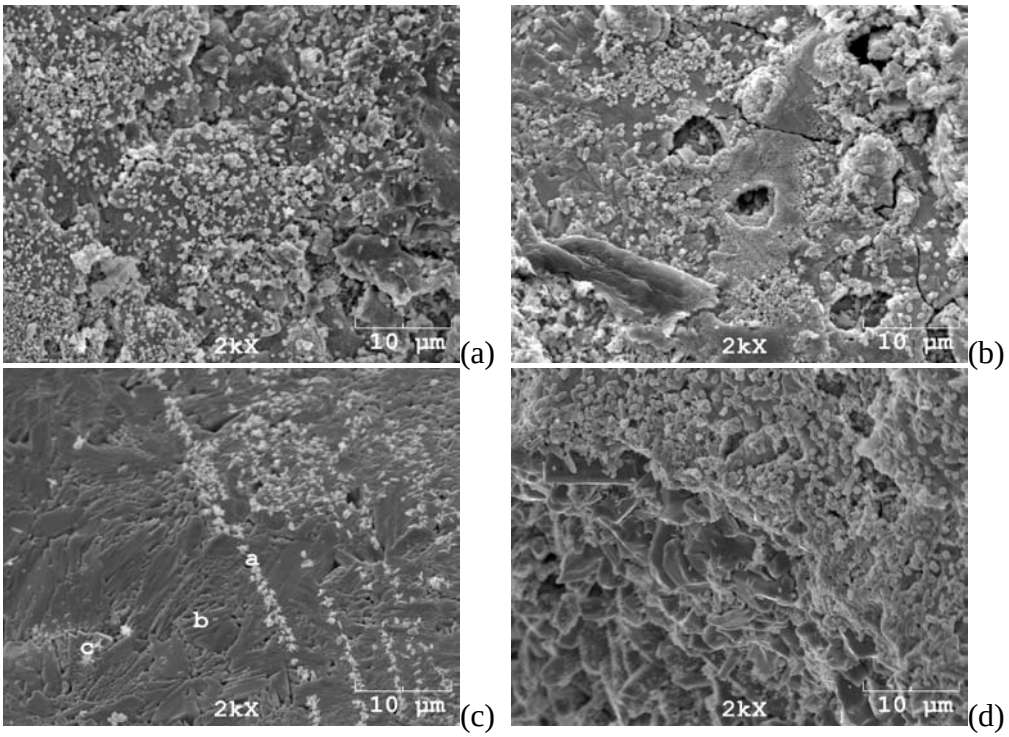

Figure 4.8 : SEM micrographs of the crystalline regions of the non-doped 0.80 GeO_2 –0.20 PbF_2 glass samples which was heat treated at 630 °C: (a) 2000x, (b) 2000x, (c) 2000x, (d) 2000x, (e) 3500x, (f) 3500x, (g) 5000x.

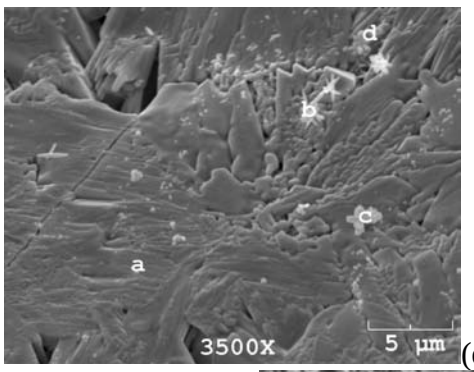

(e)

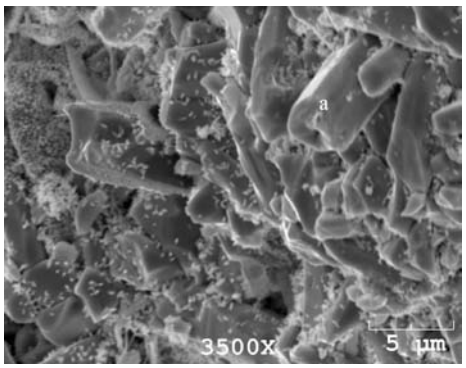

(f)

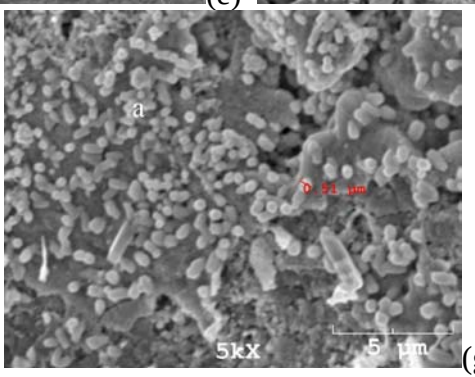

(g)

Figure 4.8 : (continued) SEM micrographs of the crystalline regions of the non-doped 0.80 GeO_2 –0.20 PbF_2 glass samples which was heat treated at 630 °C: (a) 2000x, (b) 2000x, (c) 2000x, (d) 2000x, (e) 3500x, (f) 3500x, (g) 5000x.

Figures 4.8(a) – 4.8(g) are SEM/SEI micrographs taken from surface and the cross-sectional area of the non-doped 0.80 GeO_2 – 0.20 PbF_2 glass-ceramic samples which were annealed at 630 °C for 30 min with a heating rate of 10 °C/min and quenched in water. Formation of germanium rich crystals which mainly reside at cross-sectional area of the sample can be seen as blocky-like structures in Figure 4.8(f). In addition to these structures, formation of lead and germanium rich crystals is also observed as columnar–ball like crystals at the surface of the sample in Figure 4.8(g). EDS analyses were performed on the crystalline regions (a in Figure 4.8(f) and a in Figure 4.8(g)) and showed that (41.151 wt% Ge, 40.684 wt% Pb, 17.377 wt% O, 0.788 wt% F) the blocky-like crystalline regions (labeled as a in Figure 4.8(f)) are a polymorph of $PbGe_4O_9$ crystals. The columnar–ball crystalline regions (labeled as a in Figure 4.8(g)) indicate that (24.479 wt% Ge, 69.926 wt% Pb, 2.511 wt% O, 3.083 wt% F) these structures consist of $PbGeO_3$ crystals.

4.3 0.70 GeO_2 – 0.30 PbF_2 Glass

As-cast 0.70 GeO_2 – 0.30 PbF_2 glass samples are shown in Figure 4.9. As seen in Figure 4.9, this glass shows transparency in visible light.

Figure 4.9 : As-cast 0.70 GeO_2 – 0.30 PbF_2 binary glass samples.

4.3.1 DTA investigations of the 0.70 GeO_2 – 0.30 PbF_2 glass

DTA curves for the as cast 0.70 GeO_2 – 0.30 PbF_2 glass taken at different heating rates of 5, 10, 15, 20 °C/min are presented in Figure 4.10. As seen in Figure 4.10, glass transition temperature (T_g) remains constant when the heating rate is changed like 0.90 GeO_2 – 0.10 PbF_2 and 0.80 GeO_2 – 0.20 PbF_2 glasses. Two exothermic peaks exist which shift to higher temperatures with increasing heating rates, as in 0.90 GeO_2 – 0.10 PbF_2 glass. However, exothermic peaks do not shift to higher temperature with increasing the heating rate.

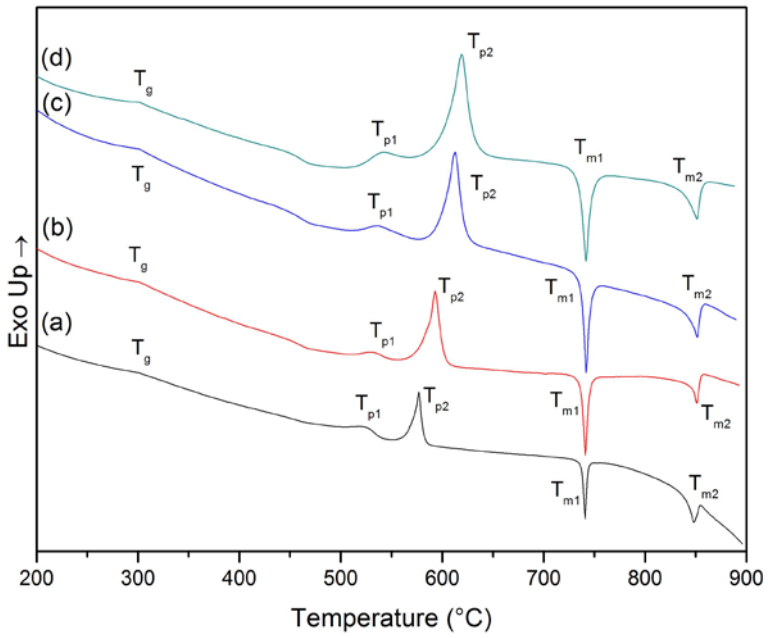

Figure 4.10 : DTA scans of the as-cast non-doped 0.70 GeO_2 – 0.30 PbF_2 glass with the heating rates of 5 (a),10 (b), 15 (c) and 20 (d) °C/min.

Characteristic temperatures and on-set crystallization temperatures (T_x) are given in Table 4.3. Glass transition temperatures (T_g) lay at 301±1 ºC while first and second crystallization peak temperatures (T_p) exist at 530±15 ºC and 600±25 ºC, respectively. Two melting temperatures (T_m) change within 741±1 ºC and 850±2 ºC, respectively. This type of thermal behavior on crystallization peak temperatures with increment of the heating rates was expected (Kissinger, 1956).

Table 4.3 : Characteristic temperatures of the 0.70 GeO_2 – 0.30 PbF_2 glass.

	0.70 GeO_2 – 0.30 PbF_2			
H.F.	5 °C/m	10 °C/m	15 °C/m	20 °C/m
T_g	301.62	301.70	301.66	301.78
T_x	216.19	229.86	235.06	238.98
T_{p1}	517.81	531.56	536.72	540.76
T_{p2}	577.06	592.98	612.58	619.21
T_{m1}	740.97	741.31	741.97	741.83
T_{m2}	848.17	850.75	851.41	851.22

Table 4.3 was used as reference for determining annealing temperatures of 0.70 GeO_2 – 0.30 PbF_2 glass for further investigations

4.3.2 XRD analysis of the 0.70 GeO_2 – 0.30 PbF_2 glass

Binary GeO_2 – PbF_2 glass containing 30 mol% PbF_2 demonstrates amorphous structure in the as-cast condition as seem in Figure 4.11(a).

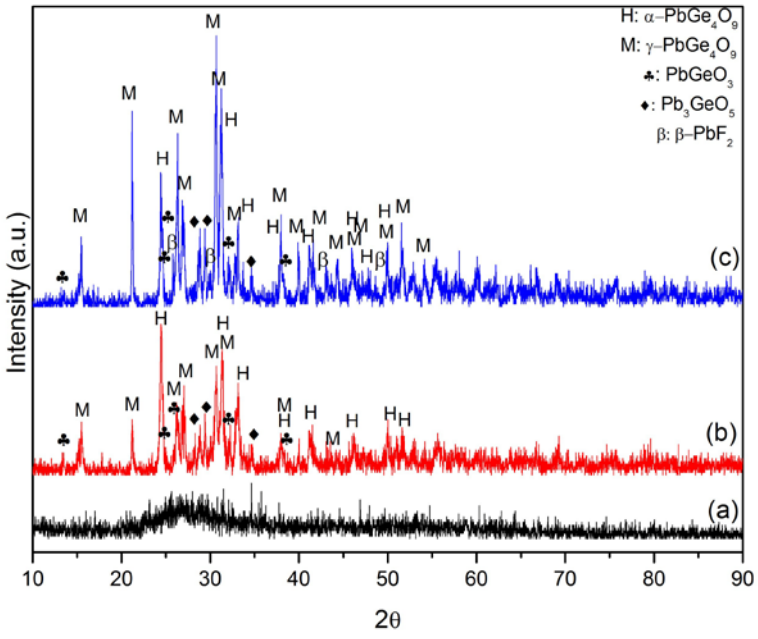

Figure 4.11 : XRD scans of the 0.70 GeO_2 – 0.30 PbF_2 non-doped glasses which are as-cast (a) and annealed at 530 °C (b) and 620 °C (c).

In order to investigate crystalline phases of the 0.70 GeO_2 – 0.30 PbF_2 glass, specimens are annealed at two different temperatures (530 °C and 620 °C) which are obtained from DTA results. As the glass heat treated at 530 °C for 20 min with the heating rate of 10 °C/min, it demonstrates α-$PbGe_4O_9$, γ-$PbGe_4O_9$ and Pb_3GeO_5 crystals with the addition of very small amount of α-GeO_2 phase and some cubic β-PbF_2 crystals in its structure. As a further step, when the glass was heat treated at 620 °C for 30 min, the same crystalline phases were observed but the intensity peaks of γ-$PbGe_4O_9$ and Pb_3GeO_5 crystals increased referring to the increment of these phases in the glass-ceramic. The structures of the crystals, lattice parameters, space groups and card numbers of the crystalline phases observed in the glasses are given in Table B.1.

4.3.3 SEM investigations of the 0.70 GeO_2 – 0.30 PbF_2 glass

In order to observe morphologically the identified in XRD investigations, SEM/SEI micrographs were taken from the surface of the non-doped 0.70 GeO_2 – 0.30 PbF_2 glass-ceramic samples which were annealed at 620 °C for 30 min with a heating rate of 10 °C/min and quenched in water afterwards. EDS measurements were taken from the crystalline regions.

Figures 4.12(a) – 4.12(m) are the SEM/SEI micrographs taken from the surface of the non-doped 0.70GeO_2 – 0.30PbF_2 glass-ceramic samples which were annealed at 620 °C for 30 min with a heating rate of 10 °C/min and quenched in water.

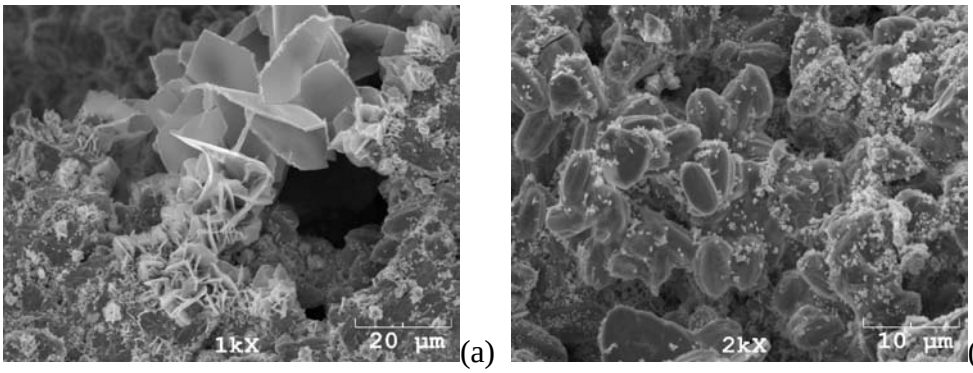

(a) (b)

Figure 4.12 : SEM micrographs of the crystalline regions of the non-doped 0.7GeO_2 –0.3PbF_2 glass samples which was heat treated at 620 °C: (a) 1000x, (b) 2000x, (c) 2000x, (d) 2000x, (e) 3500x, (f) 3500x, (g) 3500x, (h) 5000x, (i) 5000x, (j) 5000x, (k) 10000x, (l) 10000x, (m) 15000x.

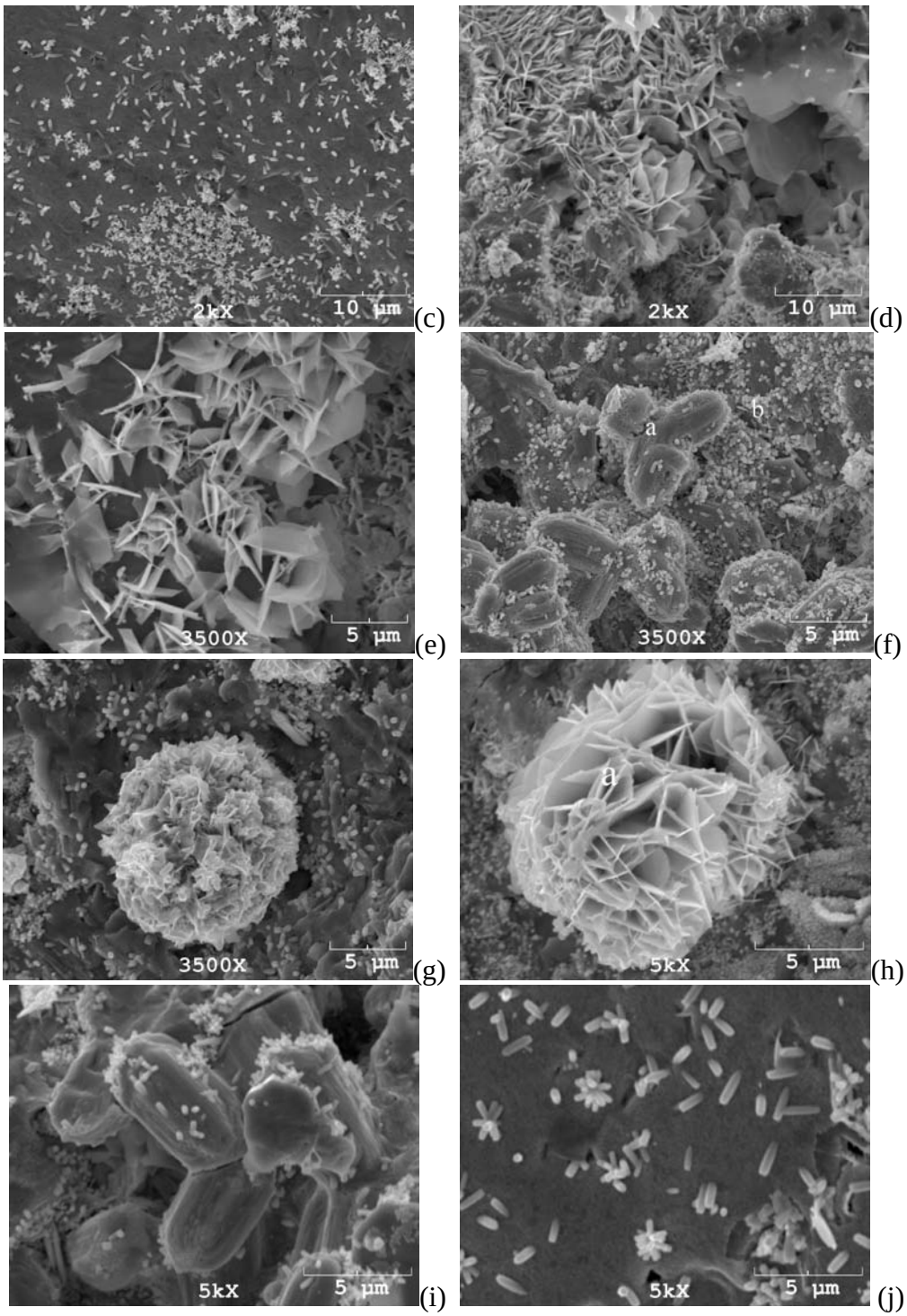

Figure 4.12 : (continued) SEM micrographs of the crystalline regions of the non-doped $0.7GeO_2$ –$0.3PbF_2$ glass samples which was heat treated at 620 °C: (a) 1000x, (b) 2000x, (c) 2000x, (d) 2000x, (e) 3500x, (f) 3500x, (g) 3500x, (h) 5000x, (i) 5000x, (j) 5000x, (k) 10000x, (l) 10000x, (m) 15000x.

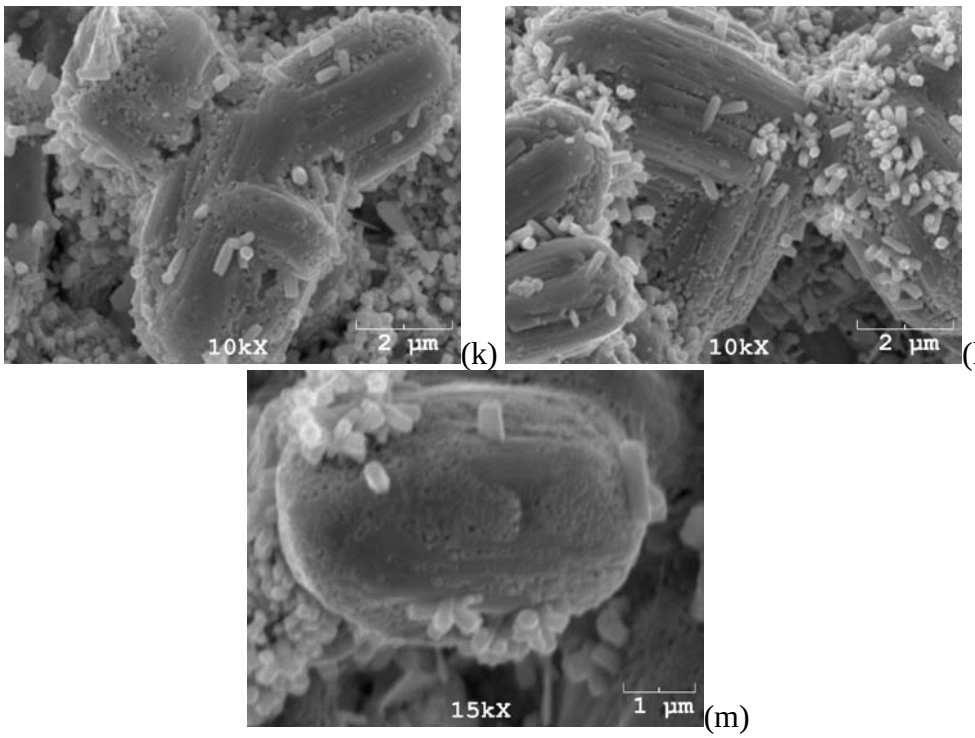

Figure 4.12 : (continued) SEM micrographs of the crystalline regions of the non-doped $0.7GeO_2$ –$0.3PbF_2$ glass samples which was heat treated at 620 °C: (a) 1000x, (b) 2000x, (c) 2000x, (d) 2000x, (e) 3500x, (f) 3500x, (g) 3500x, (h) 5000x, (i) 5000x, (j) 5000x, (k) 10000x, (l) 10000x, (m) 15000x.

Formation of Ge-rich crystals can be seen as nodular structures at the surface of the glass sample in Figures 4.12(f) and 4.12(i). In addition to these structures, formation of Pb-rich crystals is identified as in the shapes of foliated structures at the surface of the sample in Figures 4.12(g) and 4.12(h). Formation of Ge-Pb-rich crystals is also observed as columnar–ball like crystals in Figures 4.12(c) and 4.12(j) like at the non-doped 0.80 GeO_2 – 0.20 PbF_2 glass-ceramic sample. EDS analyses were performed on the crystalline regions (a and b in Figure 4.8(f) and a in Figure 4.12(h)) and showed that (48.801 wt% Ge, 50.034 wt% Pb, 4.237 wt% O, 0.706 wt% F) the nodular structures (labeled as a in Figure 4.12(f)) are a polymorph of $PbGe_4O_9$ crystals. The columnar–ball crystalline regions (labeled as b in Figure 4.12(f)) indicate that (24.479 wt% Ge, 69.926 wt% Pb, 2.511 wt% O, 3.083 wt% F) these structures consist of $PbGeO_3$ crystals as it mentioned in the non-doped $0.80GeO_2$ – $0.20PbF_2$ sample (24.479 wt% Ge, 69.926 wt% Pb, 2.511 wt% O, 3.083 wt% F). The foliated structures (labeled as a in Figure 4.12(h)) are indicated that (12.952 wt% Ge, 79.635 wt% Pb, 2.223 wt% O, 4.210 wt% F) these crystalline regions related to Pb_3GeO_5 crystals.

4.4 0.895 GeO_2 – 0.10 PbF_2 – 0.005 Er_2O_3 Glass

As-cast 0.895 GeO_2 – 0.10 PbF_2 – 0.005 Er_2O_3 glass samples are shown in Figure 4.13. As seen in Figure 4.13, this glass shows transparency in visible light.

Figure 4.13 : As-cast 0.895 GeO_2 – 0.10 PbF_2 – 0.005 Er_2O_3 glass samples.

4.4.1 DTA investigations of the 0.895 GeO_2 – 0.10 PbF_2 – 0.005 Er_2O_3 glass

DTA curve for the as cast 0.895 GeO_2 – 0.10 PbF_2 – 0.005 Er_2O_3 glass with the heating rate of 10 °C/min is presented in Figure 4.14.

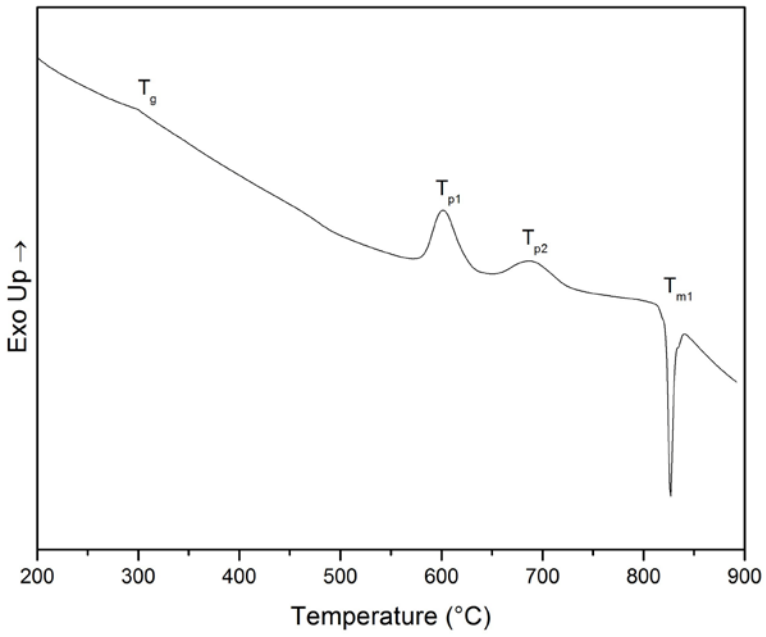

Figure 4.14 : DTA scan of the as-cast doped 0.895 GeO_2 – 0.10 PbF_2 – 0.005 Er_2O_3 glass with the heating rate of 10 °C/min.

It is showed that two exothermic peaks are present for the heating rate of 10 °C/min and it means that thermally treated 0.895 GeO_2 – 0.10 PbF_2 – 0.005 Er_2O_3 glass accommodates at least two crystallized phases. After exothermic peaks, a sharp endothermic peak follows which demonstrates the melting of the crystalline phases in glass-ceramic.

Characteristic temperatures and on-set crystallization temperatures (T_x) are given in Table 4.4. Glass transition temperature (T_g) lays at 302 ºC while first and second crystallization peak temperatures (T_p) exist at 601 ºC and 686 ºC, respectively. The melting temperature (T_m) present at 827 °C.

Table 4.4 : Characteristic temperatures of the 0.895 GeO_2 – 0.10 PbF_2 – 0.005 Er_2O_3 glass.

	0.895 GeO_2 – 0.10 PbF_2 – 0.005 Er_2O_3				
T (°C)	T_g	T_x	T_{p1}	T_{p2}	T_m
10 °C/min	302.03	299.34	601.4	686.2	826.69

Table 4.4 was used as reference for determining annealing temperatures of 0.895 GeO_2 – 0.10 PbF_2 – 0.005 Er_2O_3 glass sample for further investigations.

4.4.2 XRD analysis of the 0.895 GeO_2 – 0.10 PbF_2 – 0.005 Er_2O_3 glass

Binary GeO_2 – PbF_2 glass doped with 0.5 mol% Er_2O_3 containing 10 mol% PbF_2 demonstrates amorphous structure in the as-cast condition as seem in Figure 4.14(a).

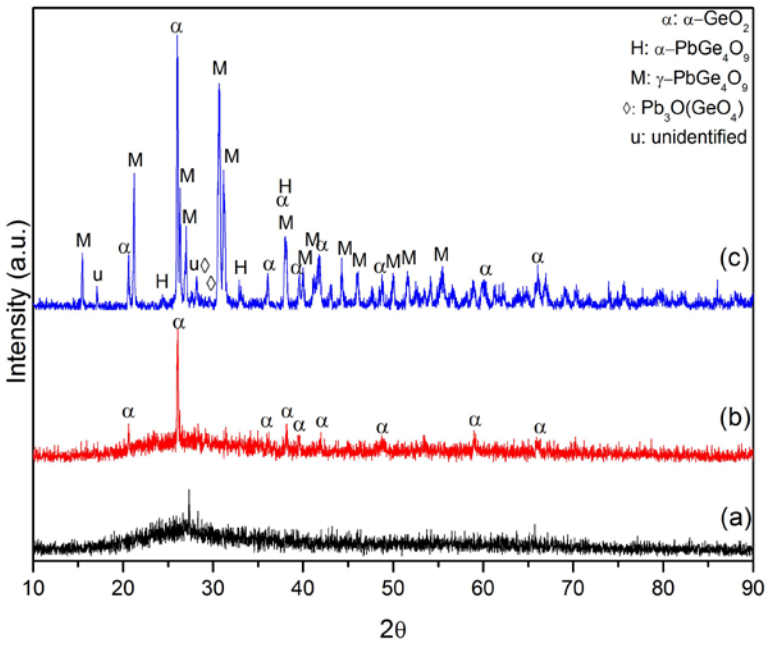

Figure 4.15 : XRD scans of the 0.895 GeO_2 – 0.10 PbF_2 – 0.005 Er_2O_3 glasses which are as-cast (a) and annealed at 630 °C (b) and 725 °C (c).

In order to investigate crystalline phases of 0.895 GeO_2 – 0.10 PbF_2 – 0.005 Er_2O_3 glass, specimens are annealed at two different temperatures (630 °C and 725 °C) which are obtained from DTA investigations. As seen in Figure 4.15(b), when the glass is quenched right after the furnace is annealed at 630 °C for 20 min with the

heating rate of 10 °C/min, only the α-GeO_2 crystalline phase is present in the microstructure. On the other hand, when the same glass is heat treated at 725 °C for 30 min, α-GeO_2 and monoclinic γ-$PbGe_4O_9$ are revealed in the microstructure (Figure 4.15(c)). In addition to these phases, hexagonal α-$PbGe_4O_9$, $Pb_3O(GeO_4)$ (Otto, 1979) and an unidentified phase (2θ = 17.1, 28.2, 33) in its structure. From these results, first exothermic peak in DTA results can be related with crystallization of α-GeO_2, while the second one corresponds to the formation of $PbGe_4O_9$ polymorphs, mainly the γ-$PbGe_4O_9$. The structures of the crystals, lattice parameters, space groups and card numbers of the crystalline phases observed in the glasses are given in Table B.1.

4.4.3 SEM investigations of the 0.895 GeO_2 – 0.10 PbF_2 – 0.005 Er_2O_3 glass

In order to observe morphologically the identified in XRD investigations, SEM/SEI micrographs were taken from the surface of the doped 0.895 GeO_2 – 0.10 PbF_2 – 0.005 Er_2O_3 glass-ceramic samples which were annealed at 725 °C for 30 min with a heating rate of 10 °C/min and quenched in water afterwards. EDS measurements were taken from the crystalline regions.

Figures 4.16(a) – 4.16(e) are the SEM/SEI micrographs taken from the surface of the doped 0.895GeO_2 – 0.10PbF_2 – 0.005 Er_2O_3 glass-ceramic samples which were annealed at 725 °C for 30 min with a heating rate of 10 °C/min and quenched in water.

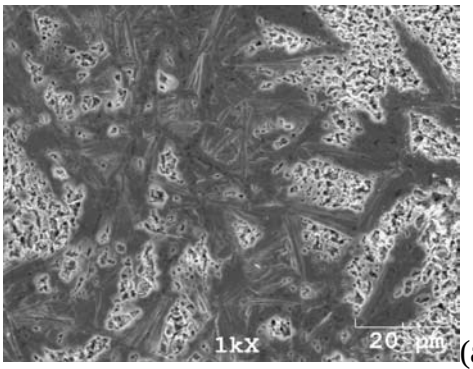

(a)
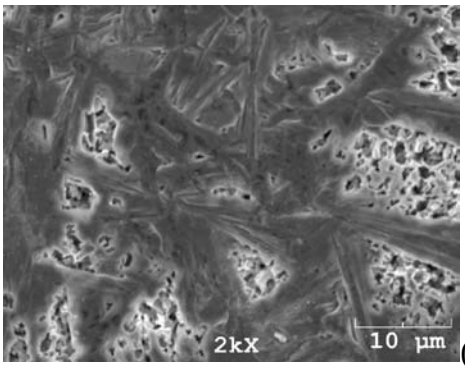

(b)

Figure 4.16 : SEM micrographs of the crystalline regions of the non-doped 0.895 GeO_2 – 0.1 PbF_2 – 0.005 Er_2O_3 glass samples which was heat treated at 725 °C: (a) 1000x, (b) 2000x, (c) 2000x, (d) 2000x, (e) 3500x.

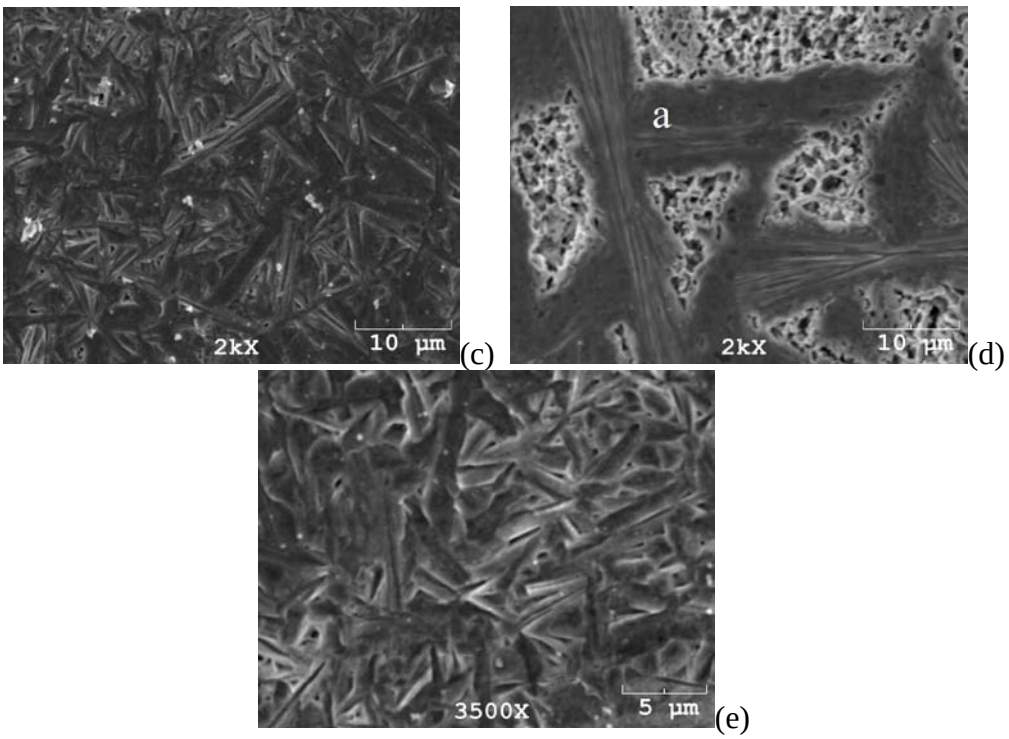

Figure 4.16 : (continued) SEM micrographs of the crystalline regions of the non-doped 0.895 GeO_2 – 0.1 PbF_2 – 0.005 Er_2O_3 glass samples which was heat treated at 725 °C: (a) 1000x, (b) 2000x, (c) 2000x, (d) 2000x, (e) 3500x.

Formation of Ge-rich crystals can be seen as blocky-like structures at the surface of the glass sample in Figures 4.16(c) and 4.16(d). EDS analyses were performed on the crystalline regions (a in Figure 4.16(d)) and showed that (49.841 wt% Ge, 26.669 wt% Pb, 21.102 wt% O, 0.000 wt% F and 4.041 wt% Er) the blocky-like structures (labeled as a in Figure 4.16(d)) are a polymorph of $PbGe_4O_9$ crystals.

4.5 0.795 GeO_2 – 0.20 PbF_2 – 0.005 Er_2O_3 Glass

As-cast 0.795 GeO_2 – 0.20 PbF_2 – 0.005 Er_2O_3 glass samples are shown in Figure 4.17. As seen in Figure 4.17, this glass shows transparency in visible light.

Figure 4.17 : As-cast 0.795 GeO_2 – 0.20 PbF_2 – 0.005 Er_2O_3 glass samples.

4.4.1 DTA investigations of the 0.795 GeO_2 – 0.20 PbF_2 – 0.005 Er_2O_3 glass

DTA curve for the as cast 0.795 GeO_2 – 0.20 PbF_2 – 0.005 Er_2O_3 glass with the heating rate of 10 °C/min is presented in Figure 4.18.

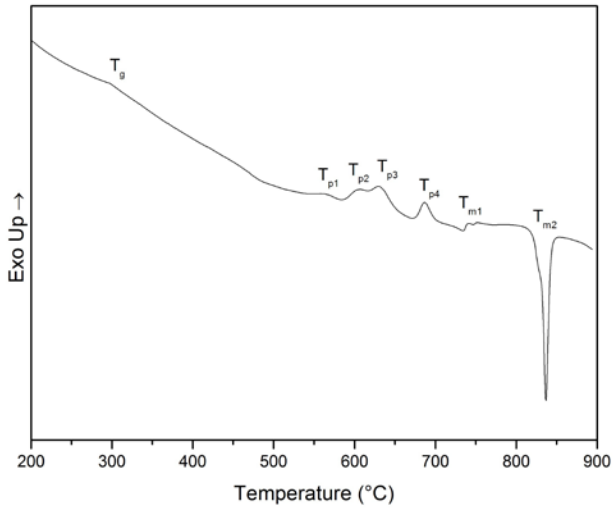

Figure 4.18 : DTA scan of the as-cast doped 0.795 GeO_2 – 0.20 PbF_2 – 0.005 Er_2O_3 glass with the heating rate of 10 °C/min.

It is showed that four exothermic peaks are present for the heating rate of 10 °C/min and it means that thermally treated 0.795 GeO_2 – 0.20 PbF_2 – 0.005 Er_2O_3 glass has at least four different crystalline phases. After exothermic peaks, a small and then a sharp endothermic peak follow which demonstrate the melting of the crystalline phases in the glass-ceramic.

Characteristic temperatures and on-set crystallization temperatures (T_x) are given in Table 4.5. Glass transition temperature (T_g) lays at 300 ºC while four crystallization peak temperatures (T_p) exist at 564 ºC, 607 ºC, 632 ºC and 687 ºC, respectively. Two melting temperatures (T_m) present at 735 ºC and 836 °C, respectively.

Table 4.5 : Characteristic temperatures of the 0.795 GeO_2 – 0.20 PbF_2 – 0.005 Er_2O_3 glass

	0.795 GeO_2 – 0.20 PbF_2 – 0.005 Er_2O_3							
T (°C)	T_g	T_x	T_{p1}	T_{p2}	T_{p3}	T_{p4}	T_{m1}	T_{m2}
10 °C/min	300.49	263.51	564.00	606.95	632.17	686.69	734.59	836.55

Table 4.5 was used as reference for determining annealing temperatures of 0.795 GeO_2 – 0.20 PbF_2 – 0.005 Er_2O_3 glass sample for further investigations.

4.4.2 XRD analysis of the 0.795 GeO_2 – 0.20 PbF_2 – 0.005 Er_2O_3 glass

Binary GeO_2 – PbF_2 glass doped with 0.5 mol% Er_2O_3 containing 20 mol% PbF_2 demonstrates amorphous structure in the as-cast condition as seem given in Figure 4.19(a).

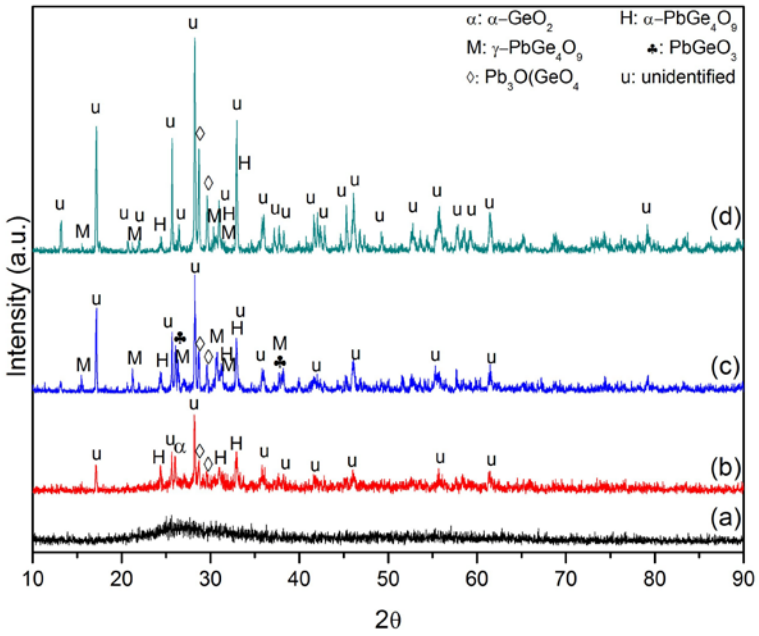

Figure 4.19 : XRD scans of the 0.795 GeO_2 – 0.20 PbF_2 – 0.005 Er_2O_3 glasses which are as-cast (a) and annealed at 600 °C (b), 645 °C (c) and 700 °C (d).

In order to investigate crystalline phases of 0.795 GeO_2 – 0.20 PbF_2 – 0.005 Er_2O_3 glass, specimens are annealed at three different temperatures (600 °C, 645 °C and 700 °C) which are obtained from DTA investigations. As seen in Figure 4.19(b), when the glass is annealed at 600 °C for 1 min with the heating rate of 10 °C/min, α-GeO_2, hexagonal α-$PbGe_4O_9$ crystal, an unidentified phase (2θ = 17.1, 28.2, 33) and little amounts of $Pb_3O(GeO_4)$ are present in the microstructure. When glass is annealed at 645 °C for 20 min with the heating rate of 10 °C/min, α-GeO_2, both monoclinic γ-$PbGe_4O_9$ and α-$PbGe_4O_9$ crystals, an unidentified phase and $Pb_3O(GeO_4)$ are present in the microstructure (Figure 4.19(c)). When glass is heated at 700 °C for 30 min with the heating rate of 10 °C/min, both γ-$PbGe_4O_9$ and α-$PbGe_4O_9$ crystals, an unidentified phase and $Pb_3O(GeO_4)$ are present in the microstructure while α-GeO_2 crystalline phases couldn't be observed for heat-treatment at 700 °C (Figure 4.19(d)). The structures of the crystals, lattice

parameters, space groups and card numbers of the crystalline phases observed in the glasses are given in Table B.1.

4.4.3 SEM investigations of the 0.795 GeO_2 – 0.20 PbF_2 – 0.005 Er_2O_3 glass

In order to examine the microstructural features in the XRD investigations, SEM/SEI were conducted. SEM/SEI micrographs were taken from the surface of the doped 0.795 GeO_2 – 0.20 PbF_2 – 0.005 Er_2O_3 glass-ceramic samples which were annealed at 700 °C for 30 min with a heating rate of 10 °C/min and quenched in water afterwards. EDS measurements were taken from the crystalline regions.

Figures 4.20(a) – 4.16(h) are the SEM/SEI micrographs taken from the surface of the doped 0.795 GeO_2 – 0.20 PbF_2 – 0.005 Er_2O_3 glass ceramic samples which were annealed at 700 °C for 30 min with a heating rate of 10 °C/min and quenched in water.

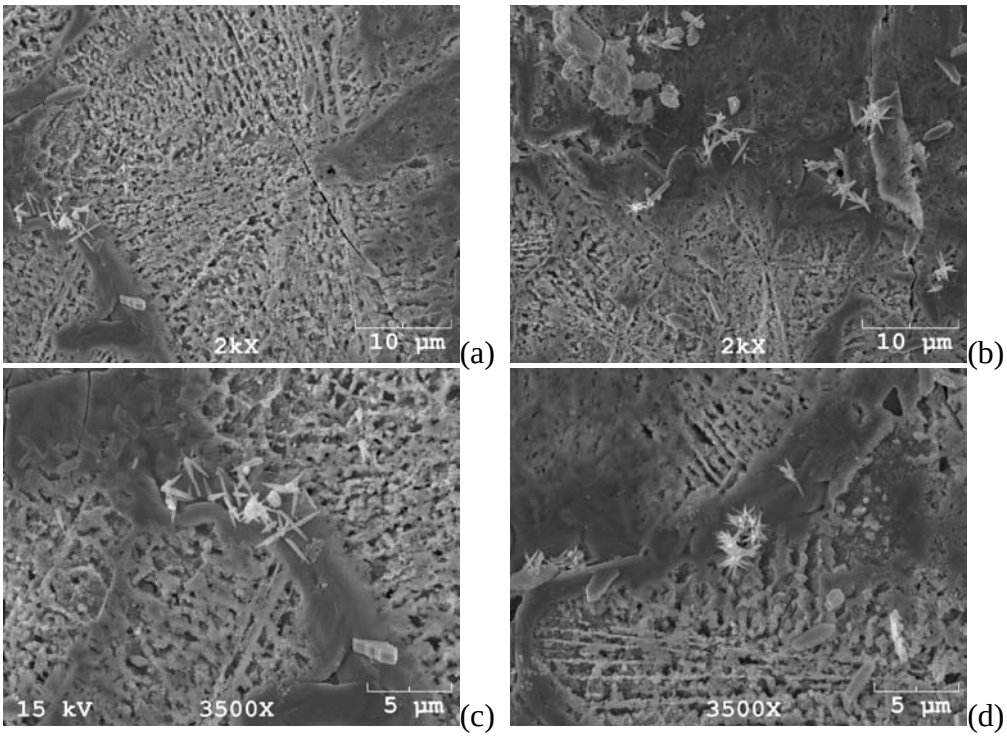

Figure 4.20 : SEM micrographs of the crystalline regions of the doped 0.795 GeO_2 – 0.20 PbF_2 – 0.005 Er_2O_3 glass samples which was heat treated at 700 °C: (a) 2000x, (b) 2000x, (c) 3500x, (d) 3500x, (e) 3500x, (f) 3500x, (g) 5000x, (h) 5000x.

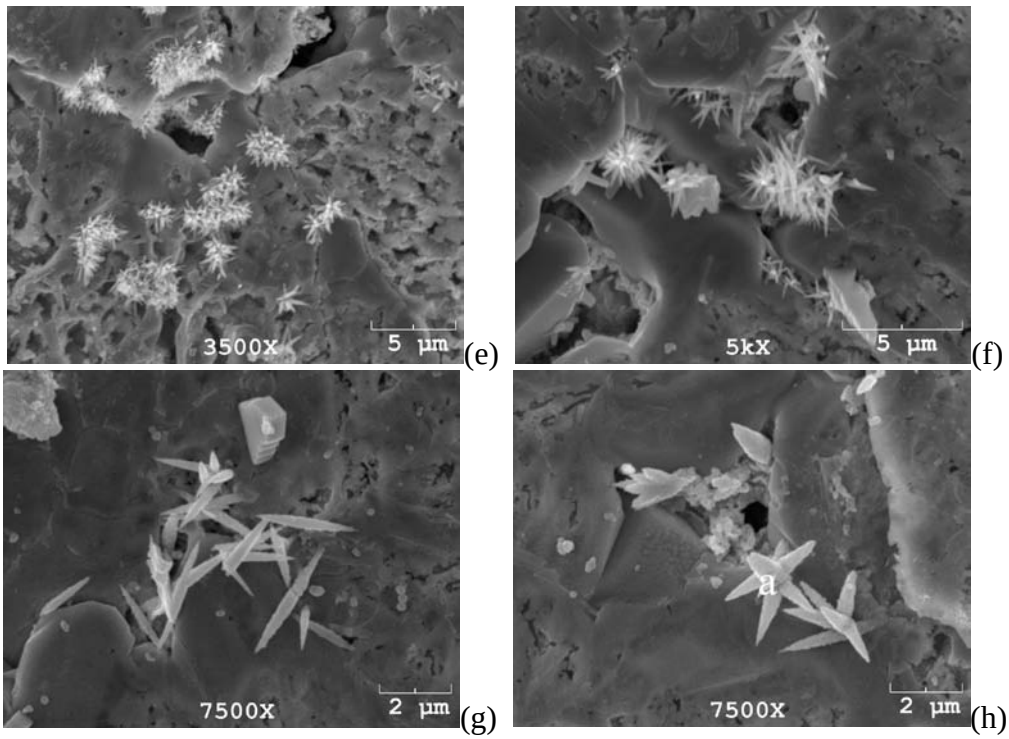

Figure 4.20 : (continued) SEM micrographs of the crystalline regions of the doped 0.795 GeO_2 – 0.20 PbF_2 – 0.005 Er_2O_3 glass samples which was heat treated at 700 °C: (a) 2000x, (b) 2000x, (c) 3500x, (d) 3500x, (e) 3500x, (f) 3500x, (g) 5000x, (h) 5000x.

Formation of needle-like structures can be seen as at the surface of the glass-ceramic samples in Figures 4.20(g) and 4.20(h). EDS were performed on the crystalline regions (a in Figure 4.20(h)) and revealed that (10.338 wt% Ge, 80.950 wt% Pb, 1.118 wt% O, 4.659 wt% F and 2.884 wt% Er) the needle-like structures (labeled as a in Figure 4.20(h)) are unidentified crystals.

4.6 0.695 GeO_2 – 0.30 PbF_2 – 0.005 Er_2O_3 Glass

As-cast 0.695 GeO_2 – 0.30 PbF_2 – 0.005 Er_2O_3 glass samples are shown in Figure 4.21. As seen in Figure 4.21, this glass shows transparency in visible light.

Figure 4.21 : As-cast 0.695 GeO_2 – 0.30 PbF_2 – 0.005 Er_2O_3 glass samples.

4.6.1 DTA investigations of the 0.695 GeO_2 – 0.30 PbF_2 – 0.005 Er_2O_3 glass

DTA curve for the as cast 0.695 GeO_2 – 0.30 PbF_2 – 0.005 Er_2O_3 glass with the heating rate of 10 °C/min is presented in Figure 4.22.

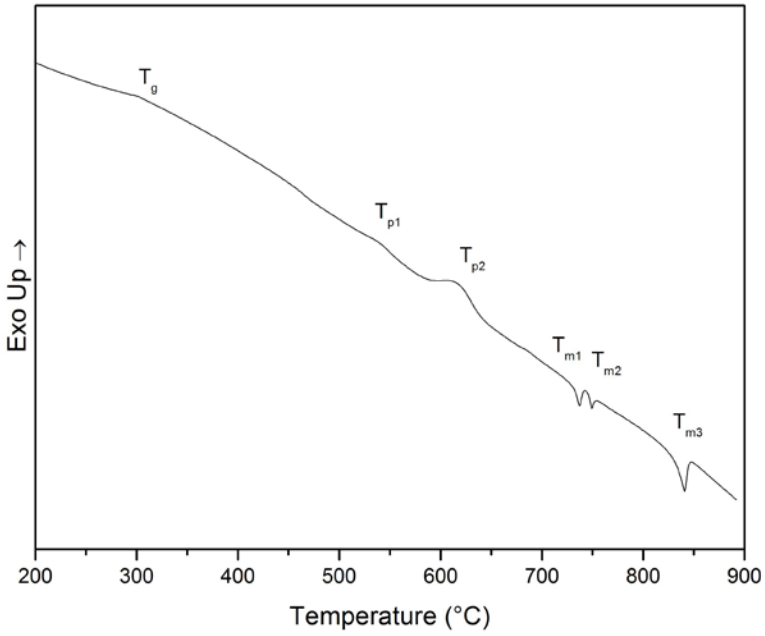

Figure 4.22 : DTA scan of the as-cast doped 0.695 GeO_2 – 0.30 PbF_2 – 0.005 Er_2O_3 glass with the heating rate of 10 °C/min.

It is showed that two exothermic peaks are present for the heating rate of 10 °C/min and it means that thermally treated 0.695 GeO_2 – 0.30 PbF_2 – 0.005 Er_2O_3 glass has at least two different crystalline phases. After exothermic peaks, two small and then a bigger endothermic peak follow which demonstrate the melting of the crystalline phases in the glass-ceramic.

Characteristic temperatures and on-set crystallization temperatures (T_x) are given in Table 4.6. Glass transition temperature (T_g) lays at 303 ºC while first and second crystallization peak temperatures (T_p) exist at 540 ºC and 616 ºC, respectively. Three melting temperatures (T_m) present at 735 ºC, 749 ºC and 837 °C, respectively.

Table 4.6 : Characteristic temperatures of the 0.695 GeO_2 – 0.30 PbF_2 – 0.005 Er_2O_3 glass.

	0.695 GeO_2 – 0.30 PbF_2 – 0.005 Er_2O_3						
T (°C)	T_g	T_x	T_{p1}	T_{p2}	T_{m1}	T_{m2}	T_{m3}
10 °C/min	303.36	236.68	540.04	616.26	734.59	749.44	836.55

Table 4.6 was used as reference for determining annealing temperatures of 0.695 GeO_2 – 0.30 PbF_2 – 0.005 Er_2O_3 glass sample for further investigations.

4.6.2 XRD analysis of the 0.695 GeO_2 – 0.30 PbF_2 – 0.005 Er_2O_3 glass

Binary GeO_2 – PbF_2 glass doped with 0.5 mol% Er_2O_3 containing 30 mol% PbF_2 demonstrates amorphous structure in the as-cast condition as seem given in Figure 4.23(a).

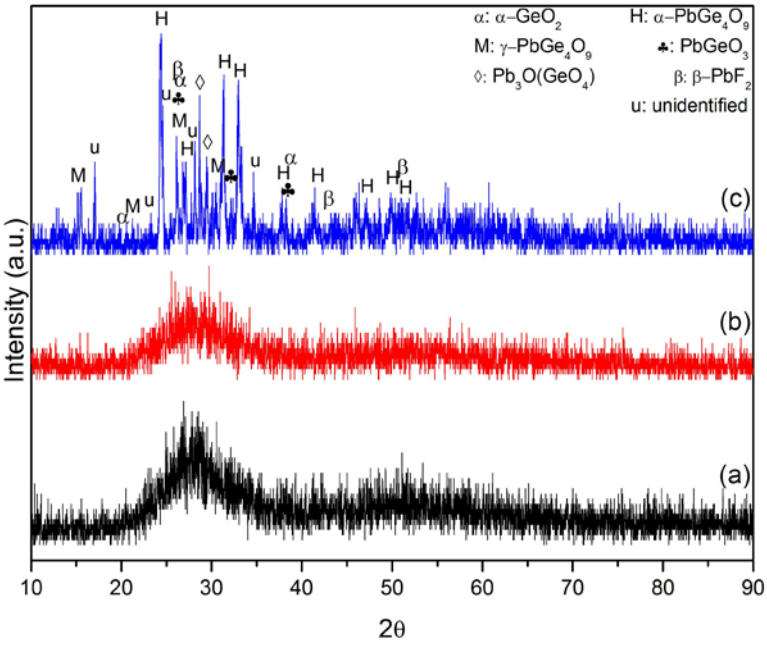

Figure 4.23 : XRD scans of the 0.695 GeO_2 – 0.30 PbF_2 – 0.005 Er_2O_3 glasses which are as-cast (a) and annealed at 580 °C (b) and 640 °C (c).

In order to investigate crystalline phases of 0.695 GeO_2 – 0.30 PbF_2 – 0.005 Er_2O_3 glass, specimens are annealed at two different temperatures (580 °C and 640 °C) which are obtained from DTA investigations. As seen in Figure 4.23(b), when the glass is heat treated at 580 °C for 20 min with the heating rate of 10 °C/min, no crystalline structures was observed in its structure. On the other hand, when glass is annealed at 640 °C for 30 min with the heating rate of 10 °C/min, both monoclinic γ-$PbGe_4O_9$ and hexagonal α-$PbGe_4O_9$ crystals, an unidentified phase (2θ = 17.1, 28.2, 33), $Pb_3O(GeO_4)$ and little amounts of α-GeO_2, cubic β-PbF_2 and $PbGeO_3$ are revealed in its microstructure (Figure 4.23(c)). The structures of the crystals, lattice parameters, space groups and card numbers of the crystalline phases observed in the glasses are given in Table B.1.

4.6.3 SEM investigations of the 0.695 GeO_2 – 0.30 PbF_2 – 0.005 Er_2O_3 glass

In order to examine the microstructural features in the XRD investigations, SEM/SEI micrographs were taken from the surface of the doped 0.695 GeO_2 – 0.30 PbF_2 –

0.005 Er_2O_3 glass-ceramic samples which were annealed at 640 °C for 30 min with a heating rate of 10 °C/min and quenched in water afterwards. EDS measurements were taken from the crystalline regions.

Figures 4.24(a) – 4.24(e) are the SEM/SEI micrographs taken from surface of the doped 0.695 GeO_2 – 0.30 PbF_2 – 0.005 Er_2O_3 glass-ceramic samples which were annealed at 640 °C for 30 min with a heating rate of 10 °C/min and quenched in water.

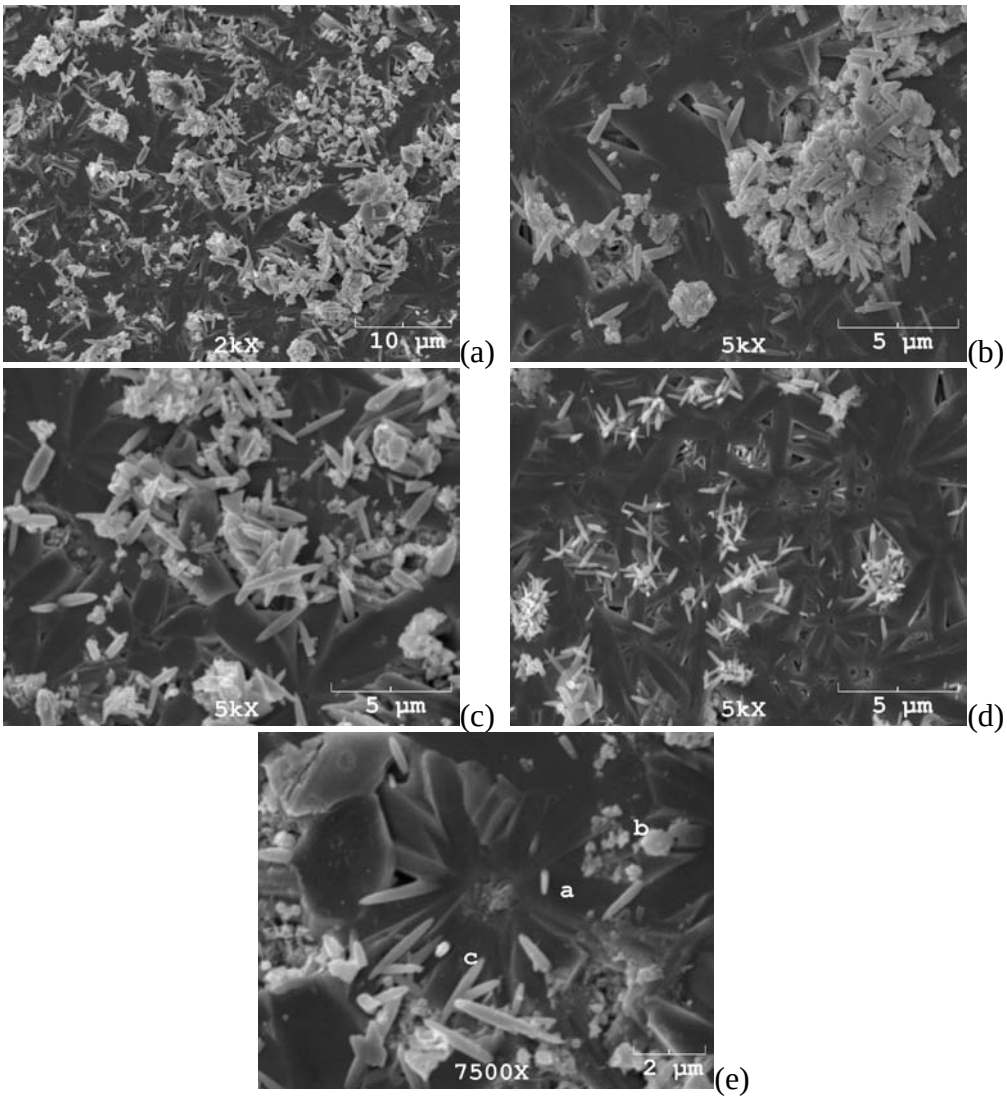

Figure 4.24 : SEM micrographs of the crystalline regions of the doped 0.695 GeO_2 – 0.30 PbF_2 – 0.005 Er_2O_3 glass samples which was heat treated at 640 °C: (a) 2000x, (b) 5000x, (c) 5000x, (d) 5000x, (e) 7500x.

Formation of Ge-rich crystals which can be seen as blocky-like structures in Figures 4.24(b) – 4.24(d) and formation of needle-like structures in Figures 4.24(a) and 4.24(e) are observed at the surface of the glass sample. EDS analyses were

performed on the crystalline regions (a and c in Figure 4.24(e)) and showed that (49.841 wt% Ge, 26.669 wt% Pb, 21.102 wt% O, 0.000 wt% F and 4.041 wt% Er) the blocky-like structures (labeled as a region in Figure 4.24(e)) are a polymorph of $PbGe_4O_9$ crystals while the needle-like (10.338 wt% Ge, 80.950 wt% Pb, 1.118 wt% O, 4.659 wt% F and 2.884 wt% Er) structures (labeled as b region in Figure 4.24(e)) are unidentified crystalline phases.

4.7 0.88 GeO_2 – 0.10 PbF_2 – 0.02 Er_2O_3 Glass

As-cast 0.88 GeO_2 – 0.10 PbF_2 – 0.02 Er_2O_3 glass samples are shown in Figure 4.25. As seen in Figure 4.25, this glass shows opacity in visible light.

Figure 4.25 : As-cast 0.88 GeO_2 – 0.10 PbF_2 – 0.02 Er_2O_3 glass samples.

4.7.1 DTA investigations of the 0.88 GeO_2 – 0.10 PbF_2 – 0.02 Er_2O_3 glass

DTA curve for the as cast 0.88 GeO_2 – 0.10 PbF_2 – 0.02 Er_2O_3 glass with the heating rate of 10 °C/min is presented in Figure 4.26.

It is showed that two exothermic peaks are present for the heating rate of 10 °C/min and it means that thermally treated 0.88 GeO_2 – 0.10 PbF_2 – 0.02 Er_2O_3 glass has at least two different crystalline phases. After exothermic peaks, a small and then a sharp endothermic peak follow which demonstrate the melting of the crystalline phases in the glass-ceramic.

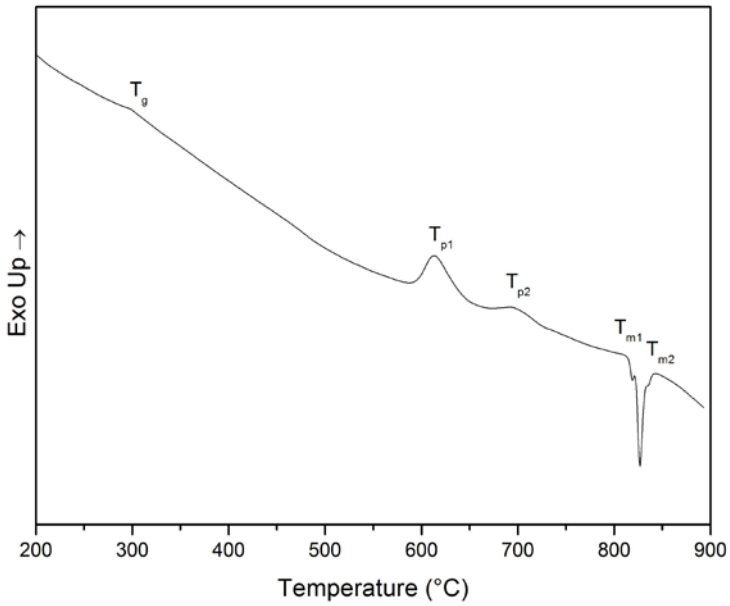

Figure 4.26: DTA scan of the as-cast doped 0.88 GeO_2 – 0.10 PbF_2 – 0.02 Er_2O_3 glass with the heating rate of 10 °C/min.

Characteristic temperatures and on-set crystallization temperatures (T_x) are given in Table 4.7. Glass transition temperature (T_g) lays at 301 ºC while first and second crystallization peak temperatures (T_p) exist at 612 ºC and 697 ºC, respectively. Two melting temperatures (T_m) present at 819 ºC and 827 °C, respectively.

Table 4.7 : Characteristic temperatures of 0.88 GeO_2 – 0.1 PbF_2 – 0.02 Er_2O_3 glass.

	0.88 GeO_2 – 0.10 PbF_2 – 0.02 Er_2O_3					
T (°C)	T_g	T_x	T_{p1}	T_{p2}	T_{m1}	T_{m2}
10 °C/min	301,16	311,22	612,38	696,62	819,04	826,82

Table 4.7 was used as reference for determining annealing temperatures of 0.88 GeO_2 – 0.10 PbF_2 – 0.02 Er_2O_3 glass sample for further investigations.

4.7.2 XRD analysis of the 0.88 GeO_2 – 0.10 PbF_2 – 0.02 Er_2O_3 glass

Binary GeO_2 – PbF_2 glass doped with 2 mol% Er_2O_3 containing 10 mol% PbF_2 demonstrates amorphous structure in the as-cast condition as seem in Figure 4.27(a).

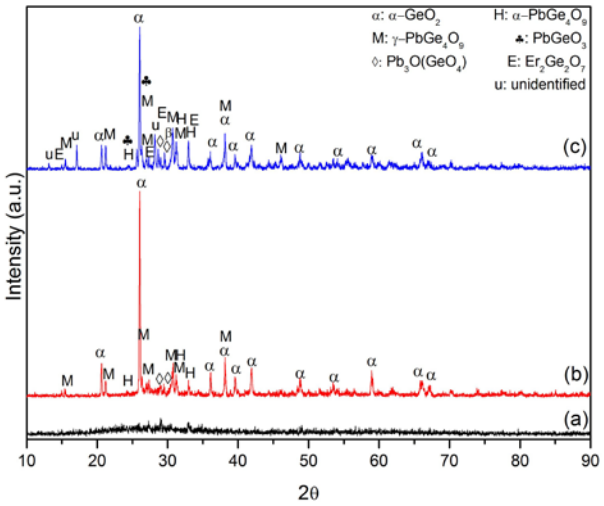

Figure 4.27 : XRD scans of the 0.88 GeO_2 – 0.1 PbF_2 – 0.02 Er_2O_3 glasses which are as-cast (a) and annealed at 640 °C (b) and 725 °C (c).

In order to investigate crystalline phases of 0.88 GeO_2 – 0.1 PbF_2 – 0.02 Er_2O_3 glass, specimens are annealed at two different temperatures (640 °C and 725 °C) which are obtained from DTA investigations. As seen in Figure 4.27(b), when the glass is heat treated at 640 °C for 20 min with the heating rate of 10 °C/min, α-GeO_2, both hexagonal α-$PbGe_4O_9$ and monoclinic γ-$PbGe_4O_9$ crystals and $Er_2Ge_2O_7$ phases are revealed in the microstructure. Also, when glass is annealed at 725 °C for 30 min with the heating rate of 10 °C/min, α-GeO_2, both γ-$PbGe_4O_9$ and α-$PbGe_4O_9$ crystals, $Er_2Ge_2O_7$ phases and formation of two additional phase which are an unidentified phase (2θ = 17.1, 28.2, 33) and $Pb_3O(GeO_4)$ crystals are present in microstructure (Figure 4.27(c)). The structures of the crystals, lattice parameters, space groups and card numbers of the crystalline phases observed in the glasses are given in Table B.1.

4.7.3 SEM investigations of the 0.88 GeO_2 – 0.10 PbF_2 – 0.02 Er_2O_3 glass

In order to examine the microstructural features in the XRD investigations, SEM/SEI micrographs were taken from the surface of the doped 0.88 GeO_2 – 0.10 PbF_2 – 0.02Er_2O_3 glass-ceramic samples which were annealed at 725 °C for 30 min with a heating rate of 10 °C/min and quenched in water afterwards. EDS measurements were taken from the crystalline regions.

Figures 4.28(a) – 4.28(c) are taken from the surface of the doped 0.88GeO_2 – 0.10PbF_2 – 0.02Er_2O_3 glass ceramic samples which were annealed at 725 °C for 30 min with a heating rate of 10 °C/min and quenched in water.

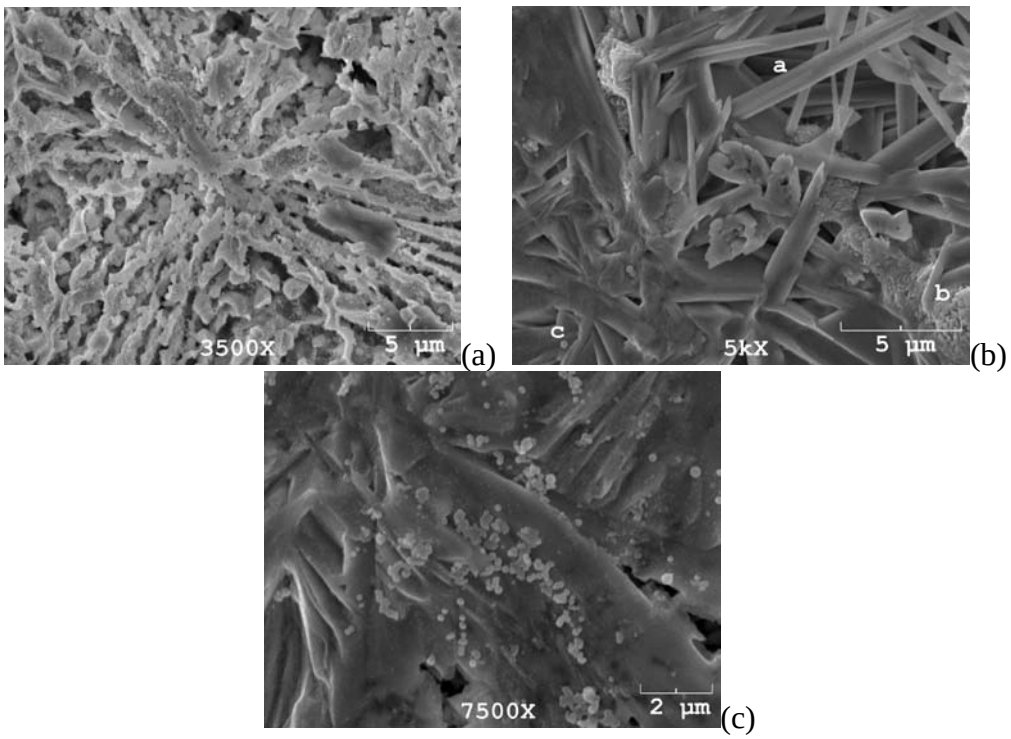

Figure 4.28 : SEM micrographs of the crystalline regions of the doped 0.88 GeO_2 – 0.1 PbF_2 – 0.02 Er_2O_3 glass samples which was heat treated at 725 °C: (a) 3500x, (b) 5000x, (c) 7500x.

Formations of Ge-rich crystals which are blocky-like structures are observed at the surface of the glass sample in Figures 4.28(a) and 4.28(b). EDS analyses were performed on the crystalline regions (a in Figure 4.28(b)) and showed that (49.841 wt% Ge, 26.669 wt% Pb, 21.102 wt% O, 0.000 wt% F and 4.041 wt% Er) the blocky-like structures (labeled as a region in Figure 4.28(b)) are a polymorph of $PbGe_4O_9$ crystals.

4.8 0.78 GeO_2 – 0.20 PbF_2 – 0.02 Er_2O_3 Glass

As-cast 0.78 GeO_2 – 0.20 PbF_2 – 0.02 Er_2O_3 glass samples are shown in Figure 4.29. As seen in Figure 4.29, this glass shows transparency in visible light.

Figure 4.29 : As-cast 0.78 GeO_2 – 0.20 PbF_2 – 0.02 Er_2O_3 glass samples.

4.8.1 DTA investigations of the 0.78 GeO_2 – 0.20 PbF_2 – 0.02 Er_2O_3 glass

DTA curve for the as cast 0.78 GeO_2 – 0.20 PbF_2 – 0.02 Er_2O_3 glass with the heating rate of 10 °C/min is presented in Figure 4.30.

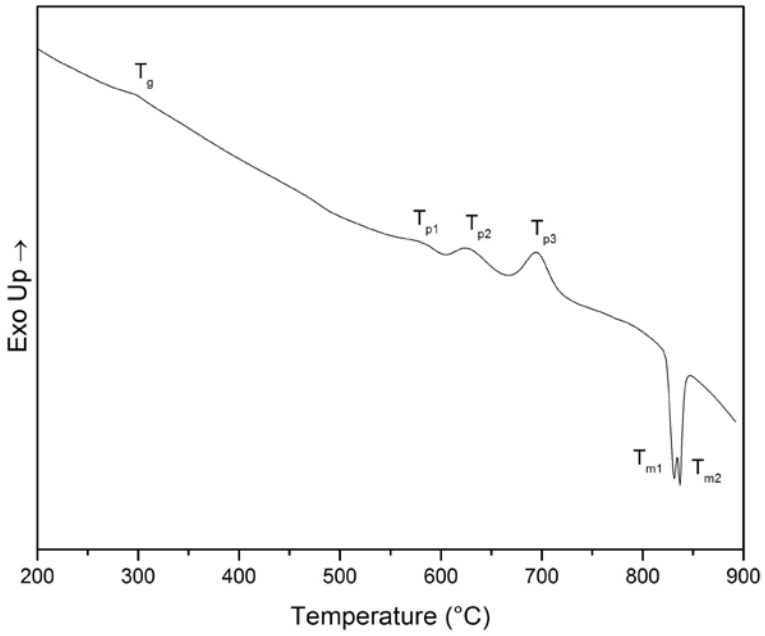

Figure 4.30 : DTA scan of the as-cast doped 0.78 GeO_2 – 0.20 PbF_2 – 0.02 Er_2O_3 glass with the heating rate of 10 °C/min.

It is showed that three exothermic peaks are present for the heating rate of 10 °C/min and it means that thermally treated 0.78 GeO_2 – 0.20 PbF_2 – 0.02 Er_2O_3 glass has at least three different crystalline phases. After exothermic peaks, two sharp endothermic peaks follow which demonstrate the melting of the crystalline phases in the glass-ceramic.

Characteristic temperatures and on-set crystallization temperatures (T_x) are given in Table 4.8. Glass transition temperature (T_g) lays at 299 ºC while three crystallization peak temperatures (T_p) exist at 580 ºC, 624 ºC and 695 ºC, respectively. Two melting temperatures (T_m) present at 831 ºC and 837 °C, respectively.

Table 4.8 : Characteristic temperatures of 0.78 GeO_2 – 0.20 PbF_2 – 0.02 Er_2O_3 glass.

	0.78 GeO_2 – 0.20 PbF_2 – 0.02 Er_2O_3						
T (°C)	T_g	T_x	T_{p1}	T_{p2}	T_{p3}	T_{m1}	T_{m2}
10 °C/min	298,73	281,21	579,94	623,68	695,46	831,34	836,93

Table 4.8 was used as reference for determining annealing temperatures of 0.78 GeO_2 – 0.20 PbF_2 – 0.02 Er_2O_3 glass sample for further investigations.

4.8.2 XRD analysis of the 0.78 GeO_2 – 0.20 PbF_2 – 0.02 Er_2O_3 glass

Binary GeO_2 – PbF_2 glass doped with 2 mol% Er_2O_3 containing 20 mol% PbF_2 demonstrates amorphous structure in the as-cast condition as seem in Figure 4.31(a).

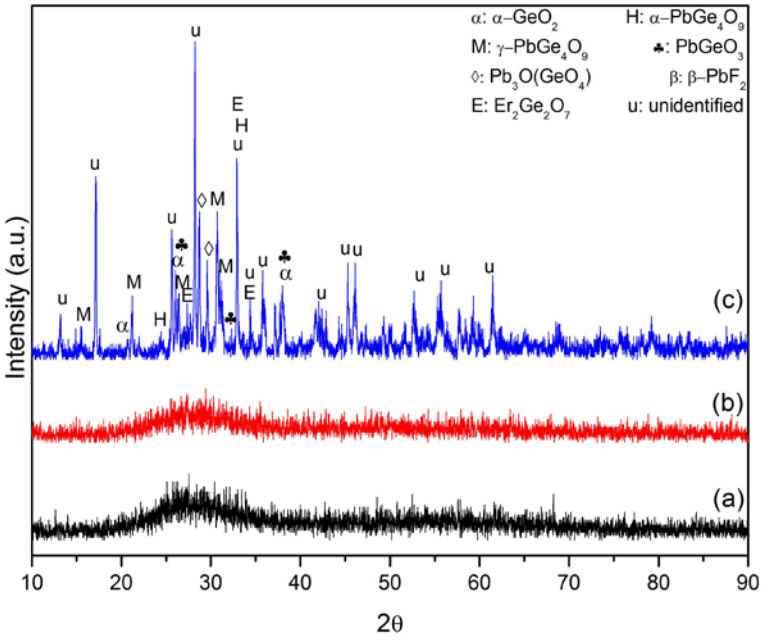

Figure 4.31 : XRD scans of the 0.78 GeO_2 – 0.20 PbF_2 – 0.02 Er_2O_3 glasses which are as-cast (a) and annealed at 600 °C (b) and 715 °C (c).

In order to investigate crystalline phases of 0.78 GeO_2 – 0.20 PbF_2 – 0.02 Er_2O_3 glass, specimens are annealed at two different temperatures (600 °C and 715 °C) which are obtained from DTA investigations. As seen in Figure 4.31(b), when the glass is heat treated at 600 °C for 20 min with the heating rate of 10 °C/min, no crystalline structures was observed in the microstructure. On the other hand, when glass is annealed at 715 °C for 30 min with the heating rate of 10 °C/min, α-GeO_2, γ-$PbGe_4O_9$ and $Pb_3O(GeO_4)$ crystals, an unidentified phase (2θ = 17.1, 28.2, 33) and little amounts of α-$PbGe_4O_9$, $PbGeO_3$, $Er_2Ge_2O_7$ are present in the microstructure. The structures of the crystals, lattice parameters, space groups and card numbers of the crystalline phases observed in the glasses are given in Table B.1.

4.8.3 SEM investigations of the 0.78 GeO_2 – 0.20 PbF_2 – 0.02 Er_2O_3 glass

In order to observe morphologically the crystalline phases which are identified in the XRD investigations, SEM/SEI micrographs were taken from the surface of the doped

0.78 GeO_2 – 0.20 PbF_2 – 0.02 Er_2O_3 glass-ceramic samples which were annealed at 715 °C for 30 min with a heating rate of 10 °C/min and quenched in water afterwards. EDS measurements were taken from the crystalline regions.

Figures 4.32(a) – 4.32(i) are SEM/SEI micrograph taken from the surface of the doped 0.78 GeO_2 – 0.20 PbF_2 – 0.02 Er_2O_3 glass-ceramic samples which were annealed at 715 °C for 30 min with a heating rate of 10 °C/min and quenched in water.

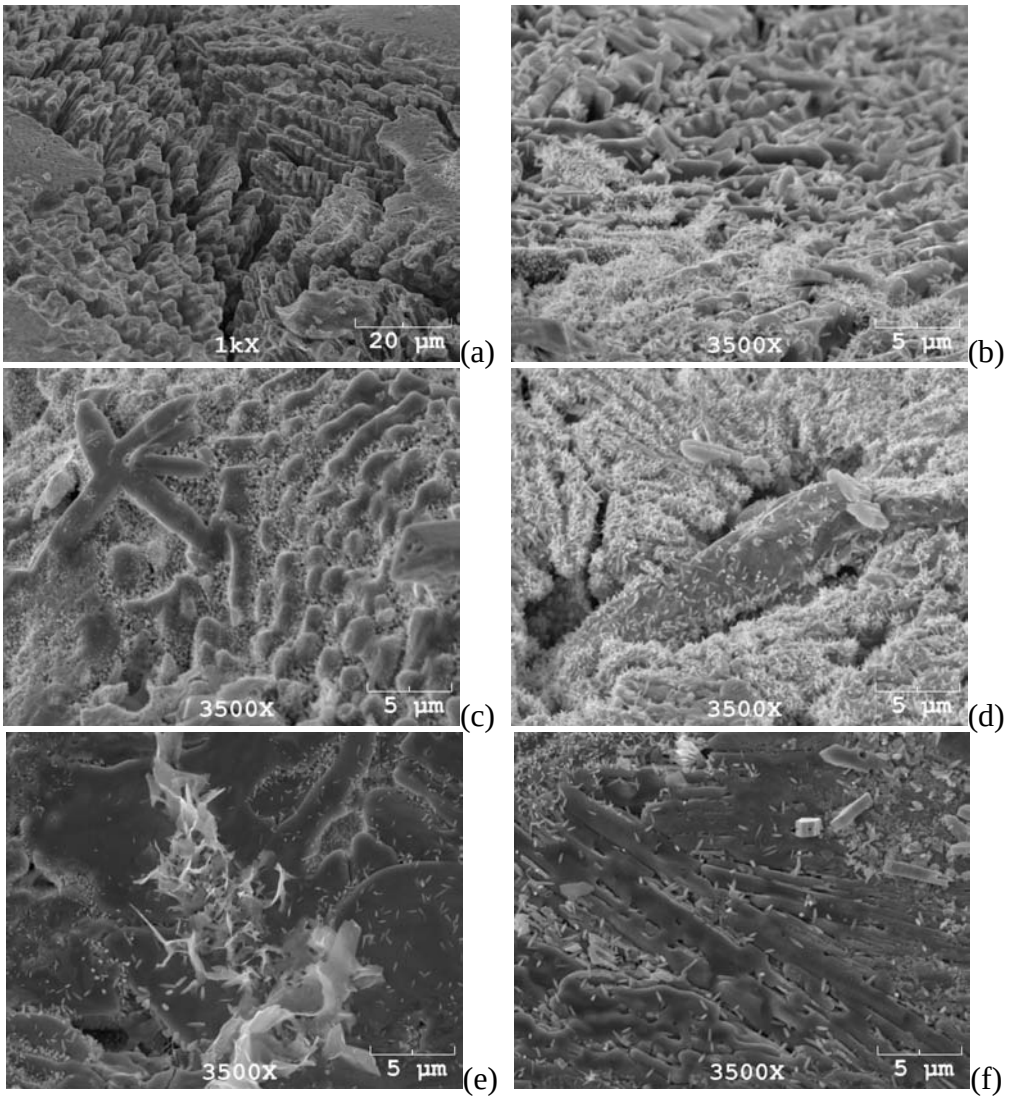

Figure 4.32 : SEM micrographs of the crystalline regions of the doped 0.78 GeO_2 – 0.20 PbF_2 – 0.02 Er_2O_3 glass samples which was heat treated at 715 °C: (a) 1000x, (b) 3500x, (c) 3500x, (d) 3500x, (e) 3500x, (f) 3500x, (g) 5000x, (h) 5000x, (i) 7500x.

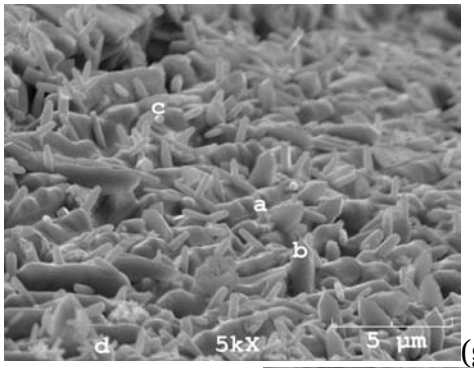

(g)
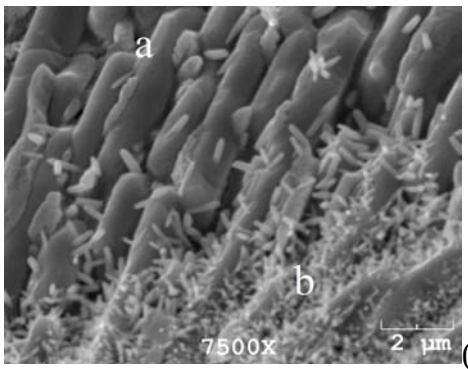

(h)
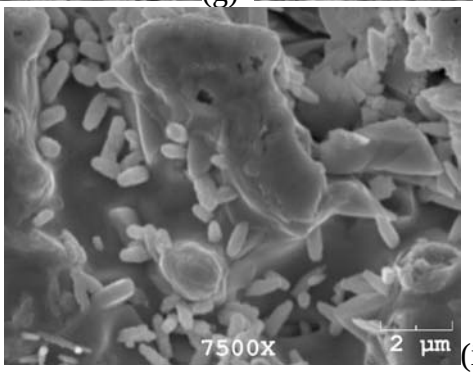

(i)

Figure 4.32 : (continued) SEM micrographs of the crystalline regions of the doped 0.78 GeO_2 – 0.20 PbF_2 – 0.02 Er_2O_3 glass samples which was heat treated at 715 °C: (a) 1000x, (b) 3500x, (c) 3500x, (d) 3500x, (e) 3500x, (f) 3500x, (g) 5000x, (h) 5000x, (i) 7500x.

Formation of Ge-rich crystals which can be seen as blocky-like structures in Figure 4.32(h) and Ge-Pb-rich crystals are observed as columnar structures in Figure 4.32(d) at the surface of the glass sample. EDS analyses were performed on the crystalline regions (a and b in Figure 4.32(h)) and showed that (49.841 wt% Ge, 26.669 wt% Pb, 21.102 wt% O, 0.000 wt% F and 4.041 wt% Er) the blocky-like structures (labeled as a region in Figure 4.32(h)) are a polymorph of $PbGe_4O_9$ crystals while columnar crystalline regions (24.479 wt% Ge, 69.926 wt% Pb, 2.511 wt% O, 3.083 wt% F) consist of $PbGeO_3$ (labeled as b region in Figure 4.32(h)) crystalline regions.

4.9 0.68 GeO_2 – 0.30 PbF_2 – 0.02 Er_2O_3 Glass

As-cast 0.68 GeO_2 – 0.30 PbF_2 – 0.02 Er_2O_3 glass samples are shown in Figure 4.33. As seen in Figure 4.33, this glass shows transparency in visible light.

Figure 4.33 : As-cast 0.68 GeO_2 – 0.30 PbF_2 – 0.02 Er_2O_3 glass samples.

4.9.1 DTA investigations of the 0.68 GeO_2 – 0.30 PbF_2 – 0.02 Er_2O_3 glass

DTA curve for the as cast 0.68 GeO_2 – 0.30 PbF_2 – 0.02 Er_2O_3 glass with the heating rate of 10 °C/min is presented in Figure 4.34.

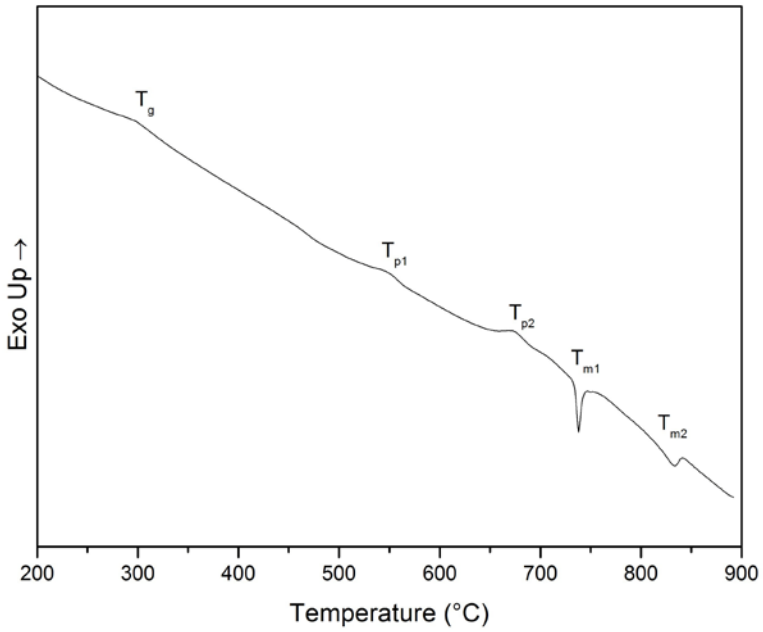

Figure 4.34: DTA scan of the as-cast doped 0.68 GeO_2 – 0.30 PbF_2 – 0.02 Er_2O_3 glass with the heating rate of 10 °C/min.

It is showed that two exothermic peaks are present for the heating rate of 10 °C/min and it means that thermally treated 0.68 GeO_2 – 0.30 PbF_2 – 0.02 Er_2O_3 glass has at least two different crystalline phases. After exothermic peaks, a sharp and then a small endothermic peak follow which demonstrate the melting of the crystalline phases in the glass-ceramic.

Characteristic temperatures and on-set crystallization temperatures (T_x) are given in Table 4.9. Glass transition temperature (T_g) lays at 299 ºC while first and second crystallization peak temperatures (T_p) exist at 546 ºC and 674 ºC, respectively. Two melting temperatures (T_m) present at 738 ºC and 833 °C, respectively.

Table 4.9: Characteristic temperatures of 0.68 GeO_2 – 0.30 PbF_2 – 0.02 Er_2O_3 glass.

	0.68 GeO_2 – 0.30 PbF_2 – 0.02 Er_2O_3					
T (°C)	T_g	T_x	T_{p1}	T_{p2}	T_{m1}	T_{m2}
10 °C/min	298,62	247,57	546,19	673,56	738,12	832,8

Table 4.9 was used as reference for determining annealing temperatures of 0.68 GeO_2 – 0.30 PbF_2 – 0.02 Er_2O_3 glass sample for further investigations.

4.9.2 XRD analysis of the 0.68 GeO_2 – 0.30 PbF_2 – 0.02 Er_2O_3 glass

Binary GeO_2 – PbF_2 glass doped with 2 mol% Er_2O_3 containing 30 mol% PbF_2 demonstrates amorphous structure in the as-cast condition as seem in Figure 4.35(a).

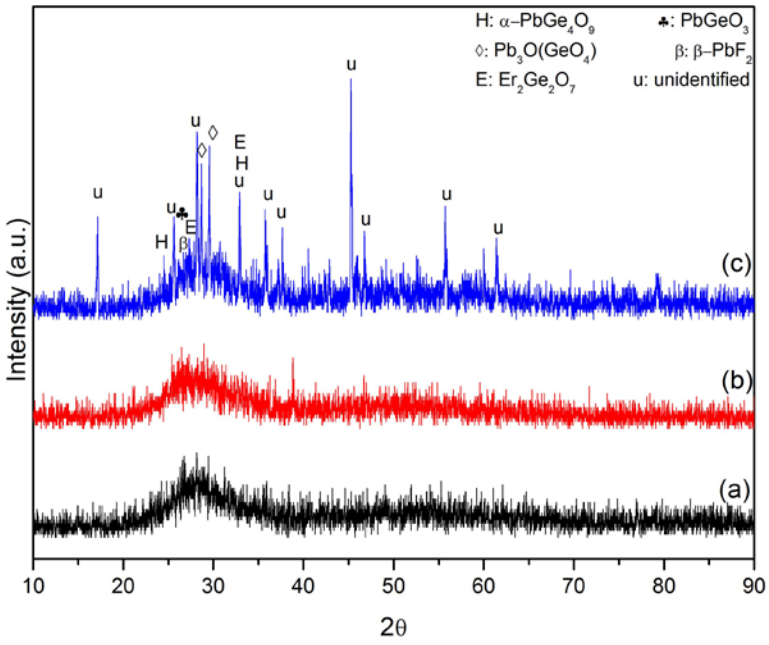

Figure 4.35 : XRD scans of the 0.695 GeO_2 – 0.30 PbF_2 – 0.02 Er_2O_3 glasses which are as-cast (a) and annealed at 580 °C (b) and 688 °C (c).

In order to investigate crystalline phases of 0.68 GeO_2 – 0.30 PbF_2 – 0.02 Er_2O_3 glass, specimens are annealed at two different temperatures (580 °C and 688 °C) which are obtained from DTA investigations. As seen in Figure 4.35(b), when the glass is heat treated at 580 °C for 20 min with the heating rate of 10 °C/min, no evidence of crystalline was detected in its microstructure. However, when glass is annealed at 715 °C for 30 min with the heating rate of 10 °C/min, α-$PbGe_4O_9$, $Pb_3O(GeO_4)$ crystals, an unidentified phase (2θ = 17.1, 28.2, 33) and little amounts of $PbGeO_3$, $Er_2Ge_2O_7$ and β-PbF_2 revealed in its microstructure. The structures of

the crystals, lattice parameters, space groups and card numbers of the crystalline phases observed in the glasses are given in Table B.1.

4.9.3 SEM investigation of 0.68 GeO_2 – 0.30 PbF_2 – 0.02 Er_2O_3 glass

In order to observe morphologically the crystalline phases which are identified in the XRD investigations, SEM/SEI micrographs were taken from the surface of the doped 0.68 GeO_2 – 0.30 PbF_2 – 0.02 Er_2O_3 glass-ceramic samples which were annealed at 688 °C for 30 min with a heating rate of 10 °C/min and quenched in water afterwards. EDS measurements were taken from the crystalline regions.

Figures 4.36(a) – 4.36(p) are the SEM/SEI micrographs taken from the surface of the doped 0.68 GeO_2 – 0.30 PbF_2 – 0.02 Er_2O_3 glass-ceramic samples which were annealed at 688 °C for 30 min with a heating rate of 10 °C/min and quenched in water.

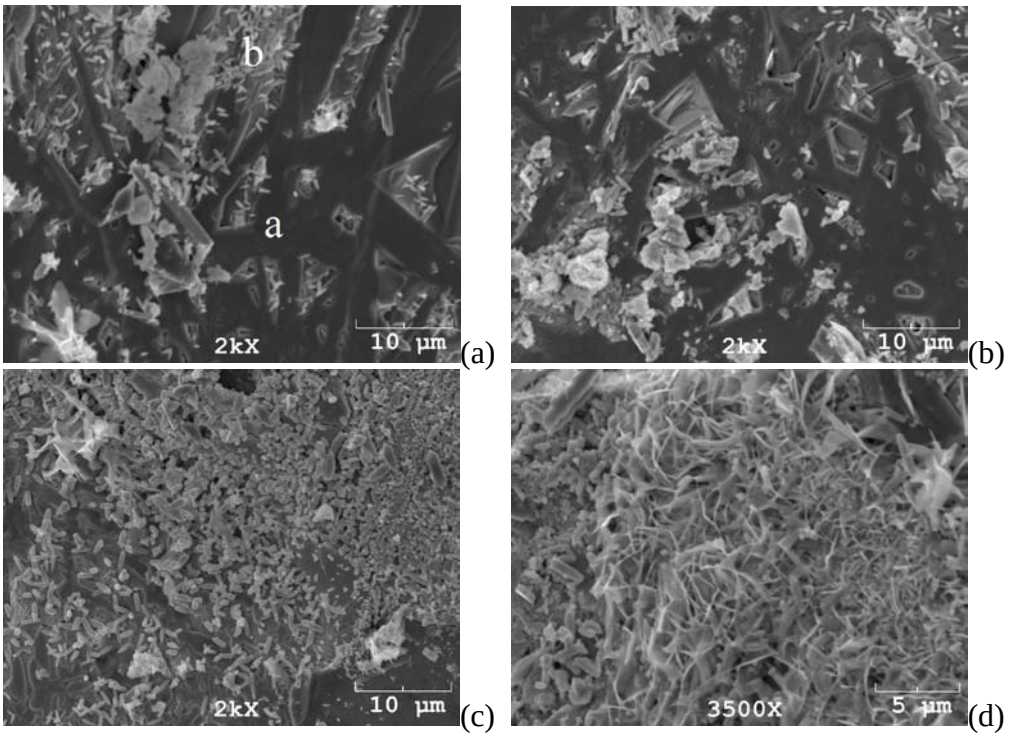

Figure 4.36 : SEM micrographs of the crystalline regions of the doped 0.68 GeO_2 – 0.30 PbF_2 – 0.02 Er_2O_3 glass samples which was heat treated at 688 °C: (a) 2000x, (b) 2000x, (c) 2000x, (d) 3500x, (e) 3500x, (f) 3500x, (g) 3500x, (h) 5000x, (i) 5000x, (j) 5000x, (k) 5000x, (l) 7500x, (m) 7500x, (n) 7500x, (o) 10000x, (p) 20000x.

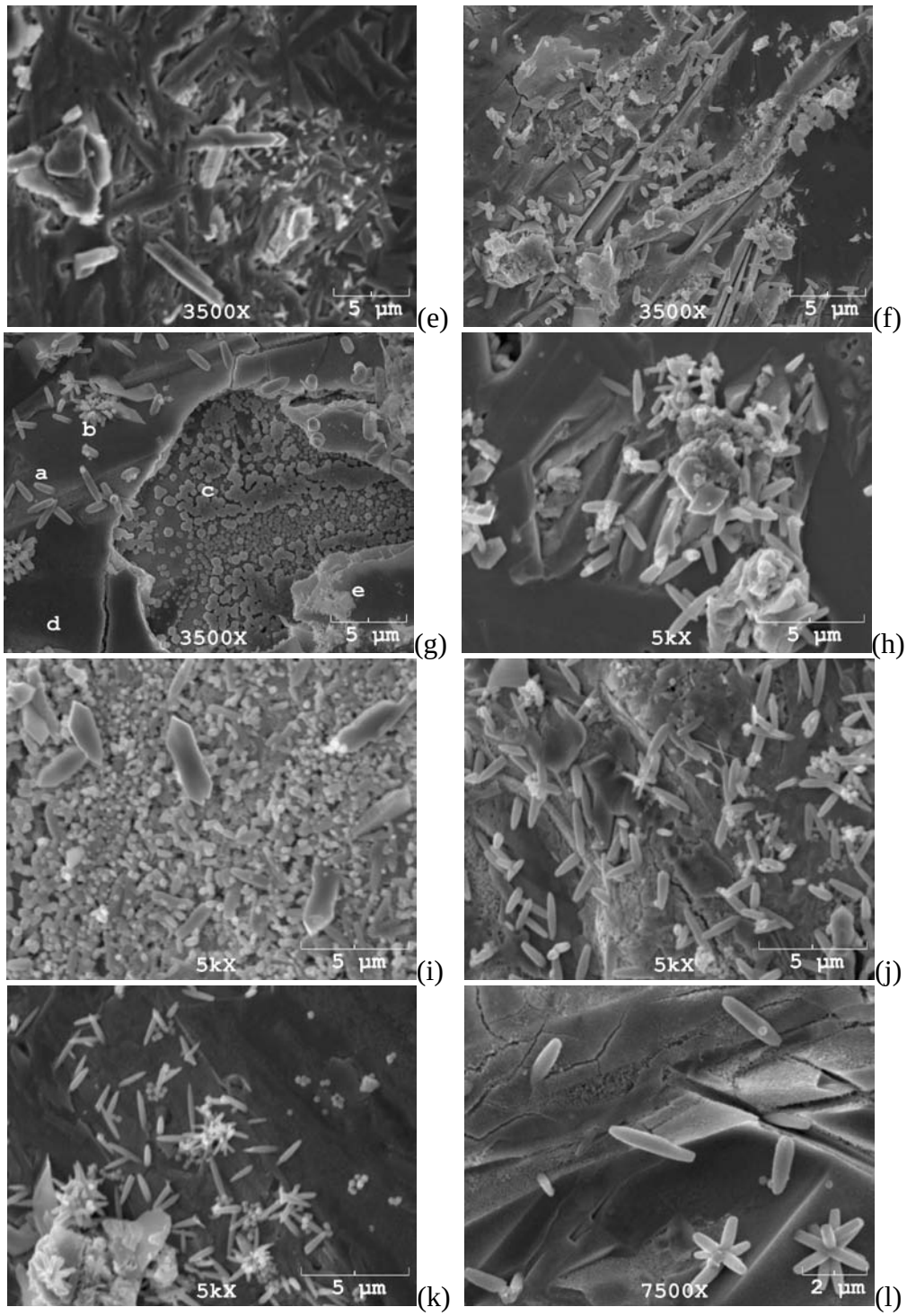

Figure 4.36 : (continued) SEM micrographs of the crystalline regions of the doped 0.68 GeO_2 – 0.30 PbF_2 – 0.02 Er_2O_3 glass samples which was heat treated at 688 °C: (a) 2000x, (b) 2000x, (c) 2000x, (d) 3500x, (e) 3500x, (f) 3500x, (g) 3500x, (h) 5000x, (i) 5000x, (j) 5000x, (k) 5000x, (l) 7500x, (m) 7500x, (n) 7500x, (o) 10000x, (p) 20000x.

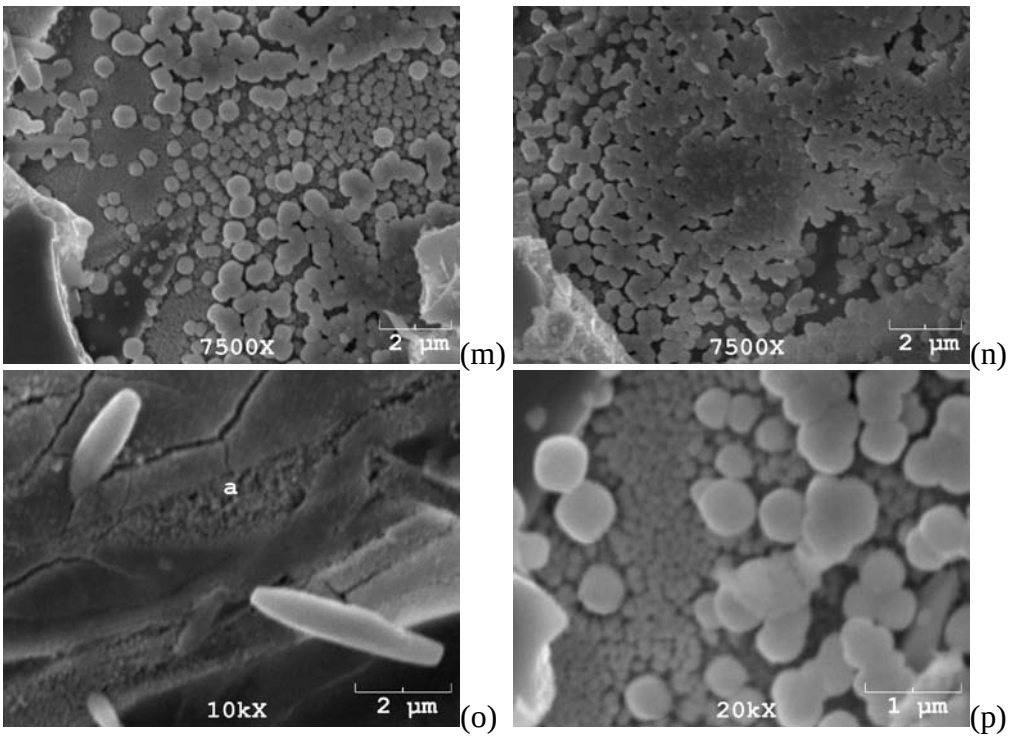

Figure 4.36 : (continued) SEM micrographs of the crystalline regions of the doped 0.68 GeO_2 – 0.30 PbF_2 – 0.02 Er_2O_3 glass samples which was heat treated at 688 °C: (a) 2000x, (b) 2000x, (c) 2000x, (d) 3500x, (e) 3500x, (f) 3500x, (g) 3500x, (h) 5000x, (i) 5000x, (j) 5000x, (k) 5000x, (l) 7500x, (m) 7500x, (n) 7500x, (o) 10000x, (p) 20000x.

Formation of Ge-rich crystals which can be seen as blocky-like structures and needle likes structures are observed at the surface of the glass sample in Figure 4.36(a) and 4.36(b). EDS were performed on the crystalline regions (a and b in Figure 4.36(a)) and showed that (41.151 wt% Ge, 40.684 wt% Pb, 17.377 wt% O, 0.788 wt% F) the blocky-like structures (labeled as a region in Figure 4.36(a)) are a polymorph of $PbGe_4O_9$ crystals while (10.338 wt% Ge, 80.950 wt% Pb, 1.118 wt% O, 4.659 wt% F and 2.884 wt% Er) the needle-like structures (labeled as b region in Figure 4.36(a)) are unidentified crystals.

4.10 Discussion

In order to understand the thermal behavior of the glasses changing with the increasing amount of PbF_2 as a network modifier, different glass compositions of the glass systems were heated with the heating rate of 10 °C/min which are given in Figures 4.37–4.39.

On the basis of DTA scans shown in Figure 4.37, the addition of PbF_2 into the glass system does not change the glass transition temperature. The exothermic peaks in the

thermographs demonstrate the crystallization processes. Table 4.8 shows all characteristic temperatures for non-doped and doped GeO_2 – PbF_2 glass system with a heating rate of 10 °C/min.

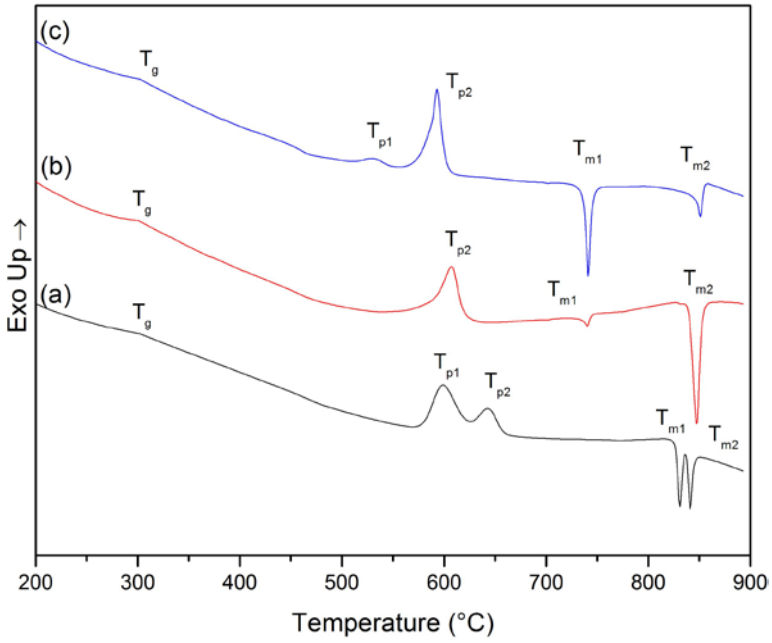

Figure 4.37 : DTA scans of the as-cast non-doped 0.90 GeO_2 – 0.10 PbF_2 (a), 0.80 GeO_2 – 0.20 PbF_2 (b), 0.70 GeO_2 – 0.30 PbF_2 (c) glasses with a heating rate of 10 °C/min.

0.90 GeO_2 – 0.10 PbF_2 glass has two exothermic peaks while 0.80 GeO_2 – 0.10 PbF_2 glass sample has only one distinguishable exothermic peak. Further PbF_2 content evoke a second crystallization peak for the 0.70 GeO_2 – 0.30 PbF_2, thus unique crystallization can occur with the increment of PbF_2 content. It is also noticed that similar of behavior was observed for endothermic peak which corresponds to melting point. First endothermic peak (T_{m1}) disappears with more PbF_2 content and a new endothermic peak (T_{m3}) was observed. In addition, increase in PbF_2 content in the system caused this new endothermic peak (T_{m3}) to become sharper while the second peak (T_{m2}) displays declination. As a result, it is right to say both exothermic and endothermic peaks are in agreement with each other with respect to changes the PbF_2 content in the GeO_2 – PbF_2 system.

Thermal effects of different PbF_2 content on GeO_2 – PbF_2 glass system doped with 0. 5 mol% Er_2O_3 can be seen in Figure 4.38. 0.895 GeO_2 – 0.10 PbF_2 – 0.005 Er_2O_3 glass has two exothermic peaks while 0.795 GeO_2 – 0.20 PbF_2 – 0.005 Er_2O_3 glass sample accommodates four different exothermic peaks. However, with addition of

more PbF_2 content there are only two exothermic peaks for the 0.695 GeO_2 – 0.30 PbF_2 – 0.005 Er_2O_3, while change on crystallization temperature with PbF_2 content could be due to the formation of different crystalline phases. It is also noticed that endothermic peak (T_{m1}) which corresponds to melting point shifts to higher temperatures with addition of PbF_2. On the other hand, a second broad endothermic peak (T_{m2}) is observed for 0.795 GeO_2 – 0.20 PbF_2 – 0.005 Er_2O_3 glass sample around 735 °C. Moreover, 0.695 GeO_2 – 0.30 PbF_2 – 0.005 Er_2O_3 glass sample has a new endothermic peak (T_{m3}) right after first endothermic peak while first endothermic peak (T_{m2}) is shifted to higher temperatures like the main endothermic peaks. As a result, it can be said that both exothermic and endothermic peaks shows an agreement with each other among the change on PbF_2 content even if doped with erbium content.

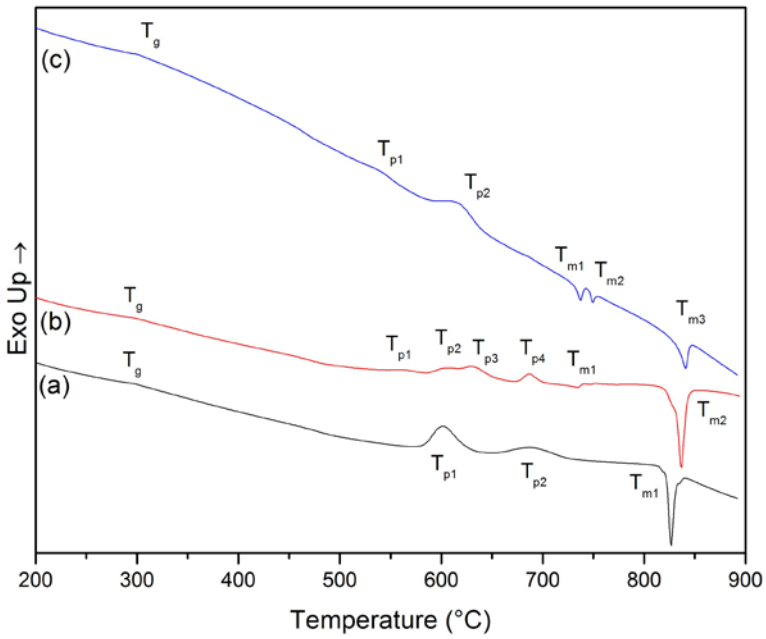

Figure 4.38 : DTA scans of the as-cast doped 0.895 GeO_2 – 0.10 PbF_2 – 0.005 Er_2O_3 (a), 0.795 GeO_2 – 0.20 PbF_2 – 0.005 Er_2O_3 (b), 0.695 GeO_2 – 0.30 PbF_2 – 0.005 Er_2O_3 (c) glasses with a heating rate of 10 °C/min.

Thermal effects of different PbF_2 content on GeO_2 – PbF_2 glass system doped with 2 mol% Er_2O_3 can be seen in Figure 4.39. 0.88 GeO_2 – 0.10 PbF_2 – 0.02 Er_2O_3 glass has two exothermic peaks while 0.78 GeO_2 – 0.20 PbF_2 – 0.02 Er_2O_3 glass sample accommodates three different exothermic peaks. However, with addition of more PbF_2 content two shallow exothermic peaks exists for the 0.68 GeO_2 – 0.30 PbF_2 – 0.02 Er_2O_3, while change on crystallization temperature with PbF_2 content could be result of the formation of different crystals. It is also noticed that endothermic peaks

which correspond to melting point are shifted to higher temperatures with addition of PbF_2 and existence of additional endothermic peak is observed at ~740 °C. Both exothermic and endothermic peaks are in agreement with each other with change on PbF_2 content even if doped with erbium content.

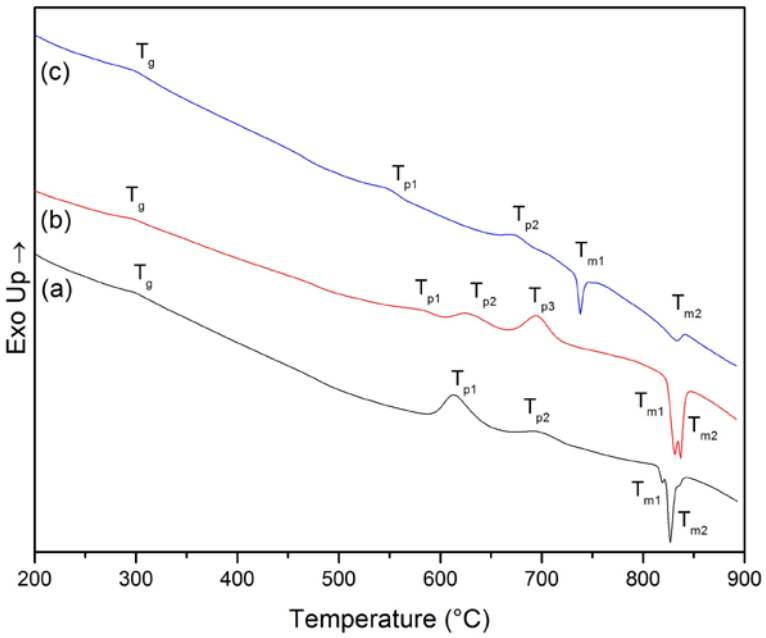

Figure 4.39 : DTA scans of the as-cast doped 0.88 GeO_2 – 0.10 PbF_2 – 0.02 Er_2O_3 (a), 0.78 GeO_2 – 0.20 PbF_2 – 0.02 Er_2O_3 (b), 0.70 GeO_2 – 0.30 PbF_2 – 0.02 Er_2O_3 (c) glasses with a heating rate of 10 °C/min.

DTA curves for as-cast (0.90 – y) GeO_2 – 0.10 PbF_2 – y Er_2O_3 (y = 0. 0.005, 0.02 mol) glasses with a heating rate of 10 °C/min are shown in Figure 4.40 and they demonstrated that glass transition temperatures are slightly affected with erbium ions and show tendency to decrease. However unlike glass transition temperatures, both exothermic crystallization peak temperatures especially second crystallization peak temperatures are shifted to higher temperatures with the addition of Er_2O_3. The second endothermic peak disappears for the y = 0.005 mol Er_2O_3 composition and first endothermic peak become sharper. For the y = 0.02 mol Er_2O_3 composition, existence of new endothermic peak (T_{m3}) was observed prior to late first endothermic peak.

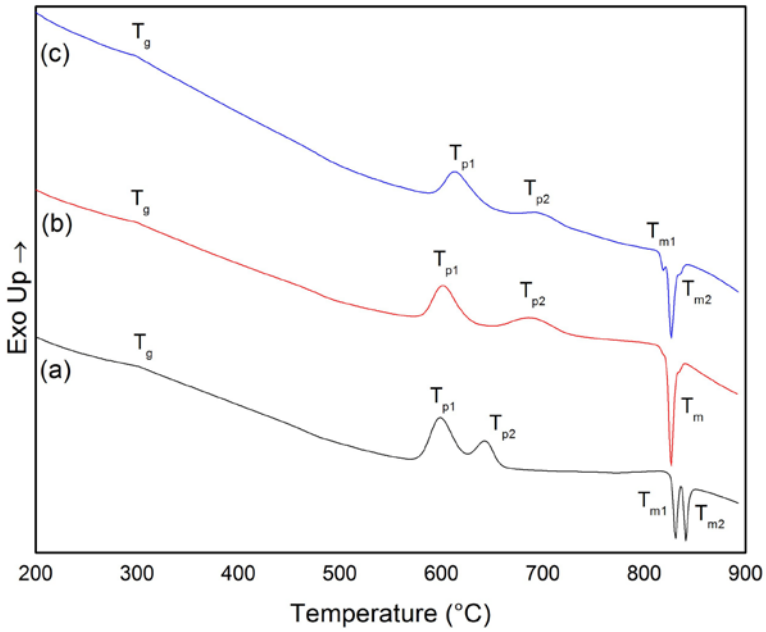

Figure 4.40 : DTA scans of the 0.90 GeO_2 – 0.10 PbF_2 (a), 0.895 GeO_2 – 0.10 PbF_2 – 0.005 Er_2O_3 (b), 0.88 GeO_2 – 0.10 PbF_2 – 0.02 Er_2O_3 (c) glasses with a heating rate of 10 °C/min.

DTA curves for as-cast (0.80 – y) GeO_2 – 0.20 PbF_2 – y Er_2O_3 (y = 0. 0.005, 0.02 mol) glasses with a heating rate of 10 °C/min are shown in Figure 4.41. As can be seen from Figure 4.41, the glass transition temperatures display slight changes and they tend to decrease to lower temperatures with the addition of erbium content. The glass transition temperatures are followed by exothermic peaks and the existence of new exothermic peaks associated with new observed crystalline formations with the introduction of erbium content to the 0.80 GeO_2 – 0.20 PbF_2 glass. Existence of four exothermic peaks can be observed for the y = 0.005 mol Er_2O_3 composition while last exothermic become shallower with addition of more erbium content (y = 0.02 mol Er_2O_3). Increasing erbium content induces endothermic peaks to shift to lower temperatures while no visible additional endothermic peaks are detected.

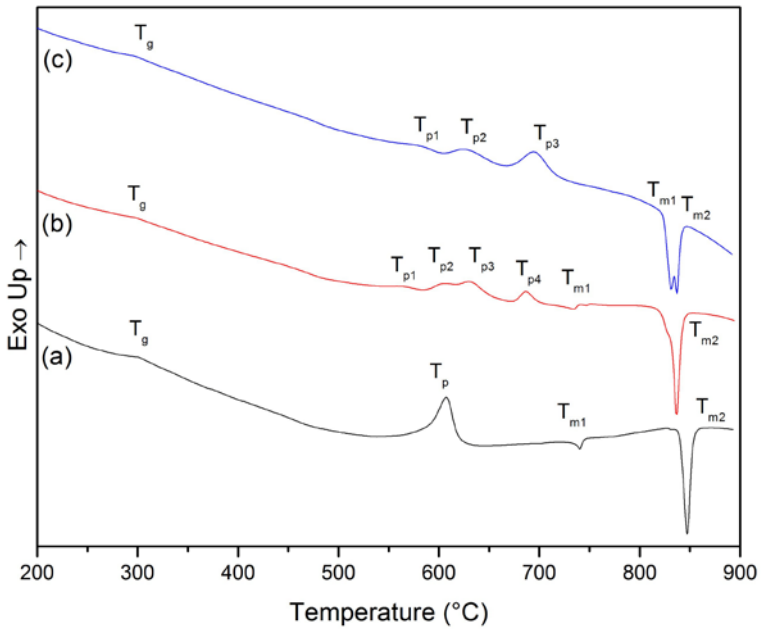

Figure 4.41 : DTA scans of the 0.80 GeO_2 – 0.20 PbF_2 (a), 0.795 GeO_2 – 0.20 PbF_2 – 0.005 Er_2O_3 (b), 0.78 GeO_2 – 0.20 PbF_2 – 0.02 Er_2O_3 (c) glasses with a heating rate of 10 °C/min.

DTA curves for the as-cast (0.70 – y) GeO_2 – 0.30 PbF_2 – y Er_2O_3 (y = 0. 0.005, 0.02) glasses with the heating rate of 10 °C/min are shown in Figure 4.42, indicating the glass transition temperature increases with the introduction of erbium. Sharper exothermic peak for non-doped 0.70 GeO_2 – 0.30 PbF_2 glass reduces with erbium content and shifts to higher temperatures, on the other hand broader exothermic peak tend to shift to lower temperatures and distant from other one. As exothermic peak behaves, endothermic peak is lowered with erbium content and existence of new endothermic peak is observed.

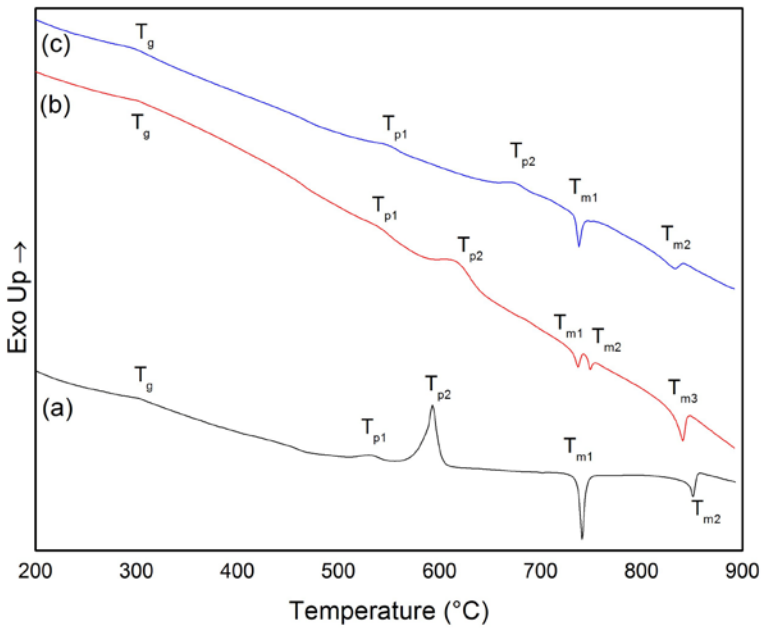

Figure 4.42 : DTA scans of the 0.70 GeO_2 – 0.30 PbF_2 (a), 0.695 GeO_2 – 0.30 PbF_2 – 0.005 Er_2O_3 (b), 0.68 GeO_2 – 0.30 PbF_2 – 0.02 Er_2O_3 (c) glasses with a heating rate of 10 °C/min.

ΔT value for corresponding glass sample was obtained from the DTA curves and difference between glass transition temperature and first crystallization temperature was given in Table 4.8 for each glass sample. The calculated value of thermal stability for 0.90 GeO_2 – 0.10 PbF_2 is 296 °C, while 0.80 GeO_2 – 0.20 PbF_2 glass sample has a higher value of 305 °C. The glass stability value for 0.70 GeO_2 – 0.30 PbF_2 decreases to 229 °C. It can be said that formation different phases can change thermal stability non-linearly. These values are much better than not only tellurite glasses, but also fluoride glasses (Silva et al, 2001; Kabalci et al., 2006; Nie et al., 2008). Studies on GeO_2 – PbO – PbF_2 and PbF_2 – based glass compositions showed that when system is provided with more PbF_2, the thermal stability decreases to lower values with nucleation of cubic β–PbF_2 crystallization (Yang et al., 2006; Zhang et al., 2005). When compared to GeO_2 – PbF_2 binary glass system, even if it shows the same behavior, formation of different phases pollute the expected results. Although it's reported that addition of a nucleating agent induces nucleation of cubic β–PbF_2 in the glass-ceramics, our thermographs show no sign of β–PbF_2.

Table 4.8 : Characteristic temperatures of the non-doped and doped $GeO_2 – PbF_2$ glasses for heating rate of 10 °C/min.

	0.90 GeO_2 – 0.10 PbF_2			**0.80 GeO_2 – 0.20 PbF_2**			**0.70 GeO_2 – 0.30 PbF_2**		
	0 Er_2O_3	0.005 Er_2O_3	0.02 Er_2O_3	0 Er_2O_3	0.005 Er_2O_3	0.02 Er_2O_3	0 Er_2O_3	0.005 Er_2O_3	0.02 Er_2O_3
Heat F.	10 °C/m	10 °C/m	10 °C/m	10 °C/m	10 °C/m	10 °C/m	10 °C/m	10 °C/m	10 °C/m
T_g	302,17	302,03	301,16	302,1	300.49	298,73	301,7	303,36	298,62
T_x	296,66	299,37	311,22	305,27	263,51	281,21	229,86	236,68	247,57
T_{p1}	598,83	601,4	612,38	607,37	564	579,94	531,56	540.04	546,19
T_{p2}	642,6	686,2	696,62	-	606,95	623,68	592,98	616,26	673,56
T_{p3}	-	-	-	-	632,17	695,46	-	-	-
T_{p4}	-	-	-	-	686,69	-	-	-	-
T_{m1}	830.98	826,69	819,04	740.29	734,59	831,34	741,31	734,59	738,12
T_{m2}	841,23	-	826,82	847,42	836,55	836,93	850.75	749,44	832,8
T_{m3}	-	-	-	-	-	-	-	841,03	-

As PbF_2 content increases from 10 mol% to 20 mol%, crystallized GeO_2 phase in the glass ceramics demonstrates a sudden decrease as shown in Figure 4.43. Neither hexagonal nor the monoclinic polymorphs of the $PbGe_4O_9$ phase in the glass ceramics change significantly in the glass compositions varying between 10-30 mol% PbF_2 content for non-doped glasses. For As PbF_2 content increases from 10 mol% to 20 mol%, crystallized GeO_2 phase in the glass ceramics demonstrates a sudden decrease as shown in Figure 5.7. Ghinga et al. (2002) reported that nucleation of GeO_2 disappear for more than 10 mol% PbO content in their GeO_2 – PbO binary glass study. As GeO_2 tend to nucleate itself, PbO addition in the germanate glass system prevents nucleation and glass system become more stable. Due to this reason Tomasi et al., (2005) reported that homogenous glass can be accomplish for more than 25 mol% PbO with prevention of GeO_2 nanocrystalline nucleation. When PbO content reaches its threshold to prevent nucleation of GeO_2, glass-transition temperature will decrease constantly with increase of the number non-bridging oxygen atoms in the glass system (Ghinga et al., 2002).

Neither hexagonal nor the monoclinic polymorphs of the $PbGe_4O_9$ phase in the glass ceramics change significantly in the glass compositions varying between 10-30 mol% PbF_2 content for non-doped glasses. In binary GeO_2-rich GeO_2 – PbO glass system, authors (Ghinga et al., 2002; Scavini et al., 2001) reported that glass system tend to crystallize as metastable $PbGe_4O_9$ crystallines, while $PbGe_3O_7$ phase which couldn't be observed in this study is crystallize with long term heating process.

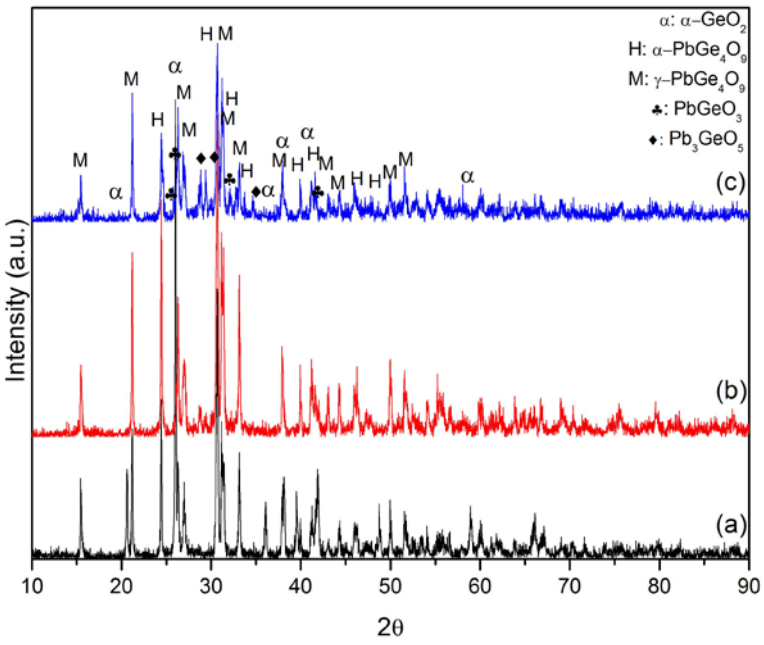

Figure 4.43 : XRD scans of the 0.90 GeO_2 – 0.10 PbF_2 (a), 0.80 GeO_2 – 0.20 PbF_2 (b) 0.70 GeO_2 – 0.30 PbF_2 (c) non-doped glasses which are annealed at 670 °C, 630 °C and 620 °C, respectively.

For the binary GeO_2 – PbO glass system, the metastable $PbGe_4O_9$ crystalline phase was observed in the compositional range of PbO being between 0–50 mol% due to the reason that it has very strong tendency for crystallization (Zhereb et al., 2008; Scavini et al., 2001; Sigaev et al., 2001; Bush et al., 2002; Dantelle et al., 2006; Dantelle et al., 2005). Even though there are no $PbGeO_3$ and Pb_3GeO_5 phases in the glass composition with 10 mol% PbF_2 content, both of these crystalline phases slowly increase as the PbF_2 content in the glass compositions varying between 10-30 mol% PbF_2 content. Even though the formation of the cubic PbF_2 phase which is also referred as β–PbF_2 is observed in $PbGeO_3$ – PbF_2 – CdF_2 and GeO_2 – PbO – PbF_2 glass systems, it is not observed in all of the compositions studied in the binary GeO_2 – PbF_2 glass system (Dominiak-Dzik et al., 2008; Bueno et al., 2008; Mortier & Patriarche, 2000; Shang et al., 2008; Gouveia-Neto et al., 2004b; Gouveia-Neto et al., 2009; Bueno et al., 2005; Bueno et al., 1999; Dantelle et al., 2006; Mortier, 2001; Labéguerie et al., 2008; Klimesz et al., 2008; Pan et al., 2007; Mortier et al., 2002). Formation of cubic PbF_2 phase is only observed in small amounts for the non-doped glass composition containing 30 mol% PbF_2 content. It is also explained in the study that Mortier and Patriarche conducted that the formation of the β–PbF_2 is not enough for compositions around 10 mol% so in order to achieve the nucleation of the cubic PbF_2 phase, another nucleation agent is necessary and even in some cases their

amount should be sufficient in the glass matrix for nucleation of the β–PbF_2 (Mortier & Patriarche, 2000; Klimesz et al., 2008). On the other hand, Shang et al. (2008) increased PbF_2 content to 47mol% and kept Er_2O_3 concentration at 0.5 mol% to obtain nucleation of β–PbF_2 in their study. The amount of the GeO_2 crystalline phase decreases with the addition of the PbF_2 content. Even though non-doped glasses demonstrate a rapid decrease in the content of the GeO_2 crystalline phase, this content changes slightly in the doped glasses. This might be due to the reason that the nucleation of the GeO_2 phase in the doped-glasses is accompanied by the Er_2O_3 which acts as a nucleation agent acting as the seeds for the inhomogeneous nucleation growth. Similar case is also observed for the GeO_2 – PbO – PbF_2 glasses (Mortier & Patriarche, 2000). The intensities of hexagonal $PbGe_4O_9$ and monoclinic $PbGe_4O_9$ phases in the non-doped GeO_2 – PbF_2 binary glasses do not change with the addition of the PbF_2 content.

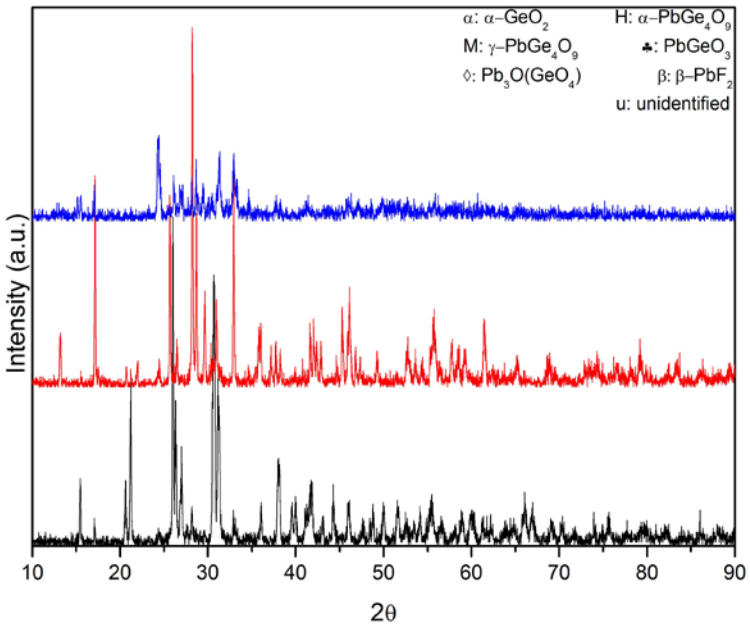

Figure 4.44 : XRD scans of the 0.90 GeO_2 – 0.10 PbF_2 – 0.005 Er_2O_3 (a), 0.80 GeO_2 – 0.20 PbF_2 – 0.005 Er_2O_3 (b) 0.70 GeO_2 – 0.30 PbF_2 – 0.005 Er_2O_3 (c) doped glasses which are annealed at 725 °C, 700 °C and 640 °C, respectively.

For the glasses containing 0.5 mol% Er_2O_3 which are shown in Figure 4.44, nucleation of GeO_2 phase is decreased rapidly with additional PbF_2 content. Although the intensity of the hexagonal $PbGe_4O_9$ phase increases, the intensity of monoclinic $PbGe_4O_9$ decreases with the addition of the PbF_2 content. The intensity of the $PbGeO_3$ phase increases with the addition of the PbF_2 content in the 0.5 mol%

Er_2O_3 doped GeO_2 – PbF_2 glasses while the amount of the crystalline $PbGeO_3$ is a slightly increase for the glasses doped with 0.5 mol% of Er_2O_3. For the doped glasses containing 0.5 mol% Er_2O_3 content, $Pb_3O(GeO_4)$ crystalline phase which has same stoichiometry with Pb_3GeO_5 is observed instead of Pb_3GeO_5 in their structure.

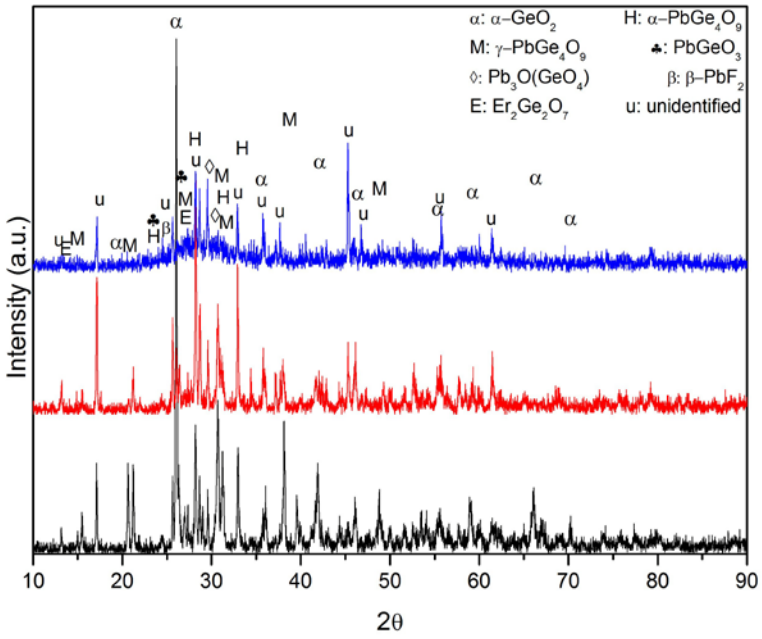

Figure 4.45 : XRD scans of the 0.90 GeO_2 – 0.10 PbF_2 – 0.02 Er_2O_3 (a), 0.80 GeO_2 – 0.20 PbF_2 – 0.02 Er_2O_3 (b), 0.70 GeO_2 – 0.30 PbF_2 – 0.02 Er_2O_3 (c) doped glasses which are annealed at 725 °C, 715 °C and 688 °C, respectively.

For the glasses containing 2 mol% Er_2O_3 which are shown in Figure 4.45, nucleation of GeO_2 phase is decreased rapidly with additional PbF_2 content. In spite of the absence of the hexagonal $PbGe_4O_9$ phase, the existence of monoclinic $PbGe_4O_9$ is observed. Monoclinic $PbGe_4O_9$ phase disappears while hexagonal $PbGe_4O_9$ phase emerges for 30 mol% PbF_2 content. The amount of the $PbGeO_3$ phase increases with the addition of the PbF_2 content in the 2 mol% Er_2O_3 doped binary GeO_2 – PbF_2 glasses, but $PbGeO_3$ phase couldn't be observed for 30 mol% PbF_2 content. For the doped glasses containing 2 mol% Er_2O_3 content, $Pb_3O(GeO_4)$ crystalline phase which has same stoichiometry with Pb_3GeO_5 is observed instead of Pb_3GeO_5 in their structure.

The results are also consistent with other studies in literature that the tetragonal GeO_2 phase which is stable below 1000 °C (Margaryan and Piliavin, 1993) was not observed in any of the studied glasses (Scavini et al., 2001; Ghigna et al., 2002). On

the other hand, Ghinga et al. (2002) could obtain rutile-like GeO_2 crystallines from quartz-like GeO_2 crystalline sample after prolong heating process which took 700 h at 750 °C. The orthorhombic $PbGe_3O_7$ phase which was observed in the binary GeO_2 – PbO glass system conducted by Scavini et al. was not observed in any of the binary GeO_2 – PbF_2 glasses that were studied in the present study (Scavini et al., 2001). The amount of the $PbGeO_3$ phase increases with the addition of PbF_2 content in the non-doped GeO_2 – PbF_2 glasses where PbF_2 content is between 10–30 mol%, which is also similar to the case where in the GeO_2 – PbO glass system with the PbO content between 20–25 mol%, intensity of $PbGeO_3$ phase increases with the addition of PbO content (Zhereb et al., 2008; Scavini et al., 2001; Sigaev et al., 2001).

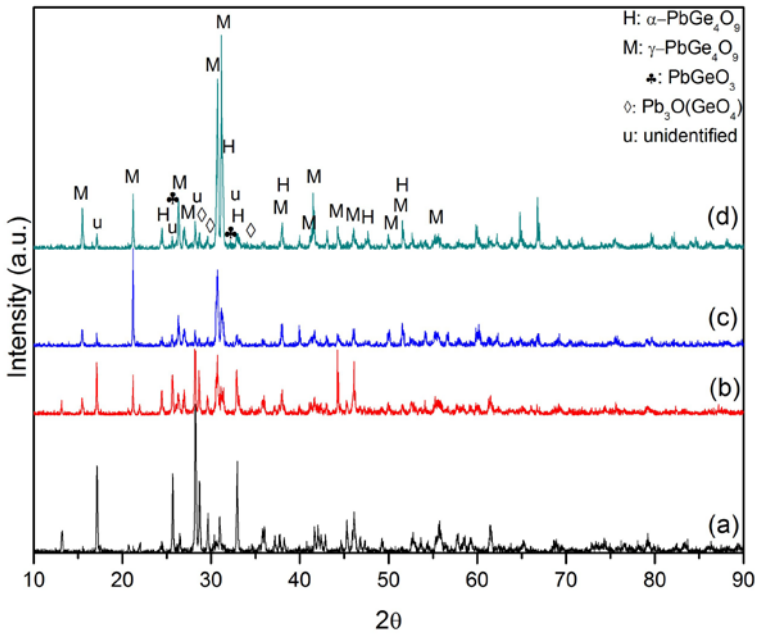

Figure 4.46 : XRD scans of the 0.80 GeO_2 – 0.20 PbF_2 – 0.005 Er_2O_3 doped glasses which are annealed at 700 °C for 30 min (a), 3 h (b), 23 h (c), 63 h (d) respectively.

In order to investigate stability of the unidentified phase, pro-long heat treatments applied to 0.80 GeO_2 – 0.20 PbF_2 – 0.005 Er_2O_3 doped glasses which has most pristine diffraction intensity peaks among studied glass samples. Heat treatments carried out at 700 °C for 30 min, 3 h, 23 h, 63 h and annealed glass were investigated with x-ray diffraction technique. For the glass sample which is annealed at 700 °C for 30 min, unidentified phase is major phase in the sample and formation of little amount of monoclinic $PbGe_4O_9$ crystals are observed. When the annealing time increases to 3 h, intensity peaks of unidentified phases decreases while amount of monoclinic phase increases. Thus, unidentified / $PbGe_4O_9$ phase ratio decreases with

annealing time. Further heat treatments (23 h at 700 °C) shows that intensity peaks of monoclinic $PbGe_4O_9$ phase increases more and amount of the unidentified phase decreases. When the heat-treatment reaches to 63 h, monoclinic $PbGe_4O_9$ phase becomes major phase in the glass-ceramic, while unidentified phase almost disappears. Different annealing times showed that unidentified phase is a metastable phase and this phase mainly transforms to monoclinic $PbGe_4O_9$ crystals.

5. CONCLUSION AND RECOMMENDATIONS

1. All glass samples show amorphous clustering and samples except 0.90 GeO_2 – 0.10 GeO_2 – 0.02 Er_2O_3 glass sample are transparent under visible light with the absence of GeO_2 crystals.

2. As effects of heating rate are investigated, no changes are observed at the glass transition temperature with varying heating rate for non-doped GeO_2 – PbF_2 glasses. On the other hand, exothermic peaks shift to higher temperatures with increasing heating rate and become more elevated. In addition to that, convolution of exothermic peaks is observed for higher heating rates. Although values of melting temperatures don't change with heating rate, they become broader like exothermic peaks.

3. The glass transition temperature tends not to change with PbF_2 content in studied non-doped and doped GeO_2 – PbF_2 glasses while these results are almost similar for studied GeO_2 – PbO glass compositions.

4. The glass transition temperature isn't affected by erbium content in studied GeO_2 – PbF_2 glasses, while literature studies showed that erbium content changes slightly the glass transition temperature in studied GeO_2 – PbO glass compositions.

5. DTA studies showed activation energy for the crystallization decreases with erbium content for all doped GeO_2 – PbF_2 glasses.

6. As PbF_2 content increased to 20 mol%, nucleation of α-GeO_2 phase a sudden decrease is observed in doped and non-doped GeO_2 – PbF_2 glasses as reported in literature for GeO_2 – PbO glass system.

7. With addition of PbF_2 content, crystallite amount decreases for both doped and non-doped studied GeO_2 – PbF_2 glasses. Moreover, doped GeO_2 – PbF_2 glasses tend to soften, due to this reason it makes difficult to obtain crystalline at relatively high temperatures and longer heat treatments at relatively lower temperatures are required.

8. As PbF_2 content increased, polymorphs of $PbGe_4O_9$ phases increases and in the absence of GeO_2 crystalline they become major phase when PbO content is increased to 20mol%. This type of behavior is almost similar to GeO_2 – PbO binary glass system.

9. $PbGeO_3$ and Pb_3GeO_5 phases nucleate with sufficient PbF_2 content for binary GeO_2 – PbF_2 glasses. Although nucleation of $PbGeO_3$ phases expected, nucleation of Pb_3GeO_5 phase is observed by limited authors in this compositional range for GeO_2 – PbO glasses.

10. In doped GeO_2 – PbF_2 glasses, formation of $Pb_3O(GeO_4)$ phase is observed instead of Pb_3GeO_5 phase which exists in studied non-doped binary GeO_2 – PbF_2 glasses. As PbF_2 content increases, amount of $Pb_3O(GeO_4)$ phases increases with $PbGeO_3$ phase.

11. The ceramic-glass samples which have 2 mol% Er_2O_3 accommodate a little amounts of $Er_2Ge_2O_7$ phase.

12. Unidentified phase which is observed for erbium doped glass is investigated for its stability. After pro-long heat treatments, unidentified phase transforms mainly into γ-$PbGe_4O_9$, thus the unidentified phase is metastable phase in doped GeO_2 – PbF_2 glass.

13. β–PbF_2 is observed for high amounts of PbF_2 content, but even 2 mol% Er_2O_3 and 30mol% PbF_2 compounds are added to glass, intensity peaks are relatively low when compared to literature studies. As it reported in literature, high amounts of PbF_2 and Er_2O_3 are required for nucleating β–PbF_2 phase.

REFERENCES

Adam, J. –L., 2001. Non-oxide glasses and their application in optics, *Journal of Non-Crystalline Solids*, **287**, 401–404.

Amato, G., Rossi, A. M., Boarino, L., Brunetto, N., 1997. On the role of germanium in porous silicon-germanium luminescence, *Philosophical Magazine Part B*, **76**, 395–403.

Anan'ev, A. V., Bogdanov, V. N., Champagnon, B., Ferrari, G. O., Karapetyan, G. O., Maksimov, L. V., Smerdin, S. N., and Solovyev, V. A., 2008. Origin of Rayleigh scattering and anomaly of elastic properties in vitreous and molten GeO_2, *Journal of Non-Crystalline Solids*, **354**, 3049–3058.

Balitsky, D. V., Balitsky, V. S.; Pushcharovsky, D. Yu,, Bondarenko, G. V., and Kosenko A. V., Growth and characterization of GeO_2 single crystals with the quartz structure, *Journal of Crystal Growth*, **180**, 212–219.

Belostotsky, V., 2007. Defect model for the mixed mobile ion effect, *Journal of Non-Crystalline Solids*, **353**, 1078–1090.

Bueno, L. A., Donoso, J. P., Magon, C. J., Dias Filho, F. A., Tambelli, C. C., Messaddeq, Y., and Ribeiro, S. J. L., 2007. Conductivity and ^{19}F NMR in $PbGeO_3$–PbF_2–CdF_2 glasses and glass-ceramics, *Journal of Non-Crystalline Solids*, **351**, 766–770.

Bueno, L. A., Gouveia-Neto, A. S., da Costa, E. B., Messaddeq, Y., and Ribeiro, S. J. L., 2008. Structural and spectroscopic study of oxyfluoride glasses and glass-ceramics using europium ion as a structural probe, *Journal of Physics: Condensed Matter*, **20**, 145201.

Bueno, L. A., Melnikov, P., Messaddeq, Y., and Ribeiro, S. J. L., 1999. Er^{3+} and Eu^{3+} containing transparent glass ceramics in the system $PbGeO_3$–PbF_2–CdF_2, *Journal of Non-Crystalline Solids*, **247**, 87–91.

Bueno, L. A., Messaddeq, Y., Dias Filho, F. A., and Riberio, S. J. L., 2005. Study of fluorine losses in oxyfluoride glasses, *Journal of Non-Crystalline Solids*, **351**, 3804–3808.

Bush, A. A., and Venevtsev, Yu. N., 1981. Phase equilibria in the $PbGeO_3$–GeO_2 system, *Russ. J. Inorg. Chem.* (Engl. Transl.), **26**, 249–253.

Bush, A. A., and Stefanovich, S. Yu., 2002. Piezoelectric and nonlinear optical properties of $PbGe_4O_9$ crystals, *Inorganic Materials*, **38**, 168–171.

Conçalves, M. C., Santos, L. F., and Almedia, R. M., 2002. Rare-earth-doped transparent glass ceramics, *Comptes Rendus Chimie*, **5**, 845–854.

Dantelle, G., Mortier, M., Vivien, D., and Patriarche, G., 2005. Effect of CeF_3 addition on the nucleation and up-conversion luminescence in transparent oxyfluoride glass-ceramics, *Chemistry of Materials*, **17**, 2216–2222.

Dantelle, G., Mortier, M., Patriarche, G., and Vivien, D., 2006. Er^{3+}-doped PbF_2: Comparison between nanocrystals in glass-ceramics and bulk single crystals, *Journal of Solid State Chemistry*, **179**, 1995-2003.

Dominiak-Dzik, G., and Ryba-Romanowski, W., 2008. Structural and luminescent properties of crystalline microstructure in the GeO_2–PbO–PbF_2 glass-ceramics doped with luminescent ions, *Journal of Alloys and Compounds*, **451**, 586-590.

Du, L.-S., Peng, L., and Stebbins, J. F., 2007. Germanosilicate and alkali germanosilicate glass structure: New insights from high-resolution oxygen-17 NMR, *Journal of Non-Crystalline Solids*, **353**, 2910–2918.

Ghingna, P., Mustarelli, P., Tomasi, C., Quartarone, E., Scavini, M., Speghini, A., and Bettinelli, M., 2002. A Combined Nuclear Magnetic Resonance and X-ray Absorption Fine Structure Study on the Local Structures of Ge and Pb in PbO–GeO_2 Glasses and Their Relationships with Thermal Properties and Devitrification Products, *Journal of Physical Chemistry B*, 106 , 9802–9809

Gouju, D., Fournier, J., and Kohlmuller R., 1968. Sur le système GeO_2 – PbO, *C. R. Seances Acad. Sci., Ser. C*, **266**, 1063–1065.

Gouveia-Neto, A. S., Bueno, L. A., do Nascimento, R. F., da Silva, E. A., and da Costa, E. B., 2009. 1540 nm fiber laser excited upconversion luminescence in erbium-doped lead–fluoride nanocrystals, *Journal of Non-Crystalline Solids*, **355**, 488–491.

Gouveia-Neto, A. S., Bueno, L. A., Afonso, A. C. M., Nascimento, J. F., Costa, E. B., Messaddeq, and Y., Ribeiro, S. J. L., 2008. Upconversion luminescence in Ho^{3+}/Yb^{3+}- and Tb^{3+}/Yb^{3+}-codoped fluorogermanate glass and glass ceramic, *Journal of Rare Earths*, **24**, 757–760.

Gouveia-Neto, A. S., da Costa., E. B., Bueno, L. A., and Riberio, S. J. L., 2004. Upconversion luminescence in transparent glass ceramics containing β–PbF2 nanocrystals doped with erbium, *Journal of Alloys and Compounds*, **375**, 224-228.

Gouveia-Neto, A. S., da Costa, E. B., Bueno, L. A., and Ribeiro, S. J. L., 2004. Intense red upconversion emission in infrared excited holmium-doped $PbGeO_3$–PbF_2–CdF_2 transparent glass ceramic, *Journal of Luminescence*, **110**, 79-84.

Hannon, A. C., Martino D. D., Santos L. F., and Almedia R. M., 2007. A model for the Ge–O coordination in germanate glasses, *Journal of Non-Crystalline Solids*, **353**, 1688-1694.

Henderson, G. S., 2007. The Germanate Anomaly: What do we know?, *Journal of Non-Crystalline Solids*, **353**, 1695-1704.

Henderson, G. S., Neuville, D. R., Cochain, B., and Cormier, L., 2009. The structure of GeO_2–SiO_2 glasses and melts: A Raman spectroscopy study, *Journal of Non-Crystalline Solids*, **355**, 468–474.

Hoppe, U., Kranold, R., Weber, H., -J., Neuefeind, J., Hannon A. C., 2000. The structure of potassium germanate glasses – a combined X-ray and neutron scattering study, *Journal of Non-Crystalline Solids*, **278**, 99–114.

Ivanova, I., 1991. Glass formation in the TeO_2-GeO_2-PbO-PbF_2 system, *Journal of Materials Science Letters*, **10**, 1309–1311.

Joubert, M. F., 1999. Photon avalanche upconversion in rare earth laser materials, *Optical Materials*, **11**, 181–203.

Kabalci, I., Özen, G., Öveçoğlu, M. L., and Sennaroğlu, A., 2006. Thermal study and linear optical properties of $(1-x)TeO_2$–$(x)PbF_2$ (x = 0.10, 0.15 and 0.25 mol) glasses, *Journal of Alloys and Compounds*, **419**, 294–298.

Kassab, L. R. P., Hora, W. G., Lozana, W. B., de Oliviera, M. A. S., and Maciel, G. S., 2007. Optical properties of Er^{3+} doped GeO_2–PbO glass: Effect of doping with Bi_2O_3, *Optics Communications*, **269**, 356–361.

Kissinger, H. E., 1965. Variation of Peak Temperature With Heating Rate in Differential Thermal Analysis, *Journal of Research of the National Bureau of Standards*, **57**, 217–221.

Klimesz, B., Dominiak-Dzik, G., Lisiecki, R., and Ryba-Romanowski, W., 2008. Systematic study of spectroscopic properties and thermal stability of lead germanate glass doped with rare-earth ions, *Journal of Non-Crystalline Solids*, **354**, 515–520.

Knoblochova, K., Ticha, H., Schwarz, J., and Tichy, L., 2009. Raman spectra and optical properties of selected Bi_2O_3–PbO–B_2O_3–GeO_2, *Optical Materials*, **31**, 895-898.

Labéguerie, J., Dantelle G., Gredin, P., and Mortier, M., 2008. Luminescence properties of PbF_2:Yb–Er nanoparticles synthesized by two different original routes, *Journal of Alloys and Compounds*, **451**, 563-566.

Lezal, D., Pedlikova, J., Kostka, P., Poulain, M., and Zavadil, J., 2001. Heavy metal oxide glasses - preparation and physical properties, *Journal of Non-Crystalline Solids*, **284**, 288–295.

Lucas, J., Smektala, F., and Adam, J. L., 2002. Fluorine in optics, *Journal of Fluorine Chemistry*, **114**, 113–118

Margaryan, A., and Piliavin M. C., 1993. *Germanate glasses: structure, spectroscopy and properties*, ARTECH HOUSE, INC., Boston.

Micolaut, M., Cormier, L., and Henderson, G. S., 2006. The structure of amorphous, crystalline and liquid GeO_2, *Journal of Non-Crystalline Solids*, **284**, 288–295.

Mortier, M., 2002. Between glass and crystal: glass–ceramics, a new way for optical materials, *Philisophical Magazine B*, **82**, 745–753

Mortier M., 2003. Nucleation and anionic environment of Er^{3+} in a germanate glass, *Journal of Non-Crystalline Solids*, **318**, 56–62

Mortier, M., Goldner, P., Chateu, M., and Genotelle, M., 2001. Erbium doped glass–ceramics: concentration effect on crystal structure and energy transfer between active ions, *Journal of Alloys and Compounds*, **323-324**, 245–249

Mortier, M., and Patriarche, G., 2000. Structural characterisation of transparent oxyfluoride glass-ceramics, *Journal of Alloys and Compounds*, **35**, 4849–4856.

Nie, Q., Lu, L., Dai, S., Xu, T., Shen, X., Zhang, X., Liang, X., and Zhang, X., 2007. Investigation of thermal stability and spectroscopic properties in Er^{3+} doped bismuth – boron – germanium glasses, *Physica B: Condensed Matter*, **392**, 195–199.

Otto, H. H., 1979. Die Kristallstruktur der ferroischen Verbindung Pb3[O|Ge04], *Zeitschrift fur Kristallographie*, **149**, 227–240.

Pan, Z., Ueda, A., Mu, R., and Morgan, S. H., 2007. Upconversion luminescence in Er^{3+}-doped germanate-oxyfluoride and tellurium-germanate-oxyfluoride transparent glass-ceramics. *Journal of Luminescence*, **126**, 251–256.

Peng, L., and Stebbins, J. F., 2007. Sodium germanate glasses and crystals NMR constraints on variation in structure with composition, *Journal of Non-Crystalline Solids*, **353**, 4732–4742.

Phillips, B., and Scroger, M. G., 1965. Phase Relations and Glass Formation in the System PbO-GeO, *Journal of the American Ceramic Society*, **48**, 398–401.

Setlur, A. A., Heward, W. J., Gao, Y., Srivastava, A. M., Chandran, R. G., Shankar, M. V., 2006. Crystal Chemistry and Luminescence of Ce^{3+}-Doped $Lu_2CaMg_2(Si,Ge)_3O_{12}$ and Its Use in LED Based Lighting, *Chemistry of Materials*, **18**, 3314–3322.

Silva, M. A. P., Messaddeq, Y., Ribeiro, S. J. L., Poulain, M., Villian, F., Briois, V., 2001. Structural studies on TeO_2–PbO glasses, *Journal of Physics and Chemistry of Solids*, **62**, 1055–1060.

Scavini, M., Tomasi, C., Speghini, A., and Bettinelli, M., 2001. Stable and Metastable Phases within the GeO_2-Rich Part of the Binary PbO–GeO_2 System, *Journal of Materials Synthesis and Processing*, **9** ,93–102.

Sigaev, V. N., Gregora, I., Pernice, P., Champgnon, B., Smelyanskaya, E. N., Aronne, A., and Sarkisov, P. D., 2001. Structure of lead germanate glasses by Raman spectroscopy, *Journal of Non-Crystalline Solids*, **279**, 136–144.

Shang, Z., Ren, G., Yang, Q., Xu, C., Liu, Y., Zhang, Y., and Wu, Q., 2008. Spectroscopic properties of Er^{3+}-doped and Er^{3+}/Yb^{3+}-codoped PbF_2–MO_x (M = Te, Ge, B) oxyfluoride glasses, *Spectrochimica Acta Part A*, **67**, 246–250.

Speranskaya, E. I., 1959. The system PbO-GeO_2, *Russian Chemical Bulletin*, **8**, 145–146.

Tambelli, C. C., Donoso, J. P., Magon, C. J., Bueno, L. A., Messaddeq, Y., Ribeiro, S. J. L., de Oliveria, L. F. C., and Kosacki, I., 2004. Glass structure and ion dynamics of lead–cadmium fluorgermanate glasses, *The Journal of Chemical Physics*, **120**, 9638–9647.

Yamane, M., and Asahara, Y., 2000. *Glasses for photonics*, Cambridge University Press, Cambridge.

Yang, Z., and Jiang, Z., 2006. Thermal stability and spectroscopic properties of Er^{3+}-doped lead fluorogermanate glasses, *Journal of Luminescence*, **121**, 149–158.

Viswanathamurti, P., Bhattarai, N., Kim, H. Y., Khil, M. S., Lee, D. R., and Suh, E. –K., 2004. GeO_2 fibers: Preparation, morphology and photoluminescence property, *The Journal of Chemical Physics*, **121**, 441–445.

Zhang, L., Sun, H., Haitao, W., Wang, J., Hu, L., and Zhang, J., 2005. Effects of PbF_2 on the spectroscopic, lasing and structural properties of Yb^{3+}-doped fluorophosphate glass, *Solid State Communications*, **135**, 150–154.

Zhereb, V. P., Kirko, V. I., Tarasova, L. S., Markosyan, S. M., Zhizhaev, A. M., El'berg, M. S., Suprunets, S. V., 2008. Phase relations in metastable equilibria of the PbO–GeO_2 system, *Russian Journal of Inorganic Chemistry*, **53**, 313–318.

APPENDICES

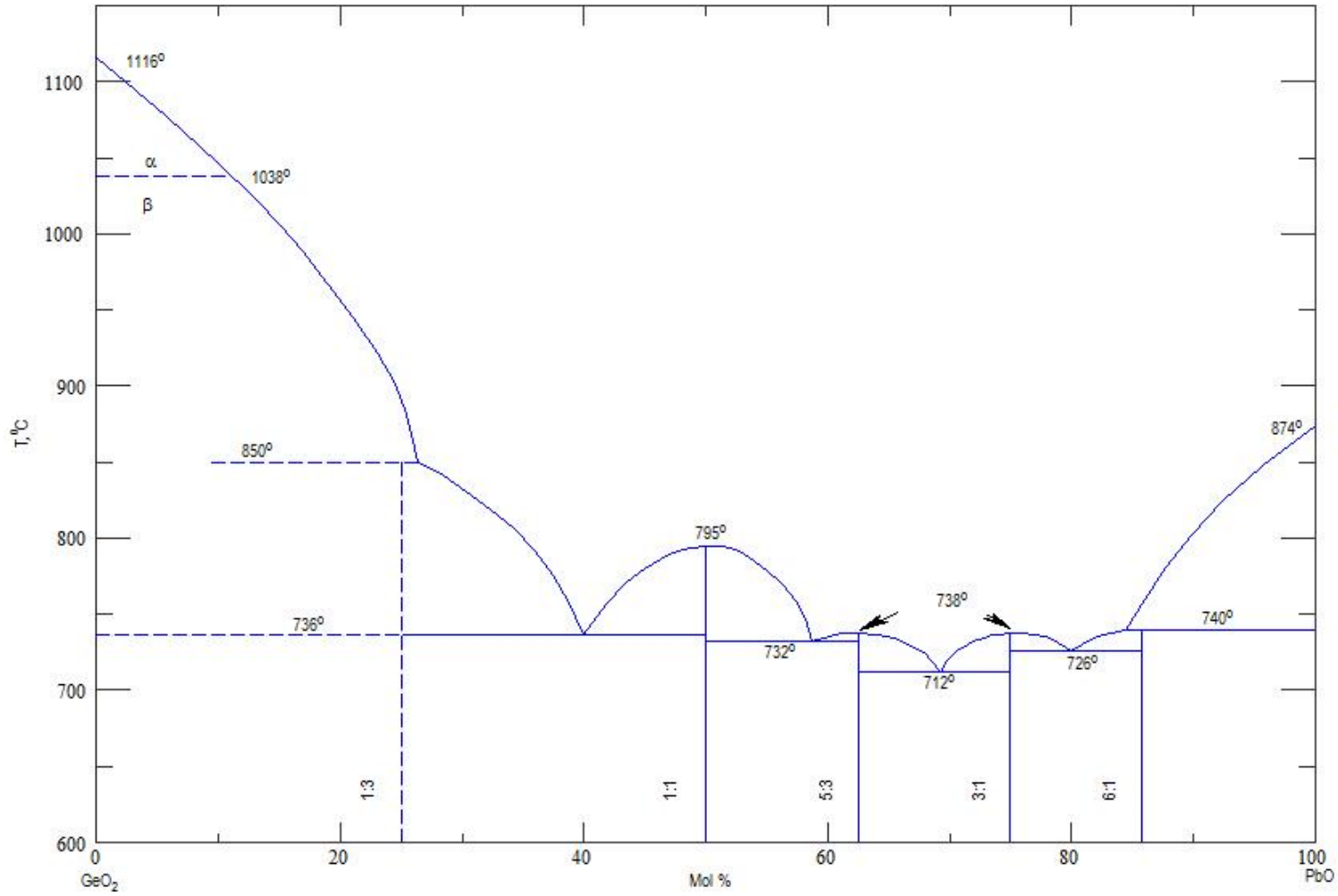

Figure A.1 : System PbO-GeO_2 (Speranskaya, 1959).

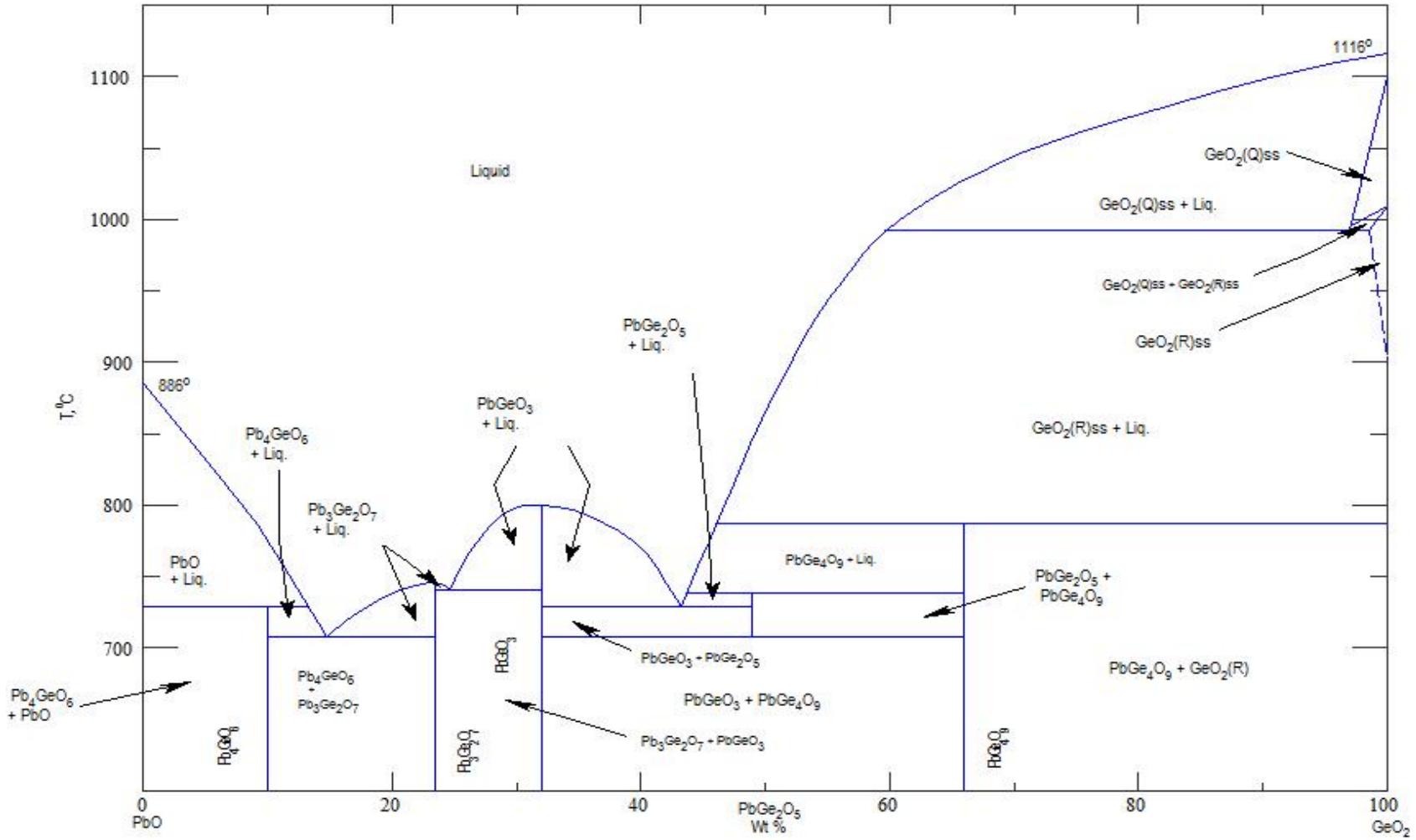

Figure A.2 : System PbO-GeO_2 (Phillips and Scroger, 1965).

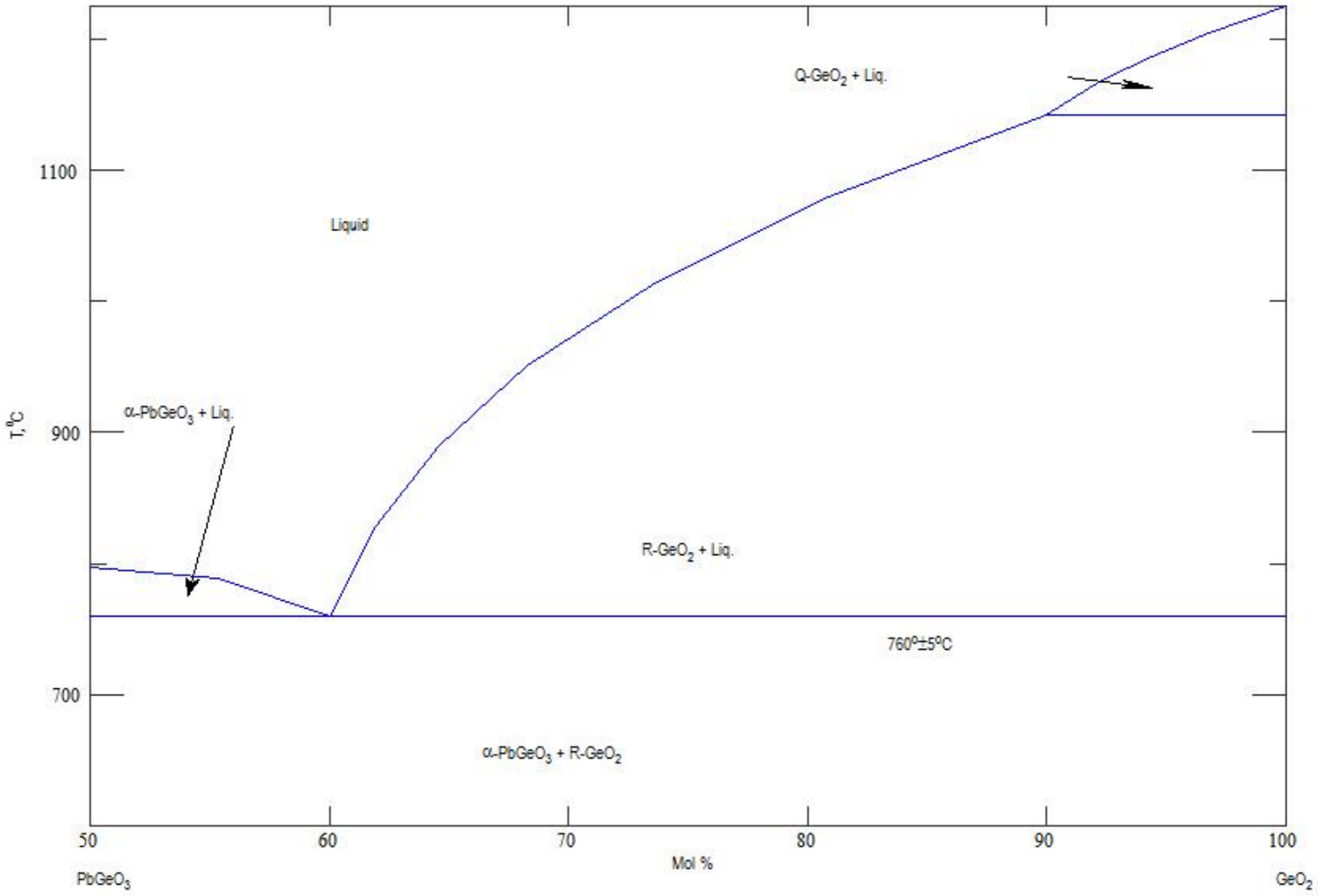

Figure A.3 : System $PbGeO_3$-GeO_2 (Bush and Venevtsev, 1981).

Table B.1 : 2θ values of unidentified phase (* indicate the highest peak)

2θ			
13.182°	32.954°	42.031°	58.480°
17.139°	35.793°	42.840°	59.268°
25.686°	36.014°	45.297°	61.489°
28.217°*	37.191°	46.106°	
28.688°	37.733°	55.732°	
30.983°	41.619°	57.761°	

Table C.1 : All of the crystals structures, lattice parameters, space groups and card numbers of the crystalline phases

Crystal	Struct.	Space Group	a(nm)	b(nm)	c(nm)	β(°)	CN
α-GeO_2	Hex.	$P3_221$(154)	4.98502		5.648	90	36-1463
α-$PbGe_4O_9$	Hex.	(0) (P321)	11.42		4.753	90	43-0969
γ-$PbGe_4O_9$	Mono.	I */*(0)	4.638	11.455	6.831	103.17	32-0516
$PbGeO_3$	Mono.	A2/a(15)	13.23	14.47	22.93	119.4	44-0945
Pb_3GeO_5	Mono.	P2(3)	5.281	5.489	5.241	91.8	83-2329
PbF_2	Cubic	Fm-3m(225)	5.934			90	77-1866
$Pb_3O(GeO_4)$	Mono.	$P2_1$(4)	5.26	10.437	5.477	92.55	83-1409
$Er_2Ge_2O_7$	Tetra.	$P4_12_12$(92)	6.7857	12.3324		90	38-0290

CURRICULUM VITAE

Candidate's full name : Mithat Cem Elbizim

Place and date of birth : Kıbrıs, 19.10.1985

Permanent Address : Soyak Yenişehir Palmiye Evleri, C-2 Blok, Daire: 22 Ümraniye/İstanbul 34770

Universities and Colleges attended : Istanbul Technical University
Physics Engineering

Publications: